NOTICE

AVIS

The quality of this microform is heavily dependent upon the quality of the original thesis submitted for microfilming. Every effort has been made to ensure the highest quality of reproduction possible.

If pages are missing, contact the university which granted the degree.

Some pages may have indistinct print especially if the original pages were typed with a poor typewriter ribbon or if the university sent us an inferior photocopy.

Reproduction in full or in part of this microform is governed by the Canadian Copyright Act, R.S.C. 1970, c. C-30, and subsequent amendments.

La qualité de cette microforme dépend grandement de la qualité de la thèse soumise au microfilmage. Nous avons tout fait pour assurer une qualité supérieure de reproduction.

S'il manque des pages, veuillez communiquer avec l'université qui a conféré le grade.

La qualité d'impression de certaines pages peut laisser à désirer, surtout si les pages originales ont été dactylographiées à l'aide d'un ruban usé ou si l'université nous a fait parvenir une photocopie de qualité inférieure.

La reproduction, même partielle, de cette microforme est soumise à la Loi canadienne sur le droit d'auteur, SRC 1970, c. C-30, et ses amendements subséquents.

Canada

University of Alberta

Response of Cylinders to Oscillatory Flow

by

Ian D. Williamson

A thesis
submitted to the Faculty of Graduate Studies and Research
in partial fulfilment of the requirements for the degree of

Master of Science

Department of Mechanical Engineering

Edmonton, Alberta

Spring 1991

Canada

University of Alberta

Release Form

Name of Author: **Ian D. Williamson**

Title of Thesis: **Response of Cylinders to Oscillatory Flow**

Degree: Master of Science

Year this degree granted: Spring 1991

Permission is hereby granted to **The University of Alberta Library** to reproduce single copies of this thesis and to lend or sell such copies for private, scholarly, or scientific research purposes only.

The author reserves other publication rights, and neither the thesis nor extensive tracts from it may be printed or otherwise reproduced without the author's written consent.

Ian Williamson

Ian D. Williamson

7 Kindle Court

Gloucester, Ontario

Canada

K1J 6E1

Date : *Feb. 5, 1991*

The University of Alberta

Faculty of Graduate Studies and Research

The undersigned certify that they have read, and recommend to the Faculty of Graduate Studies and Research for acceptance, a thesis entitled

Response of Cylinders to Oscillatory Flow
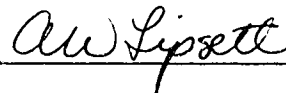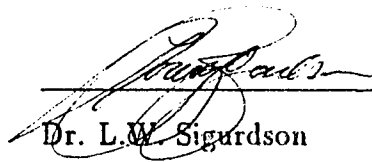
submitted by

Ian D. Williamson

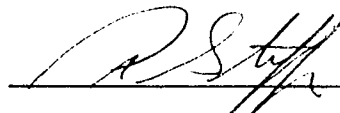in partial fulfilment of the requirements for the degree of

Master of Science.

_____

Dr. A.W. Lipsett (Supervisor)

_____

Dr. L.W. Sigurdson

_____

Dr. P.M. Steffler

Date : Jan 31, 1991

Abstract

The two-dimensional response to oscillatory flow of an elastically mounted rigid cylinder is studied experimentally and the results are compared with numerical predictions of the response. The tests are conducted in a U-tube with the Keulegan-Carpenter number, Kc, between 2 and 60, and the ratio of the natural frequency in water to the fluid oscillation frequency, f_n/f_w, between 1 and 8.6. The results of the experimental portion of the study show that the response of the cylinder depends on both Kc and f_n/f_w. For many flow conditions the cylinder was observed to respond in well defined trajectories that could be classified by the number of transverse cycles of motion completed for each cycle of water motion. One principal cycle of inline response was observed for each cycle of water motion. In general, the transverse response tended to assume integer multiples of the flow frequency, however in contrast to studies of transverse response alone, the transverse response did not necessarily occur at the integer multiple closest to the natural frequency of the cylinder. In addition, the transverse response amplitude was not any larger for cases in which f_n/f_w was an integer. Transverse response amplitudes were not observed to exceed 1.2 diameters.

Three sets of equations of motion are developed to predict the response of cylinders to oscillatory flow. Two of the models use the relative velocity formulation of the Morison equation for the fluid force inline with the flow, however each use different models of the transverse force. The third model considers lift and drag force components parallel and perpendicular to the direction of instantaneous relative velocity between the fluid and the cylinder. Comparison of the numerical models' predictions to the experimentally observed trajectories showed generally good agreement, however the models were least successful in predicting the cases in which there were abrupt changes in direction. Suggestions improvements to the models are also made.

The results of this study have identified the need for flow visualization studies of the two-dimensional response of a cylinder to oscillatory flow.

Acknowledgements

Contents

List of Tables

List of Figures

Chapter 1

Introduction

As offshore resource exploration and development progress to deeper water, further research is required to obtain an understanding of the forces on offshore structures and the resulting responses to establish safer, more efficient designs. One particular area of interest is that of the dynamics of flexible members, specifically marine risers. A riser connects a wellhead at the seabed with a surface vessel, such as a tension leg platform or a semisubmersible. Risers are typically 45 cm to 60 cm in diameter, and function as a conduit for the drilling equipment, mud and in the case of production risers, natural gas or oil. As drilling is done in greater depths of water, risers become progressively more flexible due to their increased length. Currently, risers up to about 700m in length are in use.

When the flexible riser is exposed to currents and/or wave action, its response to the fluid forces affects the fluid flow. This fluid-structure interaction may lead to an amplification of the forces on the structure and sustained large amplitude responses. Failure due to excessive load or fatigue may result. The forces causing the response of the structure may be attributed to several sources. Currents cause drag forces in the direction of the flow, and in addition there may be forces due to vortex shedding which act transversely to the flow and, less significantly, in the direction of flow. Wave action can cause forces in the inline direction (the direction of wave propagation) due

to the drag of the flow about the structure, as well as due to the acceleration of the flow. Vortex shedding due to wave action may also occur, causing both inline and transverse forces, with the added complication that the vortices shed in one half cycle become the incident flow for the next half cycle. Additional complications are that the current, wave motion, and response characteristics of the structure vary with depth, and that the current and wave effects may not be collinear.

An important design problem is to be able to predict both the forces on a structure and the response. Despite many advances in computational fluid mechanics, accurate computation of the flow and structural response for marine structures is not yet feasible. However, once the two-dimensional response of a elastically supported cylinder has been studied experimentally, the usefulness of simpler equations to predict the response can be evaluated. In particular, the Morison equation and various modifications to it have been used quite successfully to predict inline forces on fixed cylinders in oscillatory and wavy flows. The applicability of these equations to the case where the cylinder can respond in two dimensions has yet to be assessed.

Motion of the fluid due to wave action is an approximately elliptical orbit. In the case of linear inviscid wave theory for deep water, the particle motions are circular, with an amplitude that decreases exponentially to zero from a maximum at the water surface. In shallower water, the motion becomes a flatter ellipse at the surface and straight back and forth at the bottom. By far the most significant component of this type of flow is that perpendicular to the structure. To understand the basics of the fluid-structure interaction it is convenient to study this component alone in nominally two-dimensional oscillatory flow.

As a necessary step in understanding the response of structures at sea, the response of an elastically mounted rigid circular cylinder to oscillatory flow is studied in this thesis. It is hoped that by first understanding the mechanisms of two-dimensional response due to planar oscillatory flow in a U-tube, a greater understanding of the behaviour in the sea may be attained. A literature review of studies relevant to the present investigation is presented in Chapter 2. Chapter 3

contains a description of the experimental apparatus, and is followed by the experimental results in Chapter 4. In Chapter 5 simple numerical models of the behaviour of the cylinder are developed, based on previous studies of inline and transverse response alone, and are applied to the conditions studied in the U-tube. The results of the numerical predictions are compared to the experimentally observed results in Chapter 6 to assess the usefulness of the equations of motion. Finally, in Chapter 7 conclusions about the experimental results and numerical models are presented, and important topics for future studies are identified.

Chapter 2

Literature Review

To provide the groundwork required for at least a partial understanding of the response of offshore structures in waves, investigations of simpler cases of flow about cylinders are summarized in this chapter. First, the features of steady flow about fixed structures is discussed, followed by a summary of the response of flexible structures to steady flow. Studies of oscillatory flow about fixed cylinders are then considered and compared with studies of wavy flow on fixed cylinders. Finally, most of the emphasis is placed on investigations of the response of flexible structures in oscillatory flow and wavy flow. In this thesis, the term "oscillatory flow" refers to flow in which the flow field removed from the cylinder describes rectilinear harmonic motion (straight back and forth), while the term "wavy" flow refers to flow in which the flow field removed from the cylinder describes an orbital motion in a vertical plane. At the end of the chapter a synthesis is presented of the significant features of previous work as they relate to the present study.

2.1   Vortex Shedding in Steady Flow

Vortex shedding from bluff bodies in steady flow has been the subject of much research because it is encountered in many engineering situations, particularly

4

structures in wind or currents. Examples include chimneys, transmission wires, buildings, piles, offshore structures, heat exchanger tubes and reactor tubes. For a more detailed treatment of vortex shedding and flow induced vibrations in general the reader is directed to references [1, 2].

Any sufficiently bluff body will shed vortices due to the separation of the boundary layer. As the flow along the surface of a body moves from the stagnation point toward the downstream side of the object, it loses energy due to friction. Eventually the flow does not have enough kinetic energy to overcome the increasing pressure on the downstream side, and separates from the surface of the object. A shear layer is formed between the fluid flowing past the body and the slower moving fluid in the wake of the body. This shear layer which trails downstream from the separation point becomes unstable and rolls up into discrete vortices. For a wide range of Reynolds numbers, these vortices are shed alternately from each side of the body, producing a Kármán vortex street.

A Strouhal number S, can be defined as

$$S = f_v D/U, \tag{2.1}$$

which relates the vortex shedding frequency f_v (cycles/sec), the constant free stream velocity U, and a characteristic dimension of the body, D. For circular cylinders in steady flow with a Reynolds number, Re, from 300 to 3×10^5, S is approximately constant at 0.2 [1, 3]. In one cycle of vortex shedding, a vortex is shed from one side followed by another shed from the other side. In what follows the vortex shedding frequency corresponds to the shedding of a pair of vortices.

Separation also has a large effect on the pressure distribution about the cylinder, giving rise to a significant mean drag force. For large Re, viscous shear forces contributing to the drag are much smaller than the forces due to the pressure distribution. An important consequence of vortex shedding from a body such as a circular cylinder is the variation of lift and drag forces imposed on the body due to the fluctuations in the pressure on the surface of the body. Variations in the force

transverse to the flow direction, or lift forces, occur at a frequency primarily equal to the vortex shedding frequency and have zero mean value. Variations in the inline force occur primarily at a frequency that is twice the vortex shedding frequency, and are much smaller than both the mean drag and the maximum transverse force. Because of this, the inline time dependent forces are often neglected.

In the case where the cylinder is not fixed, but is able to respond in the inline or transverse directions, or both, it is possible that the natural frequency of the structure may be close to the frequency of force variations in either the inline or transverse directions and cause large amplitude response. Due to the greater magnitude of the varying forces in the transverse direction, vibration in that direction is much more common. A familiar example of this phenomenon is the vibration of power lines in the wind due to vortex shedding, causing them to "hum" or "sing".

When the natural frequency of the body is close to the vortex shedding frequency, causing significant transverse oscillations, the cylinder motion has an effect on the fluid flow that is causing the motion. The cylinder motion tends to increase the strength and organization of the vortex shedding which in turn increases the forces causing the cylinder motion. In doing so, the vortex shedding frequency shifts to the natural frequency of the structure, in deviation from the Strouhal relationship, i.e. the motion of the cylinder controls the vortex shedding. This is known as "lock-in". Other terms for this phenomenon are locking-on, synchronization, hydroelastic or fluid-elastic oscillations, wake capture, self-controlled or self-excited oscillations [4]. Lock-in is characterized by a highly nonlinear interaction between the fluid forces and structural motion and has been modelled with limited success numerically. Further discussion of these models follows shortly. Although one might expect that lock-in would cause larger and larger amplitudes of oscillation, the amplitude of cylinder oscillations has never been observed to exceed 1.5 diameters [1]. The reason for this is that "as the cylinder amplitude increases beyond approximately one half diameter, the cylinder begins to outrun the shedding vortices and the lift coefficient diminishes" [1, p.63].

The range of flow conditions over which lock-in occurs is called the range of capture, and it is usually expressed in terms of the reduced velocity of the flow,

$$U_r = U/Df_n, \qquad (2.2)$$

where D is the cylinder diameter, and f_n is the natural frequency of the cylinder. When the natural frequency of the cylinder equals the vortex shedding frequency predicted by the Strouhal relationship, the reduced velocity is the inverse of the Strouhal number. This is called the resonant point, and corresponds to a reduced velocity of about 5 for a wide range of Reynolds number. The range of capture includes the resonant point and depends on the shape of the body. For a freely oscillating circular cylinder the range of capture extends from the resonant point to higher values of reduced velocity [2]. For example, if the flow speed past a flexibly mounted circular cylinder is increased, the vortex shedding frequency also increases as predicted by the Strouhal relationship until the resonant point is reached. Further increases in flow speed do not change the response frequency or vortex shedding frequency which remain at f_n, until the upper limit of the range of capture is reached. Beyond this point the vortex shedding cannot remain at the natural frequency and returns to the frequency given by the Strouhal relationship, and the response amplitude drops considerably. There is an exception to the above generalizations. For certain cases involving dense fluids (such as water) and low reduced velocities, inline oscillations may arise accompanied by symmetric vortex shedding. [2]

As mentioned earlier, a number of models have been used to predict the response of a cylinder in steady flow. Blevins [1] presents two such models, the "harmonic" model and the "wake oscillator" model. The harmonic model assumes sinusoidal forcing at the vortex shedding frequency applied to a spring-mounted, damped rigid cylinder. On a per unit length basis the equation of motion is

$$(m + m_a)\ddot{y} + 4\pi(m + m_a)\zeta f_n \dot{y} + ky = \frac{1}{2}\rho U^2 DC_L \sin \phi, \qquad (2.3)$$

where y is the transverse displacement, m is the structural mass, m_a is the added mass, ζ is the structural damping factor, k is the stiffness, ρ is the fluid density, C_L

is the lift coefficient, and ϕ is the phase of the vortex shedding. For steady flow the vortex shedding frequency is constant, thus

$$\phi = 2\pi f_v t, \tag{2.4}$$

in which f_v is that predicted by the Strouhal relationship in Equation 2.1. This model can be solved as a single degree of freedom harmonic oscillator, however it tends to overpredict the response near resonance. Further improvements are made by including amplitude dependence in the value of the lift coefficient. The lift coefficient is based on a three-term polynomial curve fit to experimental data, such that the lift coefficient increases for amplitudes y/D up to about 0.5 and then decreases for amplitudes above that. The lift coefficient becomes negative for amplitudes significantly over one.

The wake oscillator presented by Blevins [1] employs a momentum balance in a control volume that contains the cylinder. The fluid forcing terms include a negative damping term that extracts energy from the flow and a nonlinear fluid governor term that limits the amplitude of oscillations. The coefficients used in the model are based on experiments on fixed and forced cylinders in steady flow. The wake oscillator exhibits resonance at super- and sub-harmonics due to nonlinearities in the equation, and unlike the harmonic model, it "exhibits entrainment—the frequency of vortex shedding from an elastically mounted cylinder is entrained by the natural frequency of the motion" [1, p.70].

2.2 Forces on Fixed Cylinders in Oscillatory and Wavy Flow

An important distinction must be made between oscillatory and wavy flow. While most of the research on the forces produced by these flows is ultimately aimed at estimating forces in wavy flow, it is often preferable to produce oscillatory flow in the

laboratory situation. Oscillatory flow has the advantage of separating structural and fluid effects under specific conditions from the cumulative effects of depth dependent forces and structural response characteristics encountered with vertical cylinders in wavy flow. Wavy flow is characterized by fluid particle paths that describe elliptical trajectories in a vertical plane in the direction of wave propagation. The exact shapes of these trajectories change with the depth below the fluid surface, and depend on the wave characteristics. In oscillatory flow, the fluid particles follow a trajectory that is back and forth in a straight line and sinusoidal with time. For the case of linear inviscid wave theory, oscillatory flow reproduces the normal component of the fluid motion past a vertical structure. For this reason, oscillatory flow is chosen by many researchers as a starting point for understanding the forces acting on offshore structures as well as fluid structure-interaction in waves.

Considerable research has been done to measure the forces on fixed cylinders in oscillatory flow. There are basically two types of such experiments: fixing a cylinder in oscillating fluid [5, 6, 7, 8, 9, 10] or oscillating a cylinder in still fluid [11, 12, 13]. In each case the forces are considered as inline, in the direction of fluid or cylinder motion, and transverse, normal to the fluid or cylinder motion.

2.2.1 Inline Forces on Fixed Cylinders

The most common equation used to describe the inline forces on a cylinder in oscillatory flow is that attributed to Morison et al. [14]. It is a semi-intuitive equation that expresses the net force F on a cylinder of diameter D and length L as a superposition of a drag force and a force due to the accelerating fluid as

$$F = \frac{1}{2}\rho C_d LDU|U| + \frac{\pi}{4}\rho C_m LD^2 \frac{dU}{dt}. \tag{2.5}$$

Here ρ is the density of the fluid, U is the water particle velocity, and C_m and C_d are the empirical inertia and drag coefficients respectively. The drag term incorporates $U|U|$ rather than U^2 so that it always acts in the direction of the flow. The inertia

coefficient for a fixed cylinder may be expressed as

$$C_m = C_a + 1. \tag{2.6}$$

The "1" in the Equation 2.6 accounts for the pressure gradient in the flow that causes the fluid acceleration dU/dt. When a body is immersed in a fluid with a pressure gradient, it experiences a "buoyancy force" in the direction opposite to the gradient. The added mass coefficient, C_a, accounts for the force required to accelerate the flow around the body. For inviscid flow, the value of C_a for a cylinder is 1.

The values of C_m and C_d must be determined from experimental measurements. The Fourier averages of these coefficients were found by Keulegan and Carpenter [15] to be

$$C_d = -\frac{3}{4} \int_0^{2\pi} \frac{F(t) \cos \theta}{\rho U_m^2 LD} d\theta \tag{2.7}$$

and

$$C_m = \frac{2U_m T}{\pi^3 D} \int_0^{2\pi} \frac{F(t) \sin \theta}{\rho U_m^2 LD} d\theta, \tag{2.8}$$

where $\theta = 2\pi t/T$, T is the period of fluid oscillation, $F(t)$ is the measured force and U_m is the maximum fluid velocity. Alternatively, a least squares analysis yields an identical expression for C_m and

$$C_d = -\frac{8}{3\pi} \int_0^{2\pi} \frac{F(t) \cos \theta}{\rho U_m^2 LD} d\theta. \tag{2.9}$$

Experiments to determine values for these coefficients have been conducted in wave tanks, on prototype offshore structures and in U-tubes.

A dimensional analysis of the problem reveals two important nondimensional numbers, the Reynolds number, Re, and the Keulegan-Carpenter number, Kc,

$$Re = U_m D/\nu \qquad Kc = U_m T/D = 2\pi a/D. \tag{2.10}$$

Here ν is the kinematic viscosity and a is the amplitude of fluid oscillation. The physical significance of Kc is that it gives a measure of the amplitude of fluid oscillation relative to the cylinder diameter. If Kc is very small, say $Kc < 2$, then

the flow does not separate from the cylinder. For $Kc > 2$ separation occurs with a greater number of vortices shed per half cycle for larger values of Kc.

Sarpkaya [5, 6, 7, 8] has established the most comprehensive set of data for forces on fixed cylinders using a U-tube. Instead of plotting the force coefficients against Re and Kc as might be expected, the frequency parameter $\beta = Re/Kc = D^2/\nu T$ is used. The drag and inertia coefficients are then presented as a function of Kc with β as a parameter. Note that β is constant for a set of experiments conducted in a U-tube with a given diameter cylinder and frequency of oscillation. Large values of β indicate that the shed vortices will not dissipate significantly before encountering the cylinder in the next half cycle.

It should be pointed out that C_m and C_d are actually varying throughout the cycle, and from cycle to cycle, due to vortex shedding and that the published values of C_m and C_d are the averages over many cycles. Application of the values of C_m and C_d from U-tube laboratory tests to offshore designs requires that allowances be made for the greater Reynolds number, marine growth causing larger diameters and roughnesses, complex flow conditions, etc. A survey of recommended values of C_m and C_d for design purposes are given by Sarpkaya and Isaacson [4] and Wilson [16].

2.2.2 Transverse Forces on Fixed Cylinders

Sarpkaya [5] also reported the lift forces measured on fixed cylinders in oscillatory flow by defining an rms value of lift coefficient as

$$(C_L)_{rms} = \frac{(\text{measured transverse force})_{rms}}{0.5\rho U_m{}^2 DL}.$$ (2.11)

Alternatively a maximum lift coefficient can be defined based on the maximum force. All the information regarding the amplitude and frequency is contained in these coefficients, whereas for the inline coefficients, it is assumed that C_d and C_m are constant.

Bearman et al. [17] proposed a model for the lift force on a cylinder in oscillatory flow based on a quasi-steady application of the Strouhal relationship. Starting with

the sinusoidal model for transverse forcing in a steady flow given by Equation 2.3, they proposed that the lift force in oscillatory flow be defined in terms of the instantaneous velocity, U, as

$$F_L(t) = \frac{1}{2}\rho U^2 DC_L \cos\phi. \tag{2.12}$$

Note that $U(t) = U_m \sin 2\pi t/T$. Here ϕ is the phase of the transverse force, and its rate of change with respect to time is the vortex shedding frequency

$$\frac{d\phi}{dt} = 2\pi f_v. \tag{2.13}$$

Since the vortex shedding frequency is determined by Equation 2.1, $f_v = S|U|/D$ and is a function of time. The absolute value of U is used to avoid a negative frequency. The phase of the transverse force may then be written as

$$\phi = \int_0^t 2\pi f_v dt + \psi, \tag{2.14}$$

where f_v is the vortex shedding frequency at that instant and ψ is a constant phase angle. The lift force may then be written as

$$F_L(t) = \frac{1}{2}\rho U^2 DC_L \cos\left(\int_0^t \frac{2\pi |U| S dt}{D} + \psi\right). \tag{2.15}$$

Evaluation of the integral for the first half cycle yields

$$\phi = KcS[1 - \cos(2\pi t/T)] + \psi. \tag{2.16}$$

Thus the lift force becomes

$$F_L(t) = \frac{1}{2}\rho U_m{}^2 DC_L \sin^2(2\pi t/T)\cos[KcS(1 - \cos(2\pi t/T)) + \psi]. \tag{2.17}$$

It can be shown that the same equations apply for the next half cycle.

The transverse force is dominated by vortex shedding, and a number of different methods have been suggested for modelling it. Since some transverse forcing models are proposed in the context of studies of transverse response, other models of transverse forcing are presented later in the section on transverse response.

2.2.3 Transverse and Inline Forces Due to Vortices

Maull and Milliner [10] conducted a study of sinusoidal flow past a circular cylinder, focusing on the relationship between the inline and transverse forces on a fixed cylinder and how they are affected by the production and movement of vortices. The main difference in their approach ′ this problem is that the emphasis of the analysis is on a "discrete vortex" method which attributes forces to vortex motion and inertial forces, rather than on the Morison equation. The inline force is given by

$$F = \sum \Gamma \frac{d}{dt}(\rho y) + 2\rho \frac{\pi D^2}{4} \frac{dU}{dt}, \qquad (2.18)$$

where Γ is the circulation about a vortex in the flow field, y is the vertical distance between the vortex and its image in the cylinder, and the summation is over all vortices in the flow field. The '2' in the second term is the potential flow value for C_m. The equation for the lift force is based solely on vortex action, and is

$$F_L = \sum \Gamma \frac{d}{dt}(\rho x), \qquad (2.19)$$

where x is the horizontal distance between the vortex and its image. Maull and Milliner state that this pair of equations "has the advantage that the forces can be explained in terms of the strength and motion of the vortices, and further that the lift and drag forces may be correlated since they are produced by the same mechanism."

In tests conducted in a U-tube, they measured the inline and transverse forces on a fixed cylinder as a function of time over 200 cycles. An average cycle was then determined for each set of operating conditions. Examples of inline versus transverse force adapted from those presented by Maull and Milliner [10] are shown in Figure 2.1. Here the lift force coefficient C_L is plotted against an inline force coefficient C_Γ which does not include the effect of the inertia force. Therefore these plots only consider the forces due to the development and movement of vortices. The shapes of these plots were qualitatively explained by Maull and Milliner using equations for the lift and drag caused by the motion of point vortices past a cylinder in potential flow. The important difference between the two plots in Figure 2.1 is that in (a),
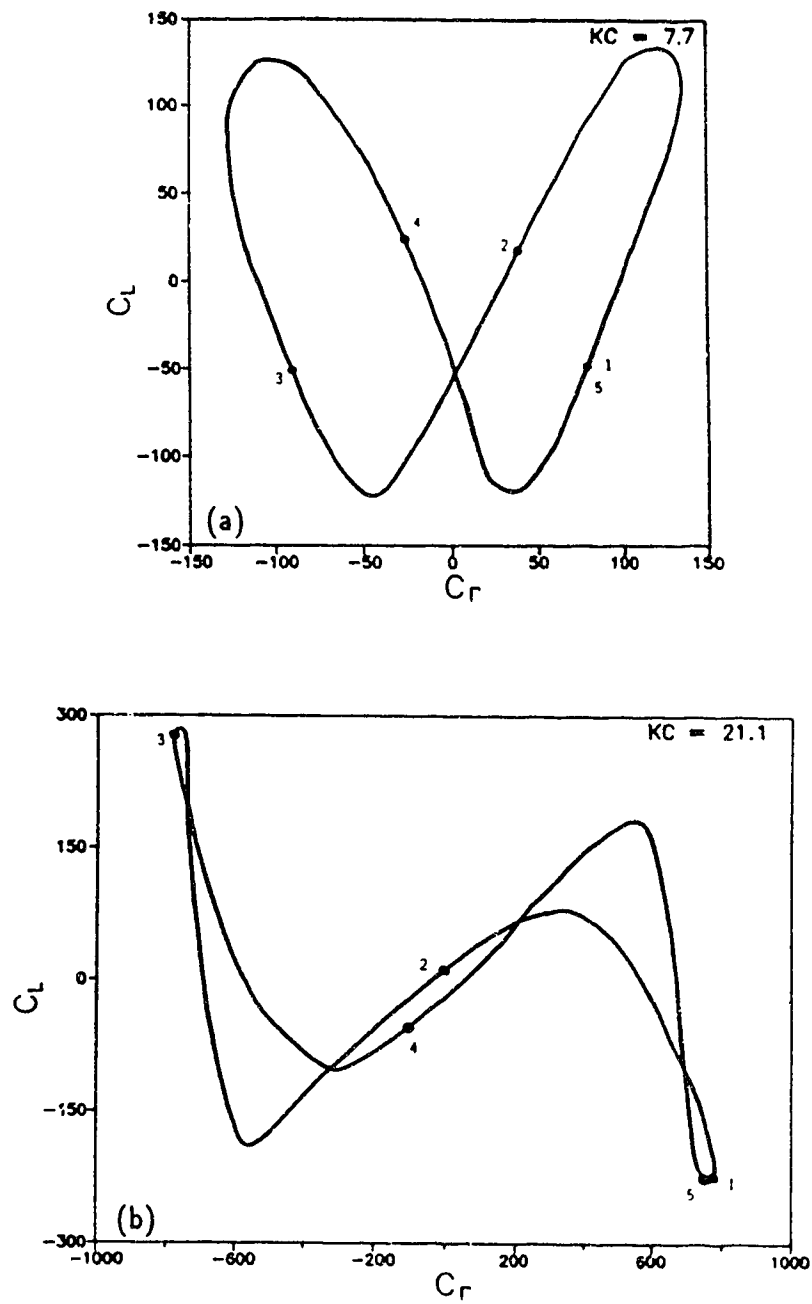
Figure 2.1 Force variations over a typical cycle, adapted from Maull and Milliner [10].

for which $Kc = 7.7$, there are two individual vortices produced in each half cycle, but in (b), for which $Kc = 21.1$, there are three. Thus in each cycle of fluid motion the transverse force varies at twice the fluid frequency in Figure 2.1(a) and at three times the fluid frequency in Figure 2.1(b). The numbers in Figure 2.1 indicate the position of the cylinder corresponding to quarter cycle increments of the motion of the fluid, starting at maximum fluid velocity from left to right.

C.H.K. Williamson [18] studied the development and motion of vortices caused by a circular cylinder oscillated in still water. Using flow visualization in a frame fixed with respect to the undisturbed fluid, he identified several repeatable patterns of vortex shedding for particular amplitudes of motion. He found that "the process of pairing of vortices from the previous half cycle with those in a present half cycle is fundamental to all the patterns." These paired vortices convect away from the cylinder in a direction that is dependent on the flow conditions. The first regime of flow occurs in the range $0 < Kc < 7$, for which symmetric pairs of small attached vortices split up upon flow reversal and pair with the new small vortices formed in the next half cycle. Pairs of vortices move away from the cylinder roughly perpendicular to the flow direction. For $Kc > 4$, the strength of the vortices becomes unequal and a lift force is produced. In the range of $7 < Kc < 15$, one large vortex is shed per cycle, producing pairs of vortices convecting away from the cylinder. At the upper end of this regime, the vortices are convected at about 45 degrees from the direction of the flow.

C.H.K. Williamson and Roshko [19] conducted a similar study of the vortex motion in the wake of a cylinder moving through the otherwise still water. The main difference here was that the cylinder was forced to oscillate transversely at a frequency higher than in the inline oscillatory motion. A number of different regimes of flow depending on the amplitude of inline motion and the relative frequency of the transverse motion were reported. The regimes of vortex motion are characterized by a wake of pairs or single vortices, or a combination of both.

2.3 Response of Cylinders to Oscillatory Flow

C.H.K. Williamson [20] studied the inline response of a cylinder to oscillatory flow, and compared the experimental results with those obtained by integrating an equation of motion in which the inline force was given by the relative velocity formulation of the Morison equation. The experiments were conducted in the vertical arm of a U-tube, with a cylinder mounted on a supporting structure that was free to respond inline with the flow. In the experiments, the Keulegan-Carpenter number ranged from 0 to 35, while the ratio of the natural frequency of the cylinder in water (f_n) to the frequency of fluid oscillations (f_w) was fixed at $f_n/f_w = 1.15$, with $\beta = 730$.

The relative velocity formulation generally was found to give good predictions of the response and phase angle between cylinder and water motion. To select coefficients for the numerical solution, the amplitude of water motion was used to select initial values for C_m and C_d. The amplitude of relative motion between the fluid and the cylinder from the solution was then used to select new values of C_m and C_d and the equation was solved again. This iterative process was repeated to converge on final values for C_m and C_d. The iteratively determined coefficients were close to the coefficients computed from experimental measurements. In most cases the iteratively determined coefficients were close to those initially chosen based on the amplitude of water motion alone. However, predictions of iteratively determined C_d and C_m differ from the initial values near the resonance region for which f_n/f_w is slightly less than 1.

Sarpkaya and Rajabi [21] conducted a study of the response of a cylinder in a U-tube that was free to move in the transverse direction but was fixed inline, in contrast to the above experiment in which the cylinder was fixed in the transverse direction but able to respond inline. They report that the frequency ratio f_v/f_n remains constant and nearly equal to unity only at "perfect" lock-in, which occurs at

a reduced velocity $U_r = 5.4$ and that the relative amplitude of oscillation at perfect lock-in for both smooth and rough cylinders is a unique function of the response parameter $R_p = m\zeta/(\rho L D^2 C_{Lmax}{}^0)$, where $C_{Lmax}{}^0$ is the maximum value of lift coefficient for the same cylinder fixed in the same flow, m is the mass of the body, and ζ is the structural damping. They also state that for inline oscillations $C_{Lmax}{}^0$ should be replaced by the normalized amplitude of the fluctuating component of the inline force. The most striking aspect of this work is the very clear relationship between the relative amplitude, y/D, and the response parameter, R_p, for perfect lock-in. A very important point made is that unlike the case of steady flow, where the relative amplitude of oscillation can be plotted as a function of $M\zeta/(\rho L D^2)$, it is necessary to include "the dynamics of the same flow past the same body when the latter is held stationary" [21]. This was achieved by including $C_{Lmax}{}^0$ in the response parameter.

McConnell and Park [12] studied the fluid lift forces and transverse cylinder responses due to an oscillating flow by harmonically driving a circular cylinder back and forth in still water. The cylinder was mounted vertically from an above water structure that was rigid in the inline direction and could be fixed or free to respond in the transverse direction. They propose that the lift force be modelled using the instantaneous fluid velocity so that

$$F_L(t) = \frac{1}{2}\rho U^2 D L C_L \sin 2\pi f_v t. \tag{2.20}$$

The results presented are principally the plots from spectral analysis of the force and response signals. These plots are used to show that the model for the lift force they propose, which uses the square of the instantaneous velocity, is more accurate than the more traditional method of using the square of the maximum velocity. They show that their model leads to

$$F_L(t) = \frac{1}{2}\rho U_m{}^2 D L C_L g(t) \tag{2.21}$$

where

$$g(t) = \sin^2 2\pi f_d t \sin 2\pi f_v t. \tag{2.22}$$

By letting $f_v/f_d = n$, where f_d is the cylinder driving frequency, the time varying portion of the lift force becomes

$$g(t) = \frac{1}{2}\sin 2\pi n f_d t - \frac{1}{4}\sin 2\pi(n+2)f_d t - \frac{1}{4}\sin 2\pi(n-2)f_d t. \tag{2.23}$$

From this the frequency components of the fluid lift force are expected to occur at f_v, $f_v - 2f_d$, and $f_v + 2f_d$. The latter two are referred to as side-band frequencies.

Their results show that the model is quite accurate in terms of frequency content. An additional result presented is the identification of three regimes of response. First, $U_r < 4.4$ to 5.3 corresponds to response near the upper side-band frequency, while 4.4 to $5.3 < U_r < 6.6$ to 7.2 corresponds to response close to the natural frequency, and $U_r > 6.6$ to 7.2 corresponds to response near the lower side-band frequency.

McConnell and Park, in a second paper [13], extended the same type of study to a larger range of Kc, showing that the Strouhal number $S = f_v D/U_m$, defined here for oscillatory flow using U_m, remains in the range of 0.15 to 0.20 except for a few cases dominated by lock-in, for both fixed and transversely free cylinders. They report also that for $Kc < 75$ an integer ratio of f_v/f_d was always found, when f_v is assumed to correspond to the largest frequency component of the force signal. For larger Kc, fractional ratios appeared. This phenomenon was attributed to the fact that for smaller Kc, the vortices have little time to decay or drift out of place, and therefore remain in a "position to interact with the cylinder when it returns to that location". This leads to a stronger and more consistent vortex shedding pattern.

Analysis of the transverse response showed that the cylinder response frequency occurs at the natural frequency, except in locked-in regions, where the response frequency changes to keep f_c/f_d an integer value. Lock-in was less evident for $Kc > 60$. The response amplitudes for the tests were generally quite small, with $y_{rms}/D < 0.40$. The maximum transverse response at a given Kc occurred at lock-in for cases in which f_n/f_d was an integer.

Finally, McConnell and Park [13] showed that their measured lift force coefficients for the transversely free cylinders, defined as $C_L = 2F_L/\rho U_m{}^2 DL$, were considerably larger than those measured by Sarpkaya [5] on fixed cylinders, however Sarpkaya's results seemed to form a lower bound on the magnitude of C_L. Their data came close to this lower bound for cases that gave low amplitude response, thus approximating Sarpkaya's fixed cylinder data as would be expected.

Bearman and Hall [22] investigated the transverse response of a cylinder in a U-tube. A vertical test cylinder was mounted in a carriage in an air filled compartment above the working section of the U-tube. The frequency parameter for these tests was $\beta = 478$, the ratio of the density of the cylinder to that of the fluid was $\rho_c/\rho = 3.28$, and the damping ratio in air was 0.08.

To aid in the analysis of the data, they propose to model the lift force using Equation 2.17. A spectral analysis of this lift force model "gives power at multiples of flow oscillation frequency and the distribution of odd and even multiples depends on the signs of consecutive half cycles" [22]. As Kc increases, the multiple for maximum power also increases. To support the model they show plots of dimensionless transverse amplitude, y/D, against Kc for given frequency ratios. Spectral analyses of conditions corresponding to two adjacent peaks in this plot show that for one peak the odd multiples of the flow frequency stand out, but for the other peak, the even multiples of the flow frequency stand out.

They conclude that transverse response depends on Kc and f_n/f_w with maximum transverse response occurring at integer frequency ratios, that the model they propose can predict frequency and amplitude modulation and maximum responses at integer frequency ratios, and that maximum response amplitudes appear to be equal to about one cylinder diameter.

Sumer and Fredsøe [23] studied the transverse vibrations of an elastically mounted cylinder to oscillatory flow for Kc between 5 and 100, and $U_r < 16$. The experimental

set-up consisted of a carriage that could be moved above a test tank, with an elastically mounted horizontal cylinder, neutrally buoyant in most cases, suspended in the water. The cylinder was free to respond in the transverse direction only. The cylinder supports protruded through a horizontal submerged plate that was designed to reduce free surface effects. The tests were conducted by setting an amplitude of oscillation, and then varying the frequency of oscillation to change the reduced velocity.

The response frequency of the cylinder, f_c, was defined as the frequency at which the highest peak occurs in a spectral analysis of the response, and it displayed a strong tendency to assume an integer multiple of the flow frequency. As the reduced velocity was increased, the ratio f_c/f_w decreased. The plots of the response amplitude (maximum and rms) against reduced velocity revealed that the response was quite large near the middle of a range in which f_c/f_w had a particular integer value, however the response dropped considerably where the jump was made to a new value of f_c/f_w. The largest maximum response tended to occur for lower reduced velocity in most cases, with the amplitude never exceeding 0.8 diameters.

Sumer and Fredsøe [23] demonstrated that the results of McConnell and Park [12], if plotted in the same fashion as their own, yield very similar trends, including the jumps to a new integer ratio of f_c/f_w. The other comparison they made was with Sarpkaya's [5] result of the number of vortices shed per cycle. Despite the fact that their cylinder could respond in the transverse direction, and Sarpkaya's results were for a fixed cylinder, the agreement between the two studies is quite good.

With stiffer springs the amplitudes of response were generally larger than for the softer springs, but displayed the same dependence on U_r. The lower response was attributed to the fact that in the stiff spring cases the cylinder is more lightly damped. When a cylinder with a specific gravity of 1.8 rather than neutrally buoyant was used, the dependence of response on U_r was virtually identical to the neutrally buoyant case, however the amplitudes of response were noticeably smaller.

Sumer et al. [24] studied the two-dimensional response of a cylinder above a scour trench on the bottom of a wave flume. The cylinder was mounted horizontally on a carriage that was oscillated in still water to create the wave action. In the tests U_r was varied between 3 and 8 for $Kc = 10$ and 40. The cylinder was positioned at different heights above the scour trench. The resulting trajectories of the cylinder showed that when the cylinder was very close to the trench, or partly in it, the responses were not vary large. In contrast, when the cylinder was positioned farther above the trench, trajectories often showed large inline and transverse responses. At $Kc = 10$, the trajectories were mainly of an "infinity" shape, while for $Kc = 40$ the trajectory was less well defined and included more transverse cycles of motion.

2.4 Response of Cylinders to Wavy Flow

Zedan et al. [25] conducted an investigation of cantilever pile dynamics in response to waves produced in a wave tank. Two series of tests were performed, one at $kd = 1.63$ and one at $kd = 2.6$, where k is the wave number and d is the water depth. For each case the natural frequency of the pile was varied by changing weights on top of the pile. The Reynolds number in all tests was between 4.0×10^4 and 7.0×10^4, while Kc remained between 10 and 15. These values were taken at the mean water level. The inline and transverse responses were measured for each test.

The results of these tests indicated that maximum transverse response was obtained for $f_n = 2f_w$. Spectral analysis indicated that most of the energy was concentrated at a frequency equal to the vortex shedding frequency and the structure's natural frequency. The vortex shedding frequency was visually determined to be twice the wave frequency. The tests reported did not extend to higher Kc, where one would expect more vortices to be shed per cycle and thus cause response at higher multiples of wave frequency. Plots of transverse deflection of the top of the pile against reduced velocity revealed a maximum near $U_r = 5.5$ with a smaller peak at $U_r = 6.2$ or 7.3, depending on the depth parameter kd.

Spectral analysis of the the inline response showed that most of the energy was concentrated near the wave frequency and near the vortex shedding frequency for tests not close to the lock-in range. Under lock-in the inline response was found to be sinusoidal at the vortex shedding frequency, and was amplified "substantially". Of particular interest is the result that under lock-in conditions, the inline response occurs at the vortex shedding frequency, rather that twice f_v. In steady flow the inline force has been observed to vary at twice the vortex shedding frequency. If the Morison equation is applicable, then the dominant frequency should be the wave frequency. The authors note that "one may speculate that transfer of energy or interaction between inline and transverse oscillations is responsible for this behaviour". The other possibility they suggest is that this behaviour is due to substantially increased inline drag under lock-in conditions, as is observed in steady flow. No mention was made of symmetric vortex shedding being observed during the tests.

An extension of the above study was made by Zedan and Rajabi [26] using the same data as [25] in a comparison of the behaviour of a pile in waves to that of a cylinder free to respond in the transverse direction only in oscillatory flow. Plots of C_L against reduced velocity for the pile in waves show two peaks: one at $U_r = 5.5$, which agrees with the results of Sarpkaya and Rajabi [21] for transverse response in oscillatory flow. A second peak occurs in the plots at $U_r = 6.2$ and 7.3 for values of $kd = 1.63$ corresponding to intermediate water depth, and at $kd = 2.6$ corresponding to deeper water, respectively.

The lift coefficient for the pile under lock-in conditions was found to be 1.6 to 1.93 times the lift coefficient measured for a cylinder fixed in harmonic flow of the same Kc. This compares closely to the value of about two reported by Sarpkaya and Rajabi [21] for a transversely free cylinder in oscillatory flow.

The frequency of the transverse force caused by waves on the pile occurred predominantly at $f_n = 2f_w$ under lock-in conditions, however as the pile natural frequency and twice the wave frequency became separated, contributions to the force

at the frequencies f_n, f_w, and $3f_w$ became more important. When f was far enough from $2f_w$, the predominant lift frequency was f_w, followed by f_n and $2f_w$.

Sawaragi et al. [27] studied the response of a pile due to vortex shedding in waves using a pile in a wave tank. The water depth was 0.35 m for all tests and Kc_{rms} ranged from 1.5 to 18. Note that Kc_{rms} is defined by the authors as "the root mean square value of the Keulegan-Carpenter number at each vertical elevation of the structure". Tests were conducted on a single cylinder by varying f_n/f_w and Kc.

The results presented include the trajectory of the displacement of the top of the pile. Four regimes of response are identified from the trajectories. Examples are shown in Figure 2.2. The first regime is defined by $f_n/f_w < 1.1$ and is characterized by predominance of the inline force and a response that is almost a straight line in the inline direction, as shown in Figure 2.2(a). The locus is approximately an ∞ shape for $1.1 < f_n/f_w < 1.7$, and for $1.7 < f_n/f_w < 2.5$ the locus is characterized by a "double ellipse", as shown in Figures 2.2(b) and (c) respectively. In this latter frequency range the response is principally in the transverse direction because "the pile is resonated by the lift force, which has the frequency two times as large as the wave frequency". A similar explanation is provide for the range $2.5 < f_n/f_w < 3.3$ in which the loci show large transverse "triple ellipses" that are caused by resonance at $f_n = 3f_w$.
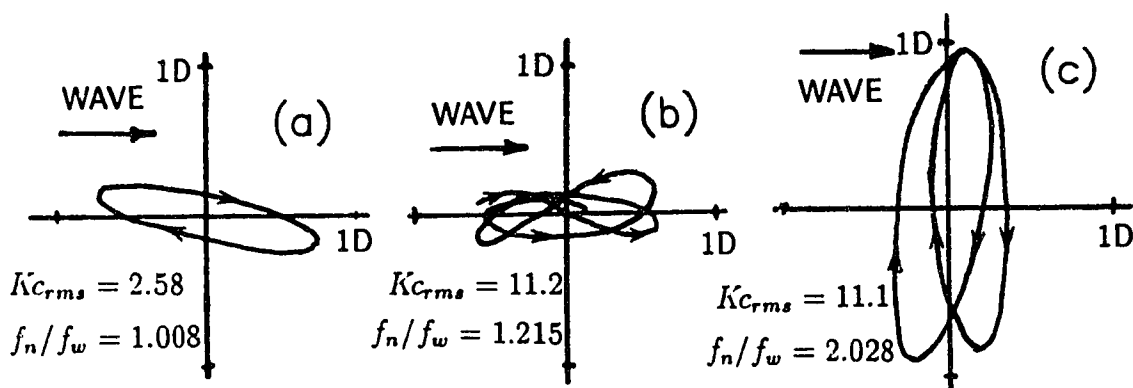

Figure 2.2 Typical responses of a pile to waves as reported by Sawaragi et al. [27]

The examples of the loci presented in [27] not only progress from $f_n/f_w = 1.1$ to 3.3 but also there is an increase in Kc_{rms} in the sequence. This is not surprising because in order to excite 2nd and 3rd multiples of the wave frequency more vortices must be shed per cycle, and as was shown by Sarpkaya [5], this is mainly a function of Kc, especially for low Reynolds numbers. Their results also show that inline response is predominant for $f_n/f_w < 1.4$, and transverse response is dominant for $f_n/f_w > 1.4$ especially when f_n/f_w is 2 and 3.

Sawaragi et al. [27] propose a formulation of the lift force that is the superposition of the first three multiples of the wave frequency. It is empirical in nature because it includes the measured spectral energy and phase angle of the lift force. However, this formulation may not be accurate for $Kc > 15$, because higher Kc would induce responses at higher multiples of the flow frequency, as found in other work.

Borthwick and Herbert [28] studied the trajectory of a rigid pile pinned at its base, held vertically with a spring mounted in the base to provide stiffness. The pile was placed in a wave tank and the response and forces were measured. Similar to the work in [27], trajectories of the displacement of the top of the pile were plotted and could be classified according to the frequency ratio f_n/f_w. When f_n/f_w approached an integer value the force and response amplitudes became large and repeatable. For $f_n/f_w = 2$ the trajectory was a horseshoe shape, while cases in which f_n/f_w was not an integer value, the trajectories were more complex, with multiple loops making up the trajectory. Higher values of f_n/f_w also tended to increase the complexity of the trajectories.

2.5 Concluding Remarks

From the papers that deal with the response of cylinders to oscillatory flow, a number of trends are evident. First, it appears that the most important parameters that govern the response are Kc and the frequency ratio f_n/f_w. Although Sarpkaya

and Rajabi [21] found that perfect lock-in occurred at a particular value of reduced velocity, this was not reported, or at least not emphasized, in other papers. The reason for this discrepancy may be that the lock-in found by Sarpkaya and Rajabi was focused strictly on cases for lock-in to the vortex shedding frequency, and that they did not encounter large responses at the other forcing frequencies suggested by McConnell and Park [12, 13] and by Bearman and Graham [9], whose work was conducted at lower values of Kc and f_n/f_w. Since Sarpkaya and Rajabi's value of f_n was about 9 times that of f_w, if McConnell and Park's suggestion that forcing occurs at f_v, $f_v + 2f_d$, and $f_v - 2f_d$ is applied, one can see that the three frequencies will be quite close. It may be that a "range of capture" phenomenon similar to the steady flow case may cause response to occur primarily at the vortex shedding frequency, and consequently excitation at the side-band frequencies would be dominated by a locking-in to the vortex shedding frequency.

McConnell and Park [12] suggested that the lift forces occur at the vortex shedding frequency and at two side-band frequencies. This does not necessarily contradict the work of Bearman et al. [17], who proposed that the lift force consists of multiples of the driving frequency with either even or odd multiples dominating depending on the flow, because McConnell and Park's model includes the three largest components of the model given by [17]. The essential difference between the two approaches is that McConnell and Park suggest that the vortex shedding frequency is constant and an integer multiple of the wave or driving frequency, while Bearman and Hall suggest that the vortex shedding frequency varies throughout the cycle. Note that as the number of vortices shed per cycle decreases, the significance of a varying frequency of vortex shedding diminishes. For simplicity in a model of the lift force, it is worth noting that Rajabi [29] found that the first three predominant harmonics of the lift force could be used to represent the lift force trace quite accurately, similar to the model proposed by McConnell and Park.

Sumer and Fredsøe [23] found that when the cylinder is free to respond in the transverse direction, the response tends to occur at a frequency that is an integer

multiple of the flow frequency and is closest to the natural frequency of the cylinder. The other frequency components are likely given by the formulation of Bearman and Hall. That is, all the other multiples of the flow frequency, with the two side-band frequencies presented by McConnell and Park as the two next strongest components of the even or odd multiples.

It seems that there is considerable consistency in the approaches to the frequency relationships, however an additional factor that must be considered is the magnitude of the response. At lock-in the maximum amplification of the transverse forces seems to be limited to about a factor of 2 while amplitudes of transverse response seem to be limited to less than one diameter. Maximum response also depends on the damping in the system—both fluid and structural damping.

The only known study of the two-dimensional response of a cylinder to oscillatory flow is that by Sumer et al. [24] in the context of pipeline vibrations in scour trenches. The study shows that there are definite patterns of response that depend on the flow conditions, and that these responses become larger as the distance from the scour trench increases.

There have been no studies known to this author of the two-dimensional response of a cylinder in oscillatory flow far removed from a solid boundary. The motion of cantilever piles in wavy flow studied by Zedan et al. [25] and Sawaragi et al. [27] and Borthwick and Herbert [28] are the close to this situation, however they measure the cumulative effects of wavy flow on a pile. In what follows an experiment to measure the two-dimensional motion of a flexibly supported rigid cylinder in oscillatory flow is discussed.

Chapter 3

Experimental Apparatus

In this chapter the experimental apparatus and instrumentation for the experimental portion of the study is described. Specifically, the U-tube, drive system, test cylinders, springs and video analysis are discussed.

3.1   The U-tube

For the experimental portion of the present study, a U-tube was chosen as the means of producing oscillatory flow. U-tubes have been used by a number of researchers for similar studies [2, 8, 10]. A schematic of the U-tube is shown in Figure 3.1. It has a cross section 0.6 m by 0.6 m and a natural frequency of oscillation of 0.31 Hz. The U-tube was made in five sections, all of which except the test section were made of 2.7 mm stainless steel, with reinforcing ribs a maximum of 0.3 m apart. The remaining section, the centre test section, was constructed from 4.8 mm (3/16 in) stainless steel sheet, with 40 mm ribs as reinforcement. The much stiffer working section proved necessary for maintaining clearances between the test cylinder and the walls of the U-tube. A removable hatch on the top of the working section provided access to the interior of the U-tube, while 10 mm thick float glass windows on both sides and in the hatch provided a view inside the tunnel. A light
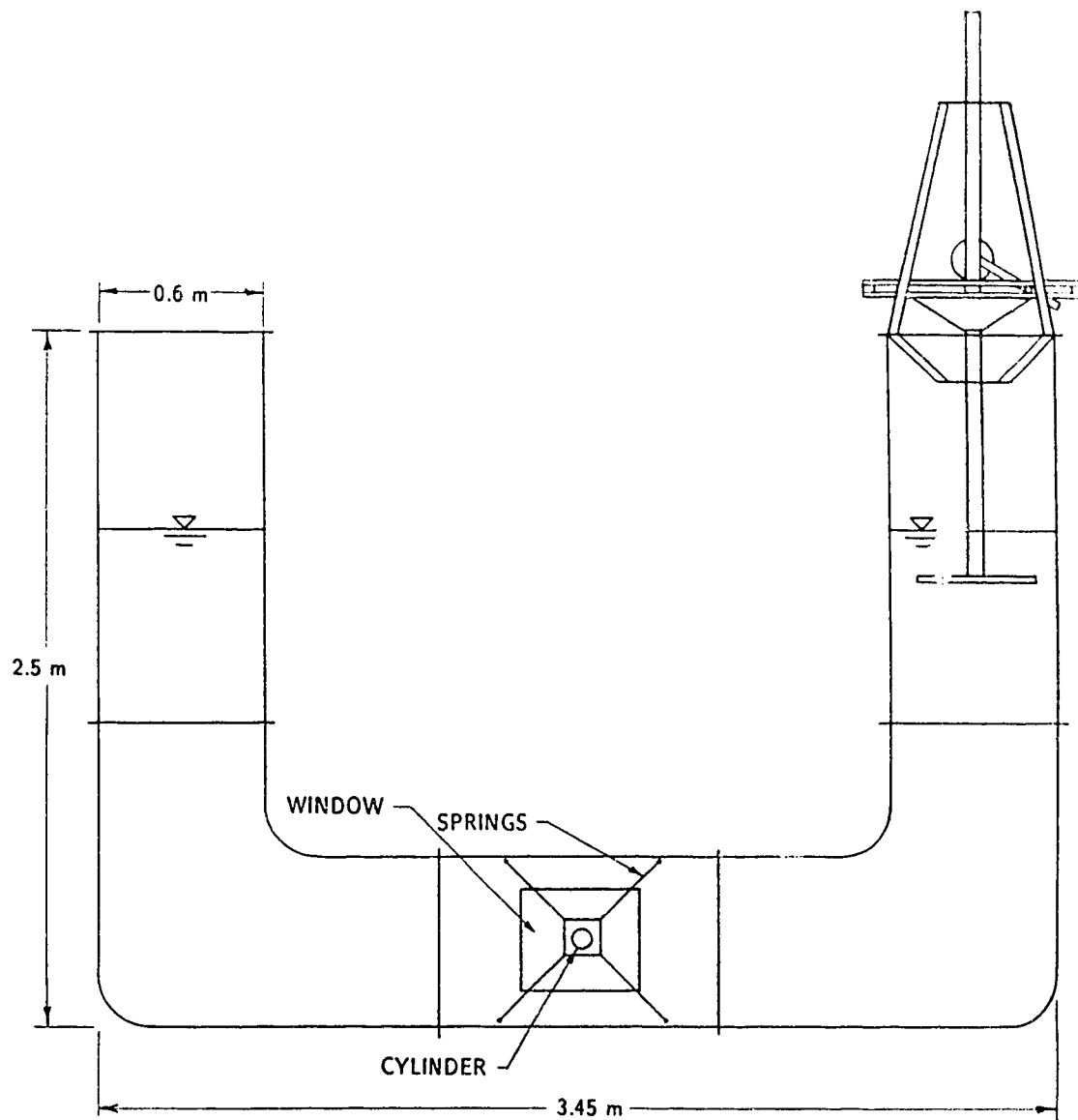
27

Figure 3.1 Schematic of U-tube.

under the centre of the working section illuminated the specimen through a window in the bottom of the section. The corners of the U-tube were streamlined to maintain harmonic flow throughout the U-tube.

Both ends were open to the atmosphere, with the drive system located in one end, and a variable capacitance depth transducer was located in the other. Pressure taps across the working section were installed to permit the measurement of the pressure gradient along the flow, which gives a measure of the acceleration of the fluid.

3.1.1 Drive system

A means of maintaining steady-state oscillations had to be devised. Initially, a large butterfly valve and air injection system were tested. The 0.4 m diameter butterfly valve was mounted on the top of one of the arms of the U-tube, and was pneumatically operated by computer. A compressed air line was also mounted on top of the same arm and controlled by computer. By closing the butterfly valve and injecting compressed air, the water could be displaced from equilibrium by the desired amount. By opening the butterfly valve, the water was set in free oscillation with a damping ratio of 0.3%.

The water level in one of the vertical arms was monitored using a variable capacitance water level transducer connected to a data acquisition system in an IBM PC compatible computer. It was intended that by controlling the opening and closing times of the air injection and butterfly valve, based on the instantaneous water level in one of the arms, the oscillations could be maintained indefinitely. The most serious problem with this method was that the natural frequency of the water oscillations was three times higher when the butterfly valve was closed than when it was open, due to the trapped volume of air at the top of one arm. The only way to avoid the higher frequency oscillations was to have the air supply inject air at exactly the right rate to match the water motion, however even with very carefully determined opening and closing times for the valve and air supply, satisfactory water

oscillations could not be attained. Although the water could be made to oscillate principally at the desired frequency, pressure differential measurements made along the test section of the U-tube showed that there was a very significant signal at the higher frequency of 1 Hz. Since fluid acceleration, which is caused by the pressure differential, causes inertia forces on a body in oscillatory flow, it became clear that an alternative method had to be developed to maintain the oscillations.

A much simpler drive system is to oscillate a small plate harmonically in one arm of the U-tube. The system shown in Figure 3.2 consisted of a 1/8 hp permanent magnet variable speed DC motor, with speed and torque control unit, driving a submerged plate via a "Scotch yoke" mechanism. The drive arm fixed to the motor output shaft had holes between 5 cm and 40 cm from the output shaft and provided a mount for a cam follower which could be bolted in one of the holes. The amplitude of
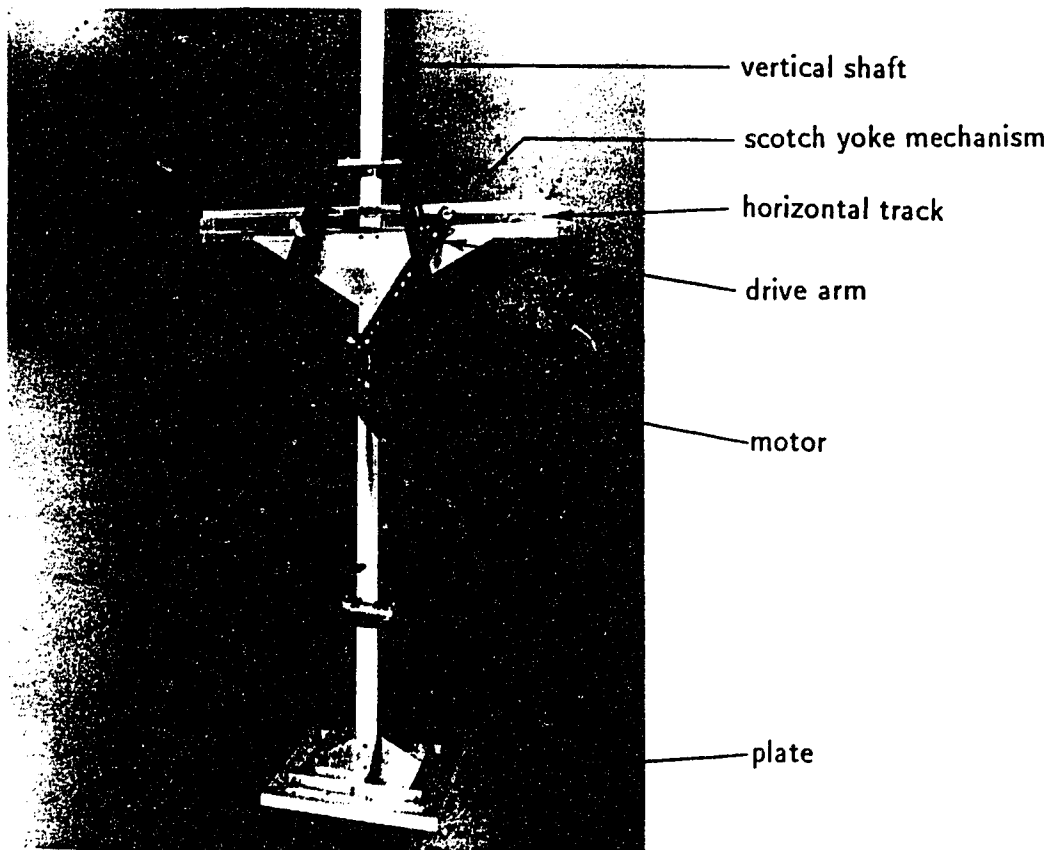
Figure 3.2 Drive system removed from the U-tube.

the plunger motion was selected by placing the cam follower the appropriate distance from the output shaft of the motor. The cam follower, when mounted in the drive arm, was also positioned in a horizontal track attached to a long vertical shaft. The vertical shaft was free to move along its length, constrained above and below by ball bearing guides. The rectangular cross section of the vertical shaft prevented it from rotating about its axis. At the bottom of the vertical shaft was a 0.4 m by 0.4 m plate that remained submerged during operation. When the motor was running, the vertical shaft and the attached plate would follow the vertical component of the position of the cam follower, thereby producing sinusoidal motion. To limit the loads placed on the motor, and to maintain constant motor speed, the plate was made of extruded polystyrene foam with a thickness such that the buoyancy of the foam just supported the weight of the vertical shaft and the attached horizontal cross track. A view of the drive system mounted in the U-tube is shown in the Figure 3.3.

The operation of the system for a particular test involved selecting the appropriate position for the cam follower, which fixed the flow amplitude, and ensuring that the motor speed was set to match the natural frequency of water oscillations. The motor was then turned on, and the speed fine tuned to match the water motion. If the motor was running too fast the plunger motion led the water motion, and vice versa.

3.2 The Test Cylinders

A system was required in which cylindrical specimens could be suspended to move freely in the inline and transverse directions, while restricting the motion to be essentially two-dimensional. The cylinders used in the test were smooth and made from thick-walled clear acrylic tubing. The 570 mm long cylinders were fitted with square, 100 mm × 100 mm × 2.5 mm, clear acrylic end plates which left approximately 12.5 mm clearance at each end between the end plate and the glass windows in the tunnel wall. The cylindrical specimens are shown in Figure 3.4 and the dimensions and masses of the cylinders are given in Table 3.1. Four teflon

Figure 3.3 The drive system mounted in the U-tube.

Table 3.1 Test Cylinders

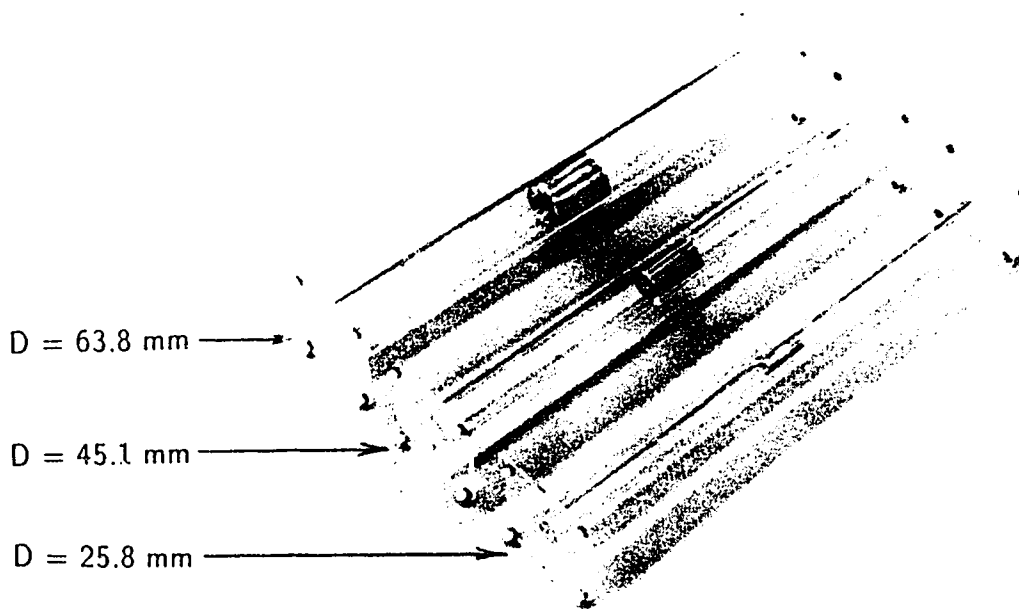| No.	Mass (g)	Diameter (mm)
1	357	25.8
2	985	45.1
3	1894	63.8

Figure 3.4 Cylinders used in the study.

"buttons" were attached to the corners of the end plates to act as spacers between the window and the end plates. Approximately 0.5–1 mm total clearance was left to permit the cylinder to move freely in the inline and transverse directions. The effect of the buttons was to suppress any motion other than the desired two-dimensional motion of the cylinder. That is, they prevent rotation about an axis perpendicular to that of the cylinder while having minimal effects due to friction when light sliding contact was made with the window.

In practice, it was found that certain flow conditions tended to produce repeatable two-dimensional motion in which the buttons did not significantly contact the window. Certain other conditions led to a very three-dimensional response with significant window to button contact. These conditions were taken as an indication of low correlation, as will be explained later.

The tendency for the cylinder to rotate about an axis perpendicular to its own was reduced by separating the rotational and translational natural frequencies as much as possible using a steel weight in the centre of the specimen to minimize the

moment of inertia. The weight was sized to make the specimen neutrally buoyant in water. Neutral buoyancy permitted the use of very soft springs to support the cylinder in its horizontal position, while maintaining its equilibrium position in the centre of the test section.

The cylinder was suspended in the test section with a set of eight matched springs. Figure 3.5 shows the cylinder at the equilibrium position in the U-tube, viewed through one of the side windows. The springs were attached at one end to the corners of the end plates on the cylinder and at the other end to small hooks on the inside of the U-tube wall. With the cylinder at rest, the springs had an orientation approximately 45 degrees to the horizontal, so that the stiffness in the inline and transverse directions were the same. The anchor points inside the U-tube for the springs were placed as far apart as possible to reduce nonlinear effects which occur for large displacements from the equilibrium position. Six sets of springs were used, and the resulting effective stiffness and frequency ratios in water are summarized in Table 3.2.
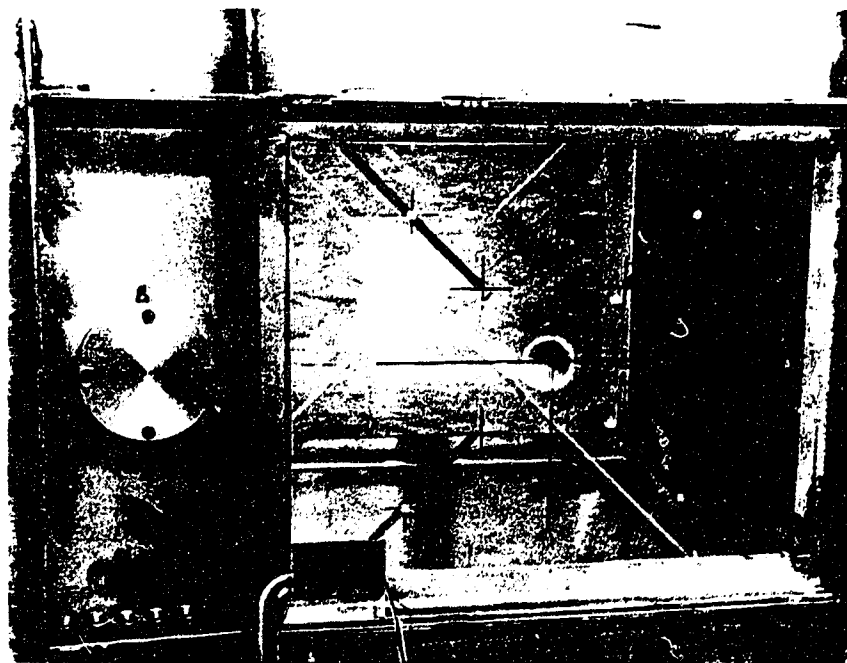

Figure 3.5 A cylinder suspended in the U-tube.

Table 3.2 Spring-Cylinder Combinations

Spring No.	Designation	k_{eff} (N/m)	f_n/f_w for Cylinder 1	f_n/f_w for Cylinder 2	f_n/f_w for Cylinder 3
1	4-15	14.2	2.49	1.42	1.07
2	4-17	24.2	3.04	1.81	1.29
3	3-16	40.8	3.81	2.29	1.68
4	2-13	56.0	4.49	2.71	1.97
5	2-15	113	6.43	3.91	2.87
6	4-26	199	8.62	5.14	3.81

The natural frequencies were calculated from slow motion play-back of video recordings of free vibration tests without the buttons on the end plates. Damping in the free vibration tests was found to be less than 5% and includes both fluid and structural damping. This value agrees well with the theoretical value for viscous unseparated flow. [1] The damping was more difficult to measure with the buttons in place because of the slight friction with the glass. This friction tended to be more significant for the small amplitude vibration tests, in which an effective ζ was measured to be as high as 20%. This should not be taken as indicative of the damping under test conditions. It is very difficult to specify a single value of ζ valid for the entire range of conditions, and would be misleading to do so. However, it is worth noting that any significant frictional forces tend to clearly disrupt the cylinder's response. Such cases are discussed in detail in Chapter 4.

Measuring the stiffness in-situ proved to be difficult because without submerging the cylinder in water, several of the springs were not able to support the weight of the cylinders. To solve this difficulty, the effective stiffnesses were measured in a frame with hooks in a layout identical to that of the hooks on the U-tube wall. A single end plate was suspended by four springs in the frame. The stiffness of this system

was assumed to be half of that of the cylinder in the U-tube, because the springs mounted in the frame reproduce the conditions at one end of the cylinder only. This assumption was tested in situ for the stiffest springs which were able to support the smallest cylinder very close to the centre position in the U-tube. The measured stiffness in this case was within 3% of the stiffness expected from measurements in the frame.

The stiffness was expected to vary somewhat with direction, however in the range of deflections encountered in the experiment, stiffnesses in either the inline or transverse direction were measured to be at most 5% less than the stiffness in the direction parallel to a spring. The stiffnesses in Table 3.2 are the means of the stiffness in the inline, transverse, and diagonal directions.

The springs had an unstretched length of about 170 mm and were made of stainless steel. The designation of the springs in Table 3.2 consist of the mean coil diameter in $1/16^{ths}$ of an inch followed by a dash and the wire diameter in $1/1000^{ths}$ of an inch.

3.3 Data Acquisition

A VHS format camera was used to record the cylinder motion while viewing it through the side window. A scale was drawn on the window with indelible ink, and a cross was placed on the end of the specimen end plate. In the field of view of the camera were a high contrast LCD digital voltmeter, and a high intensity LED. These two devices were controlled by a microcomputer which continually monitored the output of the variable capacitance depth gauge in one of the arms of the U-tube. Based on the water level with zero motion, the computer detected upward and downward zero-level crossings, and recorded maximum and minimum levels during a cycle. When an upward zero crossing was detected, the LED was switched on and the voltmeter was sent a signal that would cause the voltmeter to display the amplitude of the last cycle in tenths of a metre. When a downward zero-crossing was detected,

the LED was switched off. These two devices therefore recorded the amplitude and phase of the water motion on the videotape for later correlation with the cylinder motion. The clear end plates allowed the total cylinder behaviour, including any rotation, to be visible on the recording.

The depth gauge was calibrated by filling the U-tube past its normal operating level and monitoring the output of the capacitance gauge over the full range of water levels.

Once data for all the cases in Table 3.2 had been collected on videotape, digitizing sequences of frames was accomplished using a digital image processing board and associated software. A simple program permitted the use of a "mouse" to move a set of crosshairs on the video screen, and by "clicking" on the position of the cylinder, its coordinates could be written to a file. The scale on the window provided the necessary calibration measurements. Due to the large number of frames taken in the tests, only samples of cylinder motion were digitized for plotting. The video system recorded 30 frames per second, or about 97 frames per cycle of water motion. Typically two cycles for each spring-cylinder combination were digitized for each amplitude of water motion tested. Depending on the speed and complexity of the response, every 1st, 2nd, 3rd or 4th frame was digitized. Plots of one cycle were used in a compilation of the "overall picture", while individual plots of two or four cycles were used to examine specific cases of interest.

Chapter 4

Experimental Results and Analysis

For a large number of the tests conducted, the cylinder followed well defined trajectories. There was considerable variety in the shape and size of the trajectories, depending on the test conditions. In these tests the Keulegan-Carpenter number, Kc, ranged from about 2 to 60 and the frequency ratio, f_n/f_w, varied from about 1 to 8.5. The frequency parameter, β, is 205, 625, and 1250 for the cylinders of diameter 25.8 mm, 45.1 mm, and 63.8 mm respectively. Similarly, the maximum Reynolds numbers encountered in the tests were 13800, 29000, and 44100 for the three cylinders in order of increasing diameter. Over this diverse set of conditions the trajectories clearly were dependent on both Kc and f_n/f_w, and could not be characterized by reduced velocity alone. The response at lower frequency ratios consisted of generally more simple and repeatable trajectories, while for conditions of higher f_n/f_w, there tended to be more cycle to cycle variation of the trajectories. Consequently, these two types of responses will be considered separately in this chapter.

38

4.1 Response at Low Frequency Ratios

In general, vortex shedding from cylinders is a three-dimensional phenomenon in which vortices are shed at different times along the length of the cylinder. Therefore, a three-dimensional response would be expected from an elastically mounted rigid cylinder exposed to an oscillatory flow. However, when the conditions of vortex shedding are such that a synchronization exists between the cylinder motion and the shedding, the vortices tend to be shed simultaneously from the same side of the cylinder over a significant portion of the cylinder's length. A measure of whether the vortices are being shed simultaneously along the length of the cylinder is the "correlation length", or simply "correlation". When synchronization occurs, correlation increases, and the vortex shedding process becomes strongly two-dimensional. As a result, the response of the cylinder is also strongly two-dimensional. Conversely, when the correlation is low the response of the cylinder is three-dimensional. In what follows, a response or trajectory that is termed "strongly two-dimensional" is one that does not involve any noticeable effects of the buttons on the cylinder end plates rubbing on the glass and disrupting the cylinder motion.

Examples of strongly two-dimensional responses over two consecutive cycles are shown in Figure 4.1 for the combination of Kc and f_n/f_w identified in each figure. In all plots of trajectories given in this thesis, the dependence on time within one cycle is not shown. However, this information could be obtained from the data on videotape as further analysis might require. The trajectories themselves repeat for each cycle of water motion with very little deviation from cycle to cycle. To aid in explaining the cause of these shapes, two trajectories for a single cycle of water motion are presented in Figures 4.2(a) and (b). Figure 4.2(c) indicates the water motion as a function of time over one cycle, with five points in the cycle of water motion labelled 1 through 5. The corresponding positions of the cylinder at each of these points in time are indicated on the trajectories in Figure 4.2(a) and (b). The starting point in Figure 4.2(c), labelled "1", corresponds to maximum fluid velocity from left to right
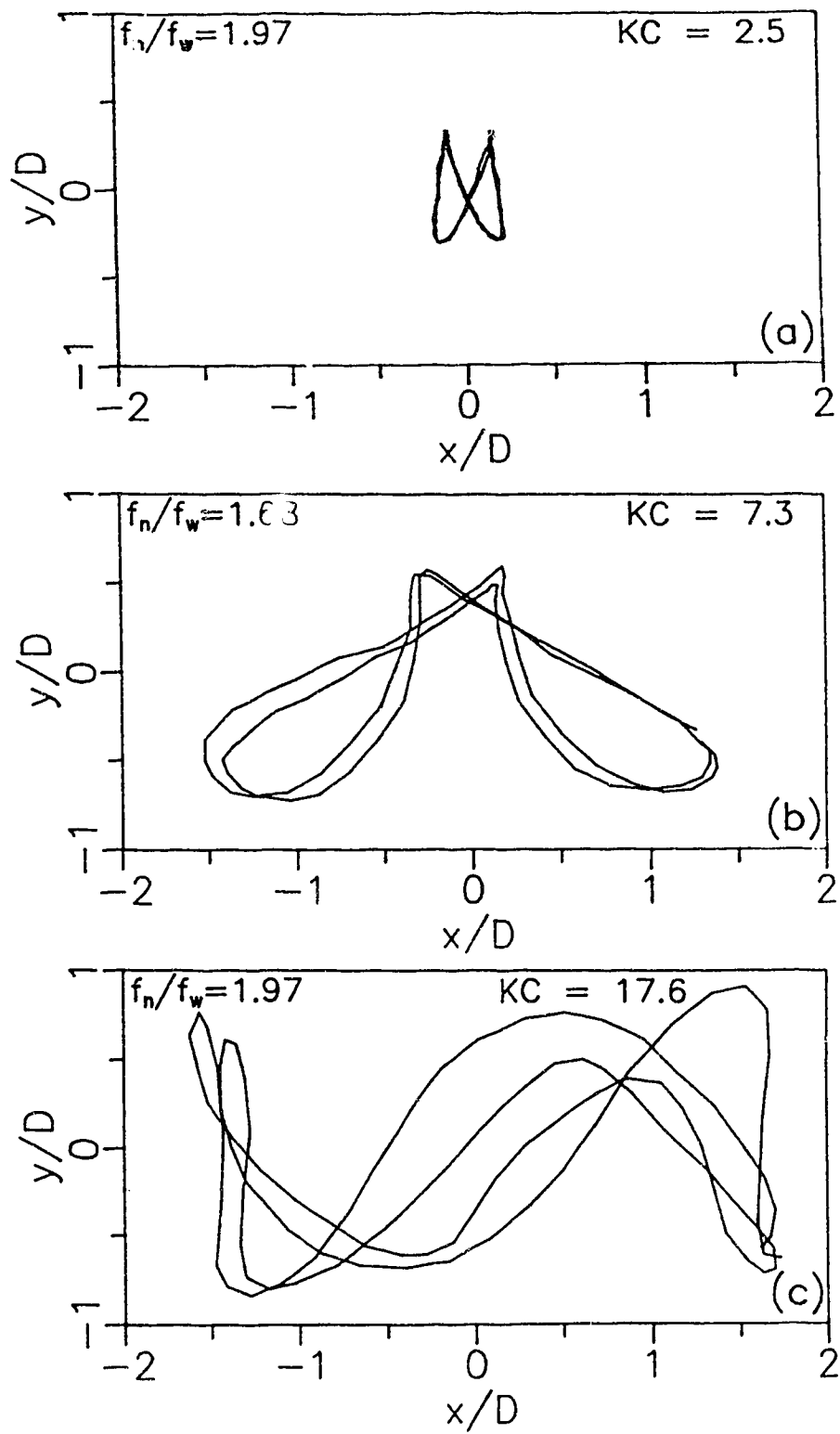
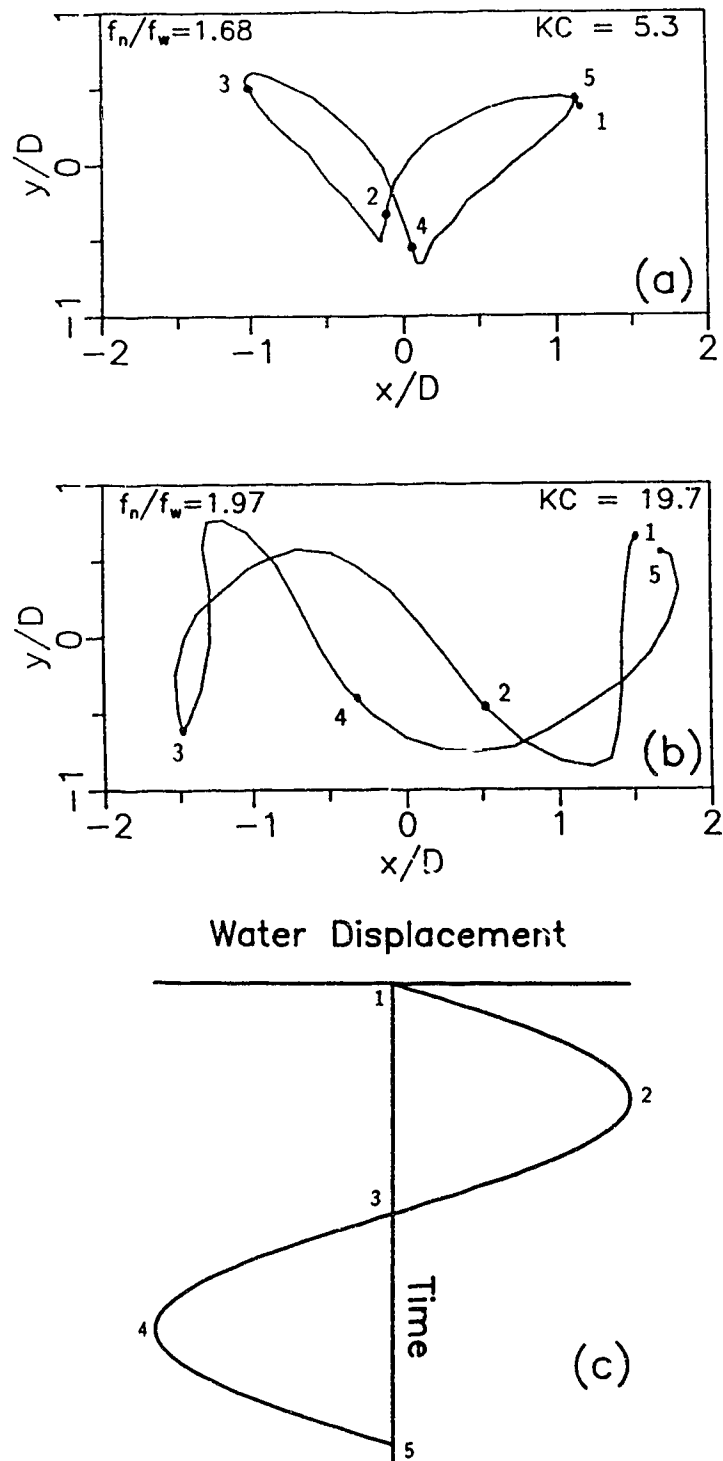Figure 4.1 Samples of strongly two-dimensional response.

Figure 4.2 Phase relationships between water motion and two typical trajectories.

and occurs when the fluid is passing its equilibrium position. At this moment the cylinder is at the point labelled "1" in Figure 4.2(a) which corresponds to maximum inline and transverse deflection to the right. The cylinder then proceeds from right to left to point 2 on the trajectory, while the fluid is moving in the opposite direction to reach its maximum displacement to the right at point 2 shown in Figure 4.2(c). The flow then reverses and both the cylinder and the fluid move from right to left until point 3 is reached, where the fluid is at its maximum velocity from right to left and the cylinder is near its largest deflection to the left and another peak in the transverse displacement. Motion of the cylinder through positions 4 and 5 completes the cycle. This analysis illustrates the phase relationship between the water motion and the response of the cylinder. A similar relationship is evident in Figure 4.2(b) for $Kc = 19.7$ and $f_n/f_w = 1.97$. It is interesting to note that the maximum displacement of the cylinder, both inline and transverse, occurs when the fluid velocity is very close to its maximum value.

The basic difference between the trajectories in Figure 4.2(a) and (b) is that for $Kc = 5.3$ there are two cycles of transverse motion for every cycle of water motion while for $Kc = 19.7$ there are three cycles of transverse motion for each water cycle. In both cases, the cylinder completes one cycle of inline motion for each cycle of fluid motion. Also, Figure 4.2(a) might be described as a distorted infinity shape while Figure 4.2(b) looks like the letter "N". The reason for these differences can be attributed to the number of vortices produced during each half cycle. In this regard the qualitative similarity of the trajectories of response in Figure 4.2 to the force plots from Maull and Milliner [10] in Figure 2.1 is very striking. Specifically, Figure 2.1(a) and Fig. 4.2(a) correspond to reasonably similar values of Kc and have a similar shape, while Figures 2.1(b) and 4.2(b) also are close in shape and correspond to Kc close to 20. Recall that in Figure 2.1(a), with $Kc = 7.7$, two vortices were produced in every half cycle while for Figure 2.1(b), with $Kc = 21.1$, three vortices were produced in each half cycle. To provide an indication of the phase of the force on the cylinder with respect to the fluid motion, the numbers 1 through

5 are also shown on Figure 2.1, indicating the water motion as given in Figure 4.2(c).

As stated earlier, strongly two-dimensional response trajectories were very repeatable, tracing out essentially the same shape each cycle. For example, Figure 4.3 shows the trajectory of the cylinder over four consecutive cycles of water motion for $Kc = 7.3$ and $f_n/f_w = 1.68$. This corresponds to a reduced velocity of 4.3. In this case the inline response amplitude is about 1.5 diameters, while the transverse response amplitude is about 0.7 diameters. As in Figure 4.2(a), there are two complete cycles of transverse motion for each cycle of water motion. One noticeable difference between Figure 4.2(a) and Figure 4.3 is that one has the opposite orientation to the other. The orientation of the trajectories depends on the initial conditions and the side of the cylinder that vortices first start. Strongly two-dimensional trajectories of the types shown in Figures 4.2(a), 4.2(b) and 4.3 do not change their orientation during the course of a test.

It may seem surprising that the strongly two-dimensional response shown in Figure 4.3 occurs for a frequency ratio of 1.68 and reduced velocity of 4.3, as these conditions do not correspond to an integer frequency ratio or a reduced velocity of 5.4 reported for transverse lock-in. McConnell and Park [12] explain that the lock-in condition is achieved for integer values of f_n/f_w because the vortices are then
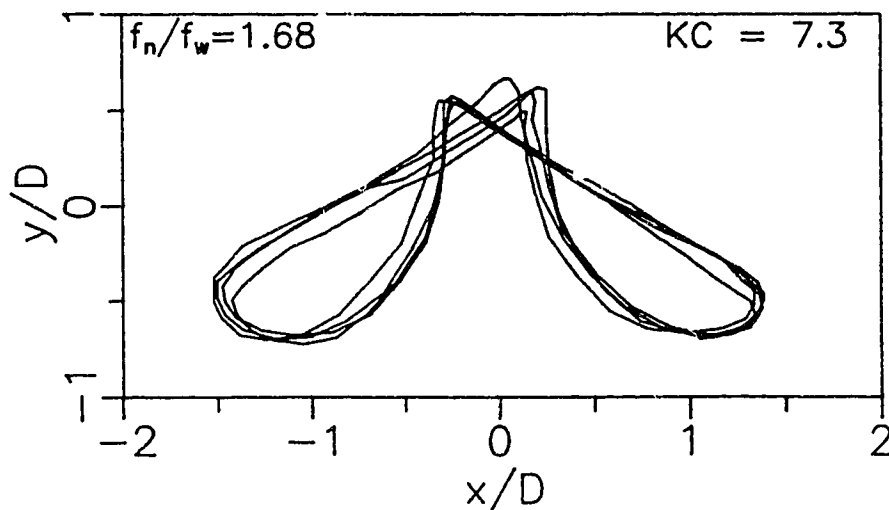

Figure 4.3 Trajectory for four consecutive cycles for $f_n/f_w = 1.68$ and $Kc = 7.3$.

able to remain in a "position to interact with the cylinder when it returns to that location". Apparently, the inline motion of the cylinder in the present study alters the conditions required for the incident flow, containing recently shed vortices, to reinforce the transver.: motion.

To obtain a more detailed picture of the response for a given set of springs, Figure 4.4 presents a sequence of trajectories for a frequency ratio of 1.97 and Kc increasing from 2.5 to 19.7. In each case two complete cycles are plotted, starting when the water in the U-tube passes its equilibrium position going from left to right. The first two cases, Figure 4.4(a) for $Kc = 2.5$ and Figure 4.4(b) for $Kc = 4.7$, show trajectories that can be described as "infinity" shapes similar to Figure 4.2(a). The first of these is very repeatable with a very small cycle to cycle variation. As Kc increases, to 7.7 in Figure 4.4(c) and then to 8.4 in Figure 4.4(d) the "infinity" shapes become distorted as shown. Although the shape has changed significantly, the cylinder still completes one inline cycle and two transverse cycles for one cycle of water motion. Note that the orientations of the trajectories in Figures 4.4(c) and (d) are different due to the different initial conditions for each test.

Figure 4.4(e) shows the trajectory for $Kc = 9.7$. In this case the correlation is low and the response is three-dimensional. No particular significance should be placed on this trajectory as it is not of the strongly two-dimensional type. The conditions for this case mark the transition between trajectories classified as having an "infinity" shape to those shaped like the letter "N". Another test was run with $Kc = 11.4$ which is not included in Figure 4.4 as its behaviour was not significantly different from that of Figure 4.4(e). For $f_n/f_w = 1.97$ with Kc between 9.7 and 11.4 the reduced velocities range between 4.9 and 5.8. It is interesting to note that in this range of reduced velocity with an integer frequency ratio, lock-in would be expected based on studies of transverse response in oscillatory flow [12]. Apparently the inline response affects the nature of the fluid-structure interaction to an extent that the results from transverse response studies are not directly applicable to the case when the cylinder responds in two dimensions.
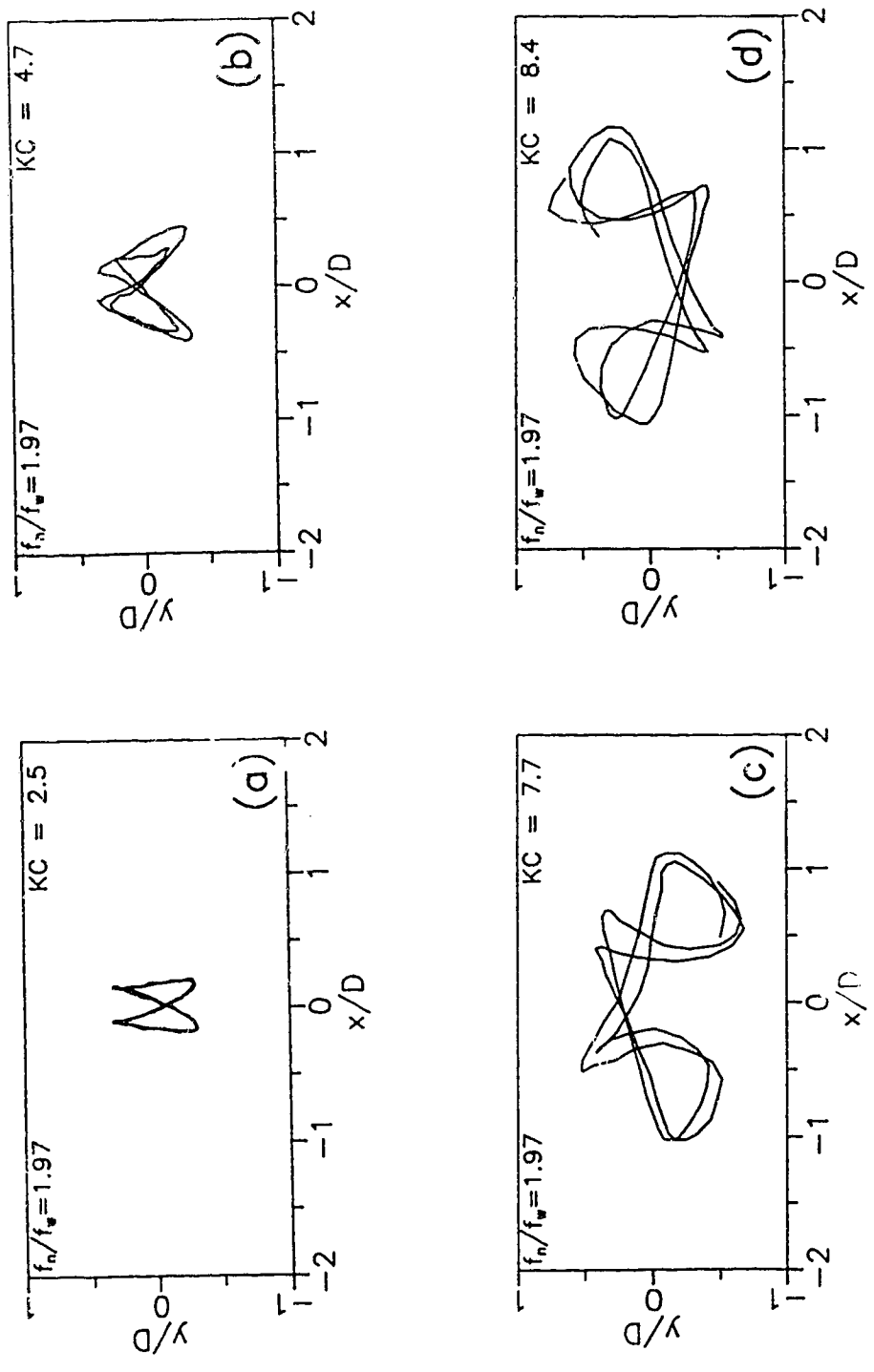
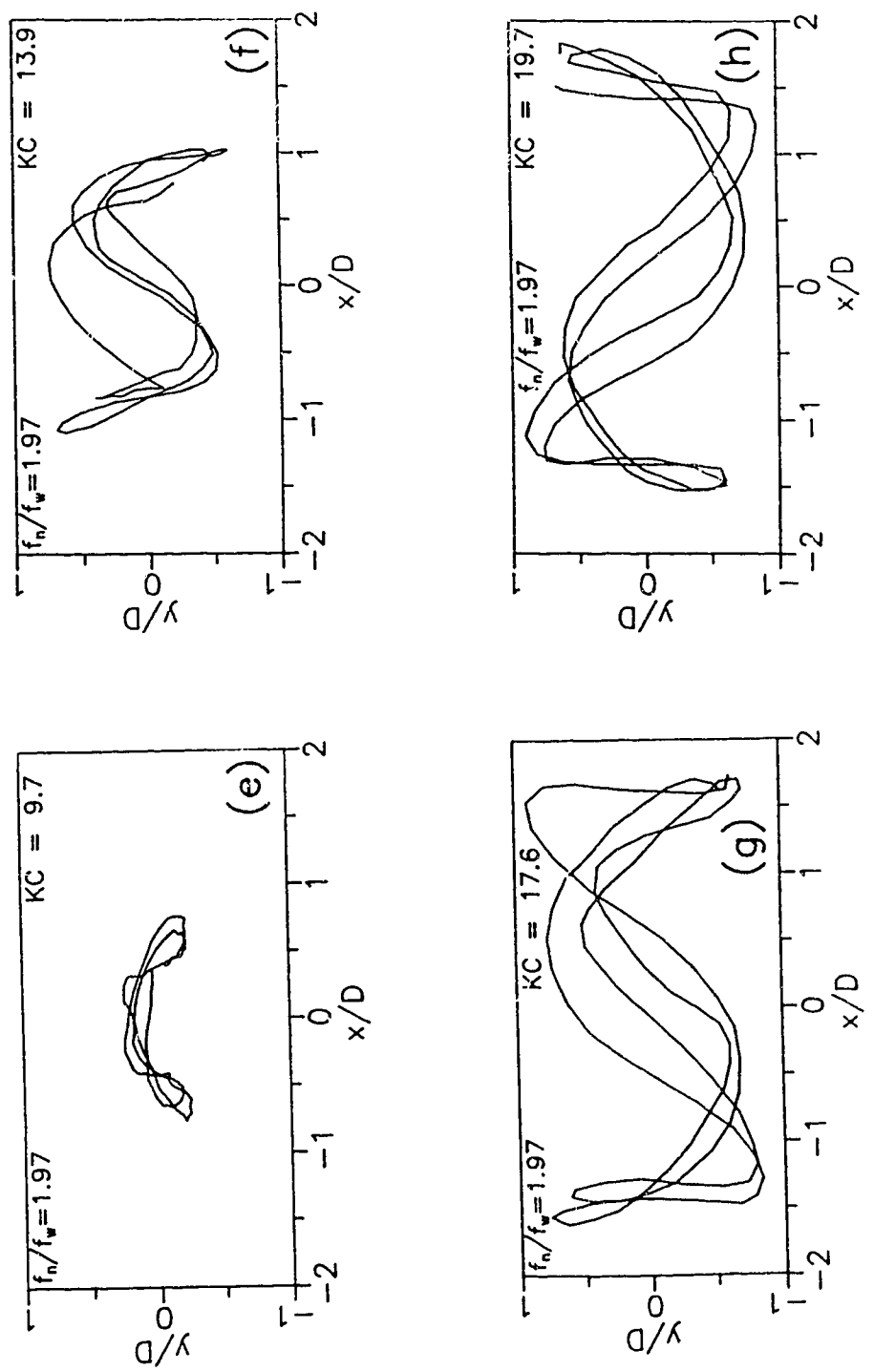Figure 4.4 Progression of trajectories for $f_n/f_w = 1.97$ and increasing Kc.

Figure 4.4 Progression of trajectories for $f_n/f_w = 1.97$ and increasing Kc (continued).

When $Kc = 13.9$ and $f_n/f_w = 1.97$, a two-dimensional trajectory occurs intermittently, and is shown in Figure 4.4(f). For a short period of time the cylinder responds in a two-dimensional fashion, but then the motion becomes three-dimensional and the buttons on the end plates contact the windows, significantly reducing the response. Subsequently a two-dimensional motion builds up again to that shown in Figure 4.4(f), with the process then repeating itself. Apparently the synchronization between the vortex shedding and the motion of the cylinder is not sufficient to maintain the two-dimensional trajectory in this case. Further increases in Kc result in a return to strongly two-dimensional and repeatable trajectories as shown in Figures 4.4(g) and (h) for $Kc = 17.6$ and 19.7 respectively. The trajectories for these two cases are now typical of those shaped like the letter "N". The different orientation in these last two figures is again due to different initial conditions. Note the amplitude of the response, both inline and transverse, has increased significantly over the responses for smaller Kc, even though the reduced velocity in this range is approximately 9.

Based on studies of transverse response alone, larger response might be expected at what McConnell and Park [12] call "side-band frequencies" which correspond to U_r slightly below 4.3 and slightly above 7.2, as discussed in Section 2.3. This transverse response would also be expected to occur at a frequency very close to the natural frequency of the structure, which for this case is 1.97 times the flow frequency. Figures 4.4(c) and (d) show a large amplitude transverse response at twice the flow frequency and a reduced velocity of about 4.0 to 4.3 as expected. However, it is not until $Kc = 18$ to 20, corresponding to $U_r = 10$, that large amplitude transverse response occurs. It occurs at 1.5 times the natural frequency of the cylinder rather than at the natural frequency, since three cycles of transverse motion are completed for each cycle of inline and water motion. A noteworthy result is that the transverse response here is larger than the response that occurs at the cylinder's natural frequency for $U_r = 4.0$ to 4.3. This phenomenon provides further evidence that the inline response alters the conditions for large amplitude transverse

res onse from those from studies of transverse response alone.

A summary of sample trajectories for f_n/f_w less than 4 is shown in Figure 4.5. The Keulegan-Carpenter number is plotted as the ordinate with the frequency ratio plotted as the abscissa. Stiffer springs correspond to increased natural frequency of the cylinder and hence increased frequency ratio. The frequency of the water motion is fixed by the natural frequency of the U-tube. All trajectories have been drawn to the same scale so the relative response amplitudes between the tests can easily be assessed. For reference purposes one cylinder diameter is shown in Figure 4.5 to provide a scale for the response amplitudes. The upper limit of Kc for each combination of cylinder and springs shown in Figure 4.5 was limited by either the response of the cylinder being too large to view it completely within the window or by the limitations of the driving mechanism. For reference purposes, lines corresponding to $U_r = 3$ to 10 are shown on Figure 4.5.

Examination of Figure 4.5 reveals that the trajectories in certain regions of the graph fall into distinct groups based on their overall appearance. The two types of trajectories that have been discussed so far are those with a basic "infinity" shape and those shaped like the letter "N". These are labelled "Group 2" and "Group 3" in Figure 4.5 in reference to the number of transverse cycles completed for each cycle of inline motion. It is believed that the numbers also correspond to the production or shedding of two and three vortices every half cycle, by comparison to the work of Maull and Milliner [10] as discussed earlier. At higher Kc and f_n/f_w, trajectories with 4 cycles of transverse motion for each one inline are evident. These trajectories fall into the region labelled "Group 4".

On Figure 4.5 those trajectories judged to involve significant contact with the glass as a result of three-dimensional response are marked with the symbol ‡ and those cases which exhibited intermittent two-dimensional trajectories, or non-repeatable trajectories are marked with the symbol *. Clearly, the three-dimensional trajectories which necessarily involved significant contact with the window cannot be considered repeatable either. Trajectories which changed orientation during steady
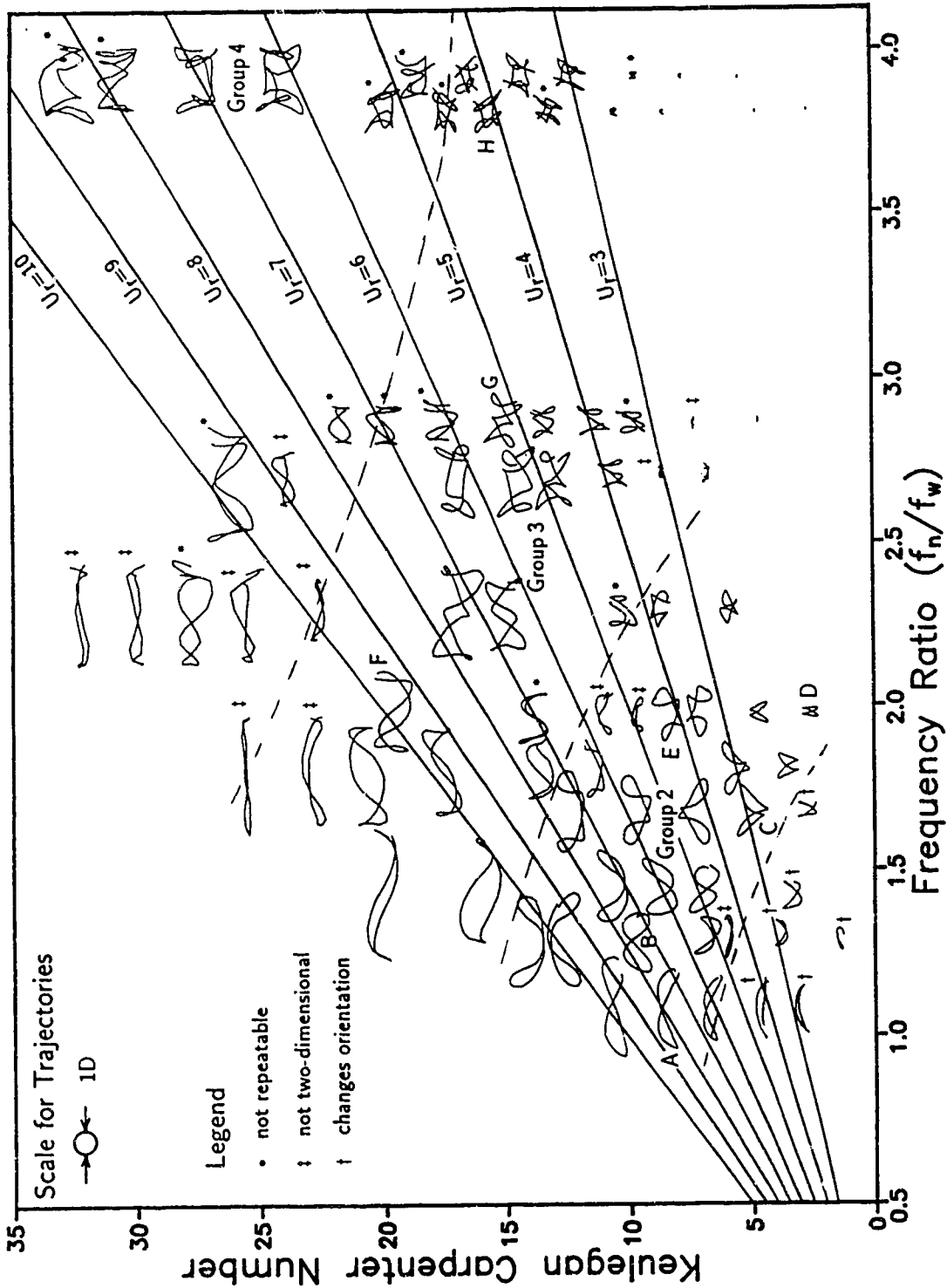
49

Figure 4.5 Typical trajectories for f_n/f_w less than four.

state flow conditions form another classification, and are marked by a †. Further discussion of this classification of trajectory follows shortly. The remaining cases are two-dimensional trajectories that follow the same shape of trajectory, but the amount of cycle to cycle variation in the trajectory depends on the case, as was evident in Figure 4.1. Attempts were made to correlate the conditions of strongly two-dimensional and repeatable response to values of r\. ˙ .ced velocity, frequency ratio, and Kc without success. Table 4.1 shows the flow conditions along with maximum inline deflections, X, and maximum transverse deflections, Y, associated with eight strongly two-dimensional trajectories. These eight trajectories are labelled A through H in Figure 4.5 and were selected because they showed smaller cycle to cycle deviations than most, while representing the different shapes of repeatable trajectories encountered. It is assumed that smaller deviations from cycle to cycle indicate a higher degree of synchronization between vortex shedding and cylinder motion. As can be seen from Table 4.1, there is no common value of reduced velocity at which these trajectories occur, nor do these responses necessarily occur at integer

Table 4.1 Flow characteristics and peak deflections from equilibrium for eight repeatable trajectories.

Key	KC	f_n/f_w	U_r	X	Y
A	8.6	1.07	8.0	1.9	0.6
B	9.4	1.29	7.3	1.3	0.7
C	5.3	1.68	3.2	1.1	0.6
D	2.5	1.97	1.3	0.2	0.4
E	8.4	1.97	4.3	1.1	0.7
F	19.7	1.97	10.0	1.7	0.9
G	15.1	2.87	5.3	1.2	0.9
H	15.8	3.81	4.1	0.9	0.6

frequency ratios.

The maximum inline deflection for the cases in Table 4.1 of 1.9 diameters occurred for $Kc = 8.6$ with $f_n/f_w = 1.07$, and the next largest deflection of 1.7 diameters ocurred for $Kc = 19.7$ with $f_n/f_w = 1.97$. Note that Keulegan-Carpenter number is a measure of the relative amplitude of fluid particle motion compared to the cylinder diameter. Specifically, $Kc = 2\pi a/D$ where a is the amplitude of fluid motion. Therefore for $Kc = 8.6$ the amplitude of fluid motion is 1.37D. In this case the inline deflection of the cylinder exceeds that of the fluid motion because the natural frequency of the cylinder is close to the fluid frequency. The maximum transverse response of 0.9 diameters occurred at both $U_r = 5.3$ and $U_r = 10.0$. Transverse deflections in all cases did not exceed one cylinder diameter, which is similar to the results reported for studies of transverse response alone.

For fixed cylinders the number of vortices shed in a cycle is principally a function of Kc. The boundaries between the groups in Figure 4.5 are thought to characterize the number of vortices produced or shed each half cycle. However these boundaries occur at smaller values of Kc than would be associated with a fixed cylinder, especially if the frequency ratio is small. This is as one might expect, because at low frequency ratios the cylinder can respond significantly in the inline direction, resulting in smaller relative motion between the cylinder and the fluid. This smaller relative motion will produce fewer vortices each cycle.

There is also a region for low values of both Kc and f_n/f_w that have similar trajectories which are basically horizontal or have a "U" shape (or an inverted "U"). As Kc is very small it is doubtful that any vortices are actually shed, although attached vortices are probably present. These trajectories could probably be classified as part of the Group 2 trajectories by virtue of their U shape which, like an "infinity" shape, completes 2 cycles of transverse motion for each cycle of inline motion. An interesting feature of these trajectories, which are marked with a † in Figure 4.5, is that they often change orientation from a U to an inverted U or vice versa under steady state flow conditions. Such a change is illustrated in Figure 4.6
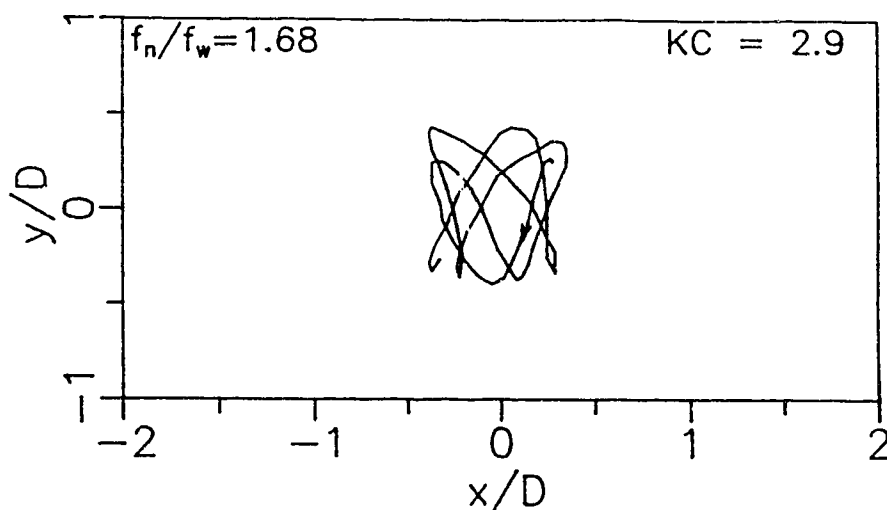
Figure 4.6 Sample of a U-shaped trajectory that changes orientation.

for which $Kc = 2.9$ and $f_n/f_w = 1.68$. By carefully following the trajectory through the 2.5 cycles shown, proceeding in the direction of the arrow, the transition from a U to inverted U shape can be seen. The change in orientation can be explained by a lack of synchronization between the development of vortices and the cylinder motion.

4.2 Response at Higher Frequency Ratios

The trajectories examined to this point have been for frequency ratios, f_n/f_w, less than four, although frequency ratios up to 8.6 were investigated. As the frequency ratio exceeds about 4 the shapes of the trajectories become more difficult to analyze due to the increased complexity and speed of the cylinder motion. The limitation is not only due to the rate at which the frames of the video recording are taken, but also due to difficulties in interpreting a trajectory with many crossing points and transverse cycles. An additional complication is that in general there is greater cycle to cycle variation of a trajectory for responses at higher frequency ratios. Thus the main features to be examined for the cases with higher frequency ratios are the

number of transverse cycles for each cycle of water motion, and whether the same basic shape of trajectory is followed for each cycle of water motion. It is difficult to apply the same criteria for classifying the trajectories at lower frequency ratios to the results at higher frequency ratios. All tests for frequency ratios greater than 4 were conducted with the two smaller diameter cylinders, and consequently the ratio of length to diameter was higher for these tests. This made highly correlated vortex shedding less likely. This tendency toward more three-dimensional behaviour was offset somewhat by the relatively stiff springs, which meant that generally larger forces were required to cause significant motion. If contact were made with the glass, the frictional force was therefore less significant compared to the other forces involved, and affected the motion to a lesser extent than for lower frequency ratios. The result of these factors was that contact with the glass was more common, but it often did not prevent trajectories of a consistent shape from occurring.

Two examples of response at higher frequency ratios are given in Figure 4.7. In Figure 4.7(a) the response shown is for $Kc = 23.7$ and $f_n/f_w = 5.14$, which corresponds to a reduced velocity of 4.6. In Figure 4.7(b) $Kc = 32.6$ and $f_n/f_w = 5.14$, giving a reduced velocity of 6.3. These trajectories are typical for U_r and f_n/f_w both greater than 4, as in each half cycle several transverse cycles of motion are completed with large amplitude transverse motion occurring near maximum inline deflection. The trajectories also tend to complete the transverse cycles by following a "C" shaped path when near the right side of the trajectory and a backward "C" shaped path near the left side of the trajectory. This "C" shape can be attributed to the phase relationship between transverse and inline forces caused by the shedding of vortices in this flow.

One difference between Figures 4.7(a) and (b) is that they exhibit different types of symmetry. In (a) there are four cycles of transverse motion completed in each cycle, while in (b) there are five. The result is that in Figure 4.7(a) the even number of cycles means that the trajectory is roughly symmetric about the y-axis, while in (b) the odd number of cycles means that the trajectory is roughly symmetric about
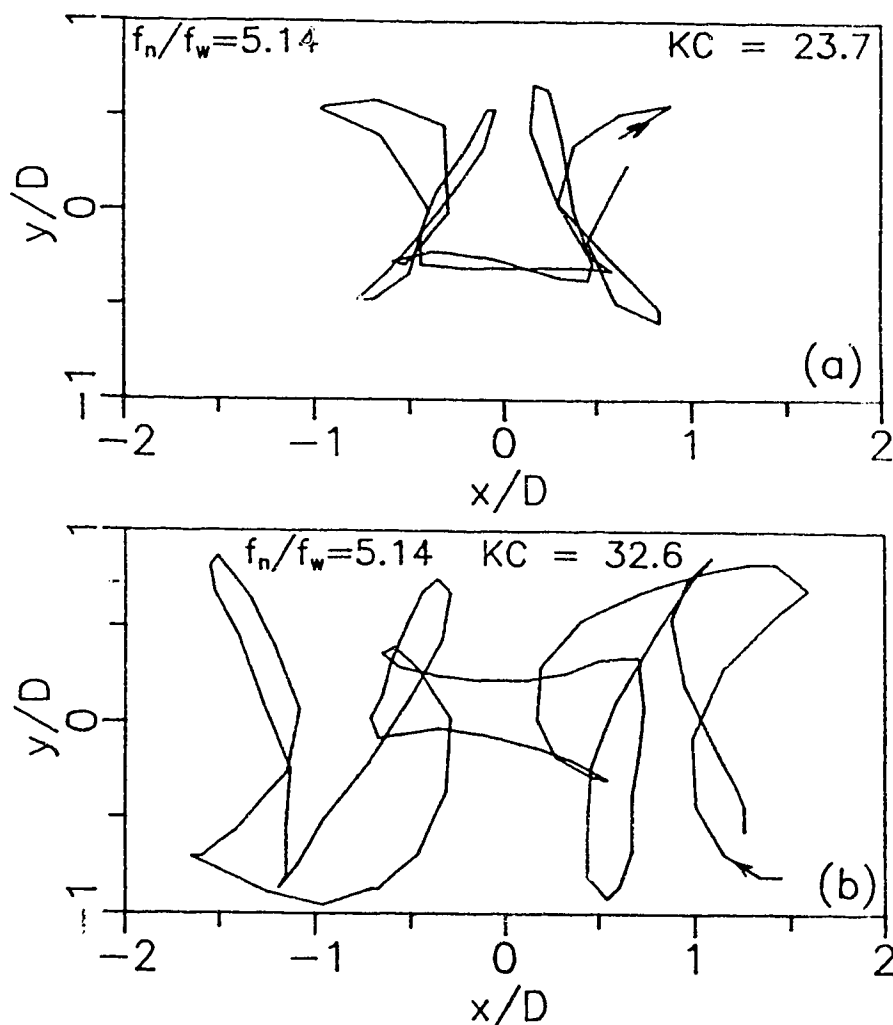
Figure 4.7 Two typical trajectories for $f_n/f_w = 5.14$. (a) $Kc = 23.7$, (b) $Kc = 32.6$

the origin.

To gain a better understanding of typical responses encountered at higher frequency ratios a sequence of trajectories is plotted in Figure 4.8 for $f_n/f_w = 6.43$ and increasing Kc. Starting at low Kc, there is very little inline response due to the relatively stiff springs, and the small fluid velocities and accelerations which cause correspondingly small drag and inertia forces. With respect to the transverse response, it is necessary to recall that at very low Kc, very few or no vortices are shed, and that as Kc increases the number of vortices shed per cycle also increases. The
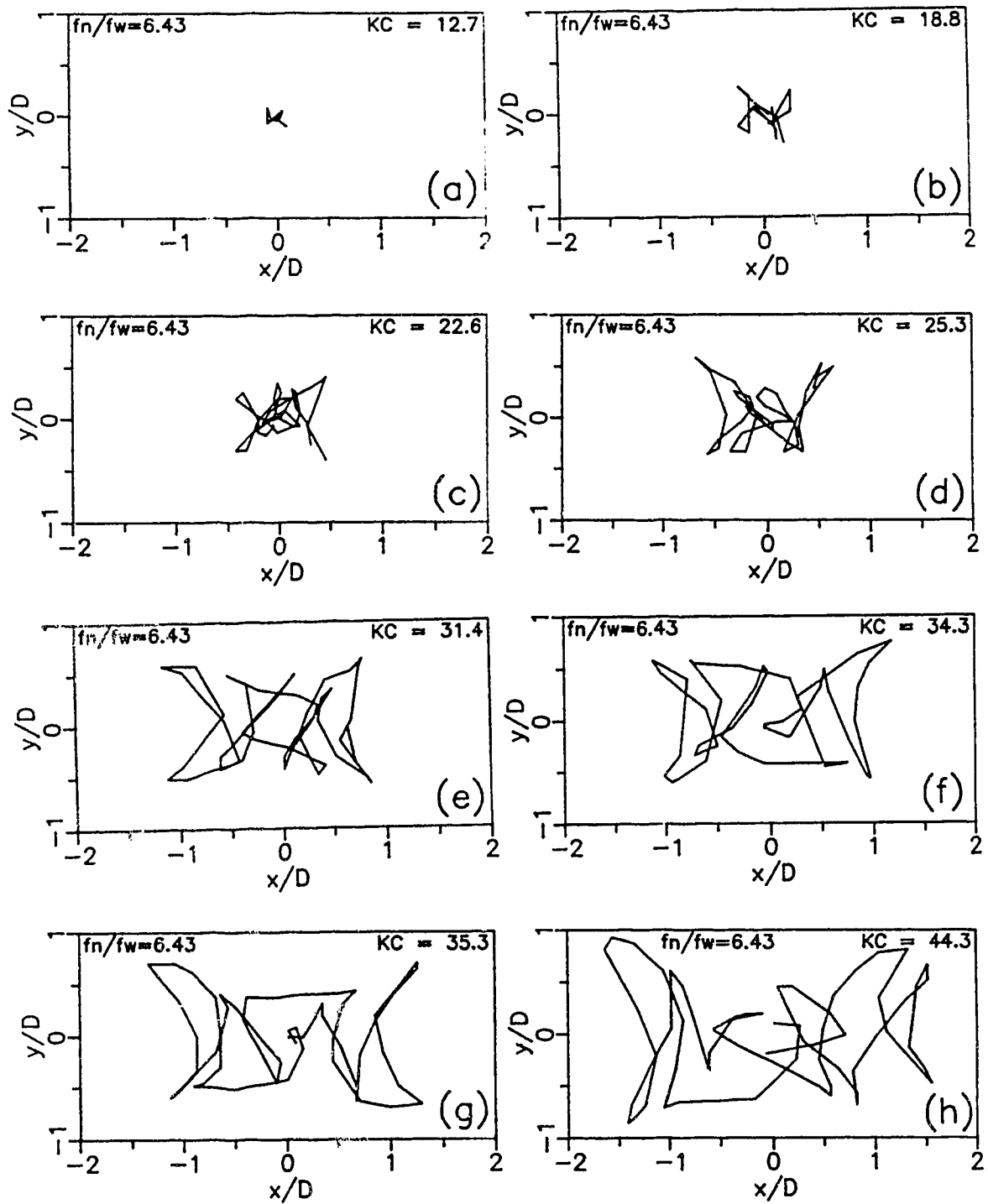
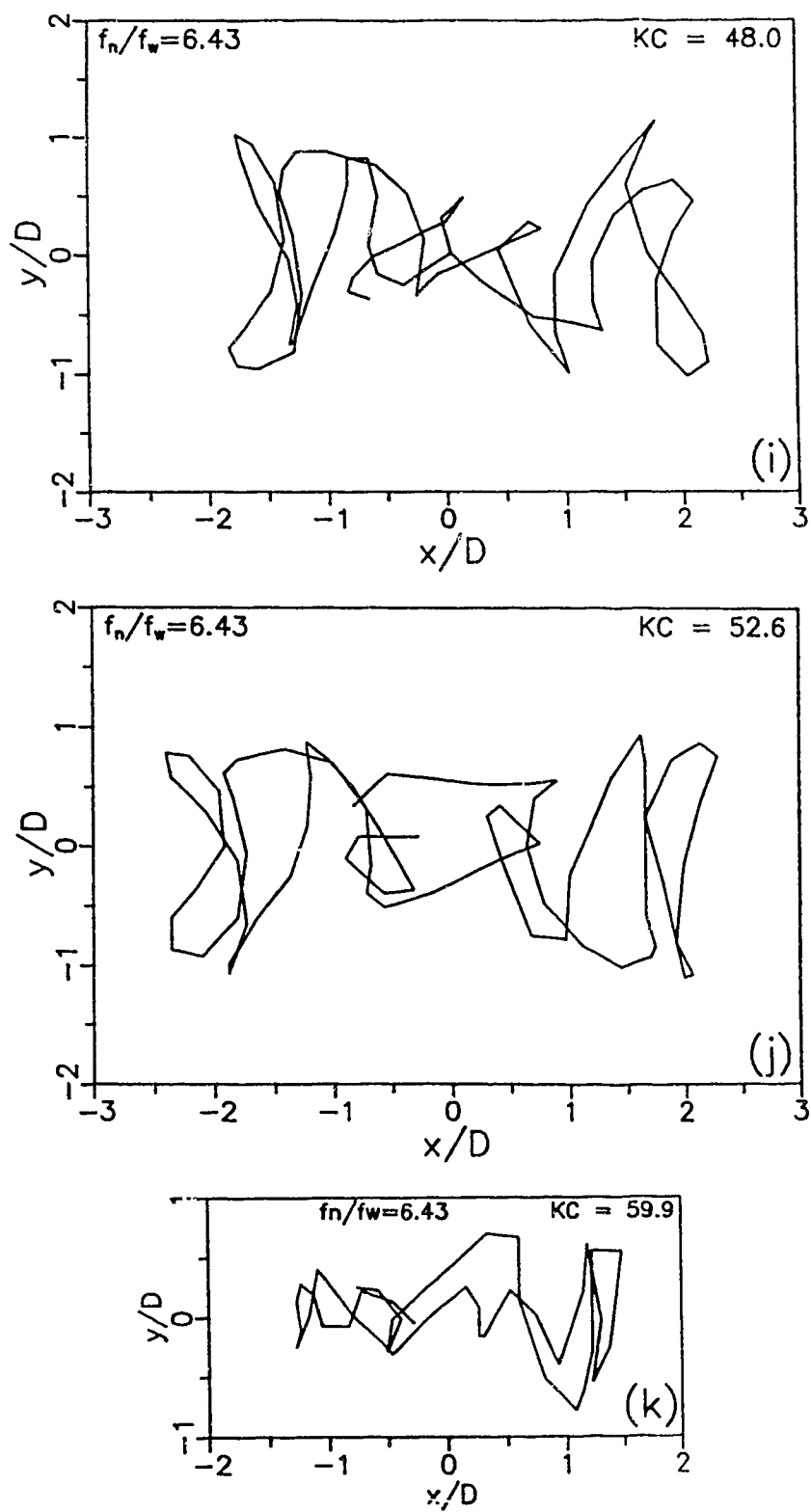Figure 4.8 Progression of trajectories for $f_n/f_w = 6.43$ and increasing Kc

Figure 4.8 Progression of trajectories for $f_n/f_w = 1.97$ and increasing Kc (continued).

small transverse response is due partly to the stiff springs, but also the number of vortices developed per cycle is much lower than the frequency ratio. This means that the frequency of transverse forcing is much lower than the natural frequency of the cylinder, and therefore lower amplitude response should be expected. As Kc increases one or two vortices appear to be shed for each half cycle, producing larger forces which cause the cylinder to respond briefly. Then, as the flow reverses the cylinder returns toward the equilibrium position where it oscillates at smaller amplitudes until the vortices shed in the next half cycle develop to the point where larger response occurs again. This type of behaviour is evident in Figures 4.8(a), (b) and (c) where roughly two significant transverse cycles of response occur for each cycle of water motion. The small amplitude oscillations make the size and direction of the first significant motion in the next half cycle of water motion unpredictable. In what follows the term "inconsistent" will be used to describe trajectories that do not follow the same basic shape in terms of the number of transverse cycles or their orientation and order of occurrence during one cycle of water motion. In Figures 4.8(a), (b) and (c), increased amplitudes of response are evident as the Keulegan-Carpenter number increases.

The plots shown in Figure 4.8 are for one cycle only due to the complexity of the trajectories. It is helpful to focus on the general shape rather than the rough details caused by the relatively low digitization frequency. Those plots that show greater symmetry and organization are generally more repeatable, and those that seem more random in shape are indicative of trajectories that are not highly repeatable. For example, Figures 4.8 (c) and (d) should only be considered as samples of inconsistent trajectories, but (e) shows much more symmetry with five transverse cycles for each inline cycle of motion. A similar shape is evident in (f) but in (g) much less symmetry is evident. Specifically, note that in (g) the path the cylinder takes from one side of the trajectory to the other, nearer the top of the trajectory, is very different in nature from the return path directly below it. It would appear that the incident vortices from the previous half cycle are not as well timed with the response of the cylinder, and consequently this "mistiming" results in an inconsistent trajectory. The

mistiming is also indicative of a transition, in this case from five transverse cycles per cycle of water motion seen in (f) to 6 cycles as seen in (h). At these higher Kc the range of amplitude of water motion, over which a trajectory with small cycle to cycle variations exists, is very small. As a result it is quite common for the amplitude to die down for about one cycle before returning to a larger number of consistent cycles similar to that shown in Figure 4.8(h). Figures 4.8(i) and (j) show relatively consistent trajectories with 7 transverse cycles of motion for each cycle of water motion, however the deviation from cycle to cycle is much greater than that for trajectories at lower f_n/f_w. Despite this larger deviation, the trajectories are quite repeatable in the number of transverse cycles completed for each inline cycle of motion. The amplitude of transverse motion appears to be limited to about 1 diameter here, similar to the maximum amplitude of a cylinder responding to vortex shedding in steady flow as well as that found for smaller frequency ratios. The inline response, on the other hand, has continued to increase to about 2 diameters. These two plots in (i) and (j) correspond to a reduced velocity of 7.5 and 8.1 respectively, yet they show the largest inline and transverse responses observed in all tests. Again it is evident that the inline motion alters the conditions for lock-in from those discovered in studies of transverse response alone. Although the reduced velocity is close to the the "upper side-band frequency" identified by McConnell and Park [12] of slightly over $U_r = 7.2$, it is interesting that a larger response did not occur for a reduced velocity close to 5.4.

It might have been expected that with a much more stiffly supported cylinder, conditions of lock-in for transverse response only might apply, but this was not the case. It is worth noting that even though $f_n/f_w = 6.43$, there were significant transverse responses at 5, 6 and 7 times the frequency of the flow. It is interesting to note that the results of Sumer and Fredsøe [23] indicate that the cylinder tends to respond at a frequency close to its natural frequency, and the vortex shedding frequency shifts to accomodate this response. This discovery was made in tests conducted at fixed values of Kc while varying U_r (ie. varying f_n/f_w). In contrast,

the present study shows that the respon?? ?? ?? to occur at different multiples of f_n although f_n/f_w is fixed and Kc is varied. The ability of the cylinder to respond at these different frequencies seems to indicate that the inline motion of the cylinder helps to accommodate the difference between the natural frequency of the cylinder and the expected vortex shedding frequency based on the Strouhal relationship.

Figure 4.8(k) shows a sample of the trajectory for $Kc = 59.9$ and $f_n/f_w = 6.43$, so that $U_r = 9.3$. In this case the response is three-dimensional and the cylinder makes significant contact with the walls of the U-tube. Consequently, the number of transverse cycles and the shape of the trajectory have very little meaning, other than to indicate a possible region of transition between conditions of larger, more consistent response.

To obtain an overview of the types of trajectories encountered, Figure 4.9 shows, in the same manner as Figure 4.5, typical trajectories for f_n/f_w greater than four. Lines corresponding to points of constant reduced velocity are again included for reference. A slightly different system of symbols is used to characterize the responses. The trajectories that were clearly not two-dimensional are marked with a ‡. Trajectories that showed no consistency of shape from one cycle to the next (that is "inconsistent") are marked with an *. The remaining trajectories generally followed the same basic shape from cycle to cycle, although there may have been slight contact with the glass, or occasional cycles where the response died down due to a slight "mistiming" of vortex shedding and cylinder motion.

From this plot a number of trends are evident. First, significant response amplitudes in the transverse direction occur for a reduced velocity of 3 or greater. Second, the largest responses in both the inline and transverse directions occur for reduced velocities larger than 6, rather than the value of 5.4 for transverse lock-in. This higher value of reduced velocity can be partly explained by the inline motion of the cylinder which would tend to reduce the amplitude of relative inline motion between the water and the cylinder. The smaller relative inline motion would tend to cause fewer vortices to be shed per cycle of water motion for a given Kc. Therefore
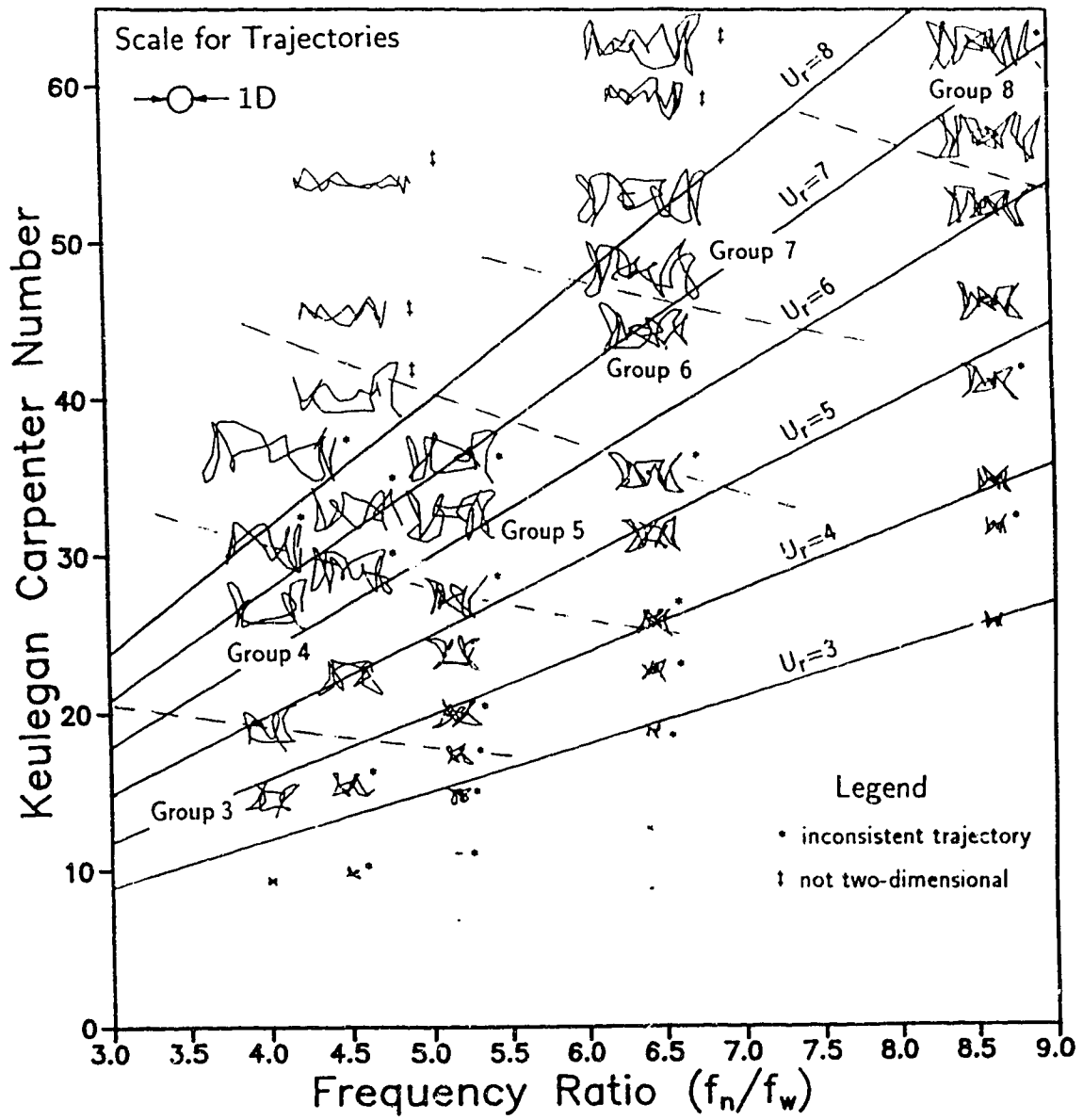
Figure 4.9 Typical trajectories for f_n/f_w greater than four.

a larger value of *Kc* would be required for enough vortices to be shed per cycle to match the natural frequency of the cylinder.

It is difficult to comment on the upper limits of the amplitude of response, if any exist, because of the experimental setup. In order to obtain larger reduced velocities over the range of frequency ratios, a smaller cylinder must be used because of the limits to the amplitude of water motion that can be achieved in the U-tube. As smaller diameter cylinders are used, the length to diameter ratio increases, thus making correlation along the full length of the cylinder more unlikely. The result is that the vortex shedding can occur out of phase along the length of the cylinder, and induce the cylinder to rotate about an axis perpendicular to its own, causing significant contact between the buttons on the end plates and the window. Any response is then disrupted and the motion can not build up. An example of this is evident in Figure 4.9 for *Kc* = 54 and a frequency ratio of about 4.5. An additional factor that may be significant is that the natural frequency of the cylinder in the rotational mode is higher than that in translation. Although the cylinder can only move a limited amount in this rotational mode, the higher natural frequency is closer to the vortex shedding frequency at high *Kc* and consequently is more easily excited than translational motion. It is also possible that large amplitude transverse responses do not occur above a limit of reduced velocity, but a different experimental apparatus would be required to investigate this possibility.

Also included in Figure 4.9 are boundaries for the different "groups" of trajectories defined by the number of transverse cycles completed for each inline cycle. For higher frequency ratios, the boundaries are less well defined, due in part to the smaller number of experiments conducted in that range. As expected, the divisions between the groups become more of a function of *Kc* alone as f_n/f_w increases, because stiffly supported cylinders more closely approximate fixed cylinders for which the number of vortices shed per cycle is mainly a function of *Kc*.

Since the shedding of a pair of vortices corresponds to one cycle of the transverse force, some similarity might be expected between the number of pairs of vortices shed

per cycle reported by Sarpkaya [5] for a fixed cylinder and the number of transverse cycles the cylinder completes for one cycle of water motion in the present study. For example, Sarpkaya [5] reports that for $Kc = 50$, 10 pairs of vortices are shed per cycle, but for the cylinder with the highest frequency ratio in the present study, the number of transverse cycles of response completed for each cycle of water motion is only 7 when $Kc = 50$. This difference can be attributed to the inline motion of the cylinder, since studies of transverse response alone by Sumer and Fredsøe [23] indicated good agreement between the number of transverse cycles completed and the number of vortices shed per cycle from a fixed cylinder.

4.3 Conclusions

This study of the two-dimensional response of a flexibly mounted cylinder in oscillatory flow has shown that the inline response significantly alters the conditions at which large amplitude, repeatable responses occur. These conditions are different from those identified in studies of transverse response only. Specifically, repeatable two-dimensional response did not occur at a common value of reduced velocity, or necessarily at the natural frequency of the cylinder. Large responses were generally observed for $U_r > 6$, while significant transverse responses did not occur for $U_r < 3$. The higher values of reduced velocity required for large transverse response than those reported for studies of transverse response alone can be attributed to the inline motion of the cylinder which reduces the amplitude of relative motion between the cylinder and the water.

In all cases, the cylinder completed one main cycle of inline motion for one cycle of water motion. The trajectories were classified according to the number of transverse cycles completed for each cycle of water motion. These different types of trajectories occurred in well defined regions on a plot with Kc and f_n/f_w, particularly for lower values of f_n/f_w. Conditions corresponding to the boundaries between these regions are those of low correlation and three-dimensional response. The shapes of the

trajectories could not be classified on the basis of reduced velocity alone. The responses for lower frequency ratios displayed less cycle to cycle variation in the trajectories than the responses at higher frequency ratios.

It was postulated that the main cause of the different groups of trajectories is the number of vortices produced or shed every half cycle, and it is clear that the next step in understanding the fluid-structure interactions will require flow visualization studies.

Finally, some assessment of the uncertainties in the measurements must be made. The uncertainty in the amplitude and phase information is quite small compared to that involved in the digitization process, since the LED and LCD were updated at about 100 Hz, which far exceeds the frame rate of the videotape of 30 Hz. The uncertainty in a coordinate is judged to be ±2 pixels on a 512 by 512 grid. This translates to an uncertainty in the position of the cylinder of about 1.7 mm, or as a percentage of the diameter of the cylinder as 6.6%, 3.7% and 2.7% for the three cylinders in order of increasing diameter.

Chapter 5

Equations of Motion

For the design of safe and efficient offshore structures in deeper waters, it is important to be able to predict the forces acting on a structure in waves and the resulting structural response. Ideally one would expect that a complete numerical solution of the time dependent Navier-Stokes equations coupled with the response of the structure would provide the complete solution to the problem, however such an undertaking is not currently feasible due to the prohibitive computational power required. Therefore various approximations need to be made to obtain useful solutions. For studies of steady and oscillatory flow about fixed and flexible structures, some knowledge of the net effects of the fluid flow has been acquired. This knowledge can be applied as a first step in formulating simple models to predict the response of a flexible structure. These models are necessarily approximate, and therefore must be evaluated by comparison with experiments to determine their usefulness and limitations.

In this chapter, models for forces on cylinders in steady and oscillatory flow will be used to formulate equations of motion to predict the two-dimensional response of a cylinder in oscillatory flow. Three different models are considered here. The first two employ a modified form of the Morison equation in the inline direction and different expressions for the transverse force, resulting in uncoupled sets of equations.

64

In the third model, the lift and drag are considered to act perpendicular and parallel to the direction of instantaneous relative velocity between the fluid and the cylinder, which results in a coupled set of equations. For each of the three models the resulting equations of motion are integrated numerically. The judgements as to whether each model accurately predicts the amplitude and or shape of the experimentally observed response are presented in the next chapter.

5.1   An Equation for Inline Motion

Due to the complex nature of the fluid-structure interaction for the problem being considered, the equations of motion necessarily depend on empirical coefficients. Ideally the equations of motion should have a minimum number of coefficients, and should have data available to provide a basis for selecting them. Given the success of the Morison equation, it is a natural starting point for approximating the inline force acting on the cylinder. The basic assumption of the "independent flow fields" approach is that the forces on a flexibly mounted cylinder can be considered as the sum of the fluid forces that a fixed cylinder would experience in the same flow, which are the "far field" effects, plus the fluid forces that the cylinder would experience if it were oscillating in still water at the amplitude of the response, which are the "near field" effects [30]. Such superposition is speculative, but has the advantage of clearly defining the sources for the empirical coefficients. The inline fluid force per unit length of cylinder for this case is

$$F_x = \rho A C_m \dot{U} + \frac{1}{2}\rho D C_d U |U| - \rho A C_a' \ddot{x} - \frac{1}{2}\rho D C_d' \dot{x}|\dot{x}|, \qquad (5.1)$$

in which A represents the cross-sectional area of the cylinder, ρ is the fluid density, x is the inline cylinder displacement and dots denote differentiation with respect to time. The first two terms on the right hand side of Equation 5.1 are the far field effects, and represent the force given by the Morison equation on a fixed cylinder, while the last two terms represent the near field effects. The values of C_m and C_d

are taken from data for a fixed cylinder in the same flow, while C_a' and C_d' are taken from data for a cylinder oscillating in still water with the same amplitude of cylinder motion. Unfortunately these latter coefficients depend on the solution; therefore, an iterative approach is required for their evaluation.

Another point of view considers the drag force terms to be based on the relative velocity between the fluid and the cylinder, giving a fluid force per unit length of

$$F_x = \rho A C_m \dot{U} - \rho A C_a' \ddot{x} + \frac{1}{2}\rho D C_d(U - \dot{x})|U - \dot{x}|. \qquad (5.2)$$

The value of C_d used for the drag force in this case should be based on the amplitude of relative motion rather than fluid or structural motion alone. In what follows it is assumed that the drag coefficient for the relative motion is not significantly different from that for the case of a fixed cylinder in a still fluid, thus avoiding an iterative solution. Further support for this assumption is presented later in this section.

To aid in assessing how to select the inertia coefficients in Equation 5.2, it is useful to use it in conjunction with an equation of motion, for example

$$m\ddot{x} + c\dot{x} + kx = \rho A C_m \dot{U} - \rho A C_a' \ddot{x} + \frac{1}{2}\rho D C_d(U - \dot{x})|U - \dot{x}|. \qquad (5.3)$$

In this equation the term containing C_m represents the contribution of two effects. The first is the pressure gradient in the flow causing the fluid acceleration $\dot{U}$, while the second is the force required to accelerate the flow about the cylinder when held fixed. In contrast, C_a' is used in the equation to represent the force required to accelerate the cylinder in otherwise still fluid at flow conditions corresponding to the amplitude of structural motion. Since C_m and C_a' correspond to different flow conditions, $C_m \neq C_a' + 1$, and as a result the two terms should be kept separate. By writing Equation 5.3 with the inertia terms separate, the inertia term due to structural motion can be brought to the left hand side so that the "mass" term includes the added mass. This then permits the equation to be written in a standard form that includes the natural frequency,

$$\ddot{x} + 2\zeta\omega_n\dot{x} + \omega_n{}^2 x = \frac{\rho A C_m \dot{U}}{m + \rho A C_a'} + \frac{\frac{1}{2}\rho D C_d(U - \dot{x})|U - \dot{x}|}{m + \rho A C_a'}, \qquad (5.4)$$

where

$$\omega_n{}^2 = \frac{k}{m + \rho A C_a'}, \qquad \zeta = \frac{c}{2(m + \rho AC \quad)\omega_n} \qquad (5.5)$$

are the natural frequency of the cy" nder, and the dar 'ng ratio in the fluid, respectively. When modelling a particular situation the due ω_n is determined from a simple free vibration test in the fluid. Such a test involves small amplitude oscillations, for which C_a' may be considered equal to 1.

Equation 5.4 is the "relative velocity" formulation of the Morison equation and has been used by C.H.K. Williamson [20] as described in Section 2.3. The values of C_d that C.H.K. Williamson obtained iteratively from the relative velocity approach in most circumstances did not differ significantly from the values based on the amplitude of water motion. However, a large difference occurred in the region of inline resonance for which f_n/f_w is slightly less than 1. For the present tests, f_n/f_w is always greater that one, therefore C_d can be based on the amplitude of water motion. For the purposes of assessing the usefulness of the Morison equation to predict the inline component of the two dimensional response of a cylinder, it is judged that Equation 5.4 represents a reasonable but necessary compromise between simplicity and accuracy.

5.2 Simple Uncoupled Model

The first set of equations is the "simple uncoupled model" which uses Equation 5.4 for the inline direction and simple sinusoidal forcing similar to Equation 2.3 for the transverse direction. Also included in the transverse direction are the near-field added mass and damping due to the transverse motion. Using the subscripts x and y to distinguish between empirical coefficients that are different in the inline, x, and transverse, y, directions, the set of equations on a per unit length basis is

$$(m + \rho A C_a')\ddot{x} + c\dot{x} + kx = \rho A C_m \dot{U} + \frac{1}{2}\rho D C_{d_x}(U - \dot{x})|U - \dot{x}|, \qquad (5.6)$$

$$(m + \rho A C_a')\ddot{y} + c\dot{y} + ky = \frac{1}{2}\rho D U_m{}^2 C_L \sin(n\omega_w t + \phi) - \frac{1}{2}\rho D C_{d_y}\dot{y}|\dot{y}|, \qquad (5.7)$$

where m represents the structural mass only, n is an integer based on the number of vortices produced per half cycle and ϕ is the phase of the vortex shedding forcing with respect to the fluid motion, $U = U_m \sin \omega_w t$. The basis for selection of the of value of n is consistent with the result reported by Maull and Milliner [10], but n is difficult to determine *a priori*. It may be estimated from sources such as Sarpkaya [5], where the number of vortices shed per cycle from a fixed cylinder are reported. These sources are of limited use, since the number of vortices may change when the cylinder is free to respond inline with the flow. Therefore, the value of n may have to be based on experimentally observed trajectories. The value of ϕ must also be based on experimentation and comparison with actual tests, because presently no data are available for its value. Further details on the selection of ϕ will be presented with the numerical results. The value of C_{d_x}, C_m and C_L are approximated by the values from data for a fixed cylinder in the same flow. C_{d_y} is based on small Kc (< 10) since the amplitude of transverse motion is expected to be small. The reason for this is that in studies of transverse response only, amplitudes of oscillation greater than 1 diameter have not been observed [22, 23]. It is useful to write the equations in non-dimensional form using the following substitutions, in which an overbar denotes a dimensionless quantity, $'$ denotes differentiation with respect to dimensionless time, and ρ_c is the density of the cylinder

$$
\begin{aligned}
x &= \bar{x}D & \dot{x} &= \bar{x}'D/T & \ddot{x} &= \bar{x}''D/T^2 \\
y &= \bar{y}D & \dot{y} &= \bar{y}'D/T & \ddot{y} &= \bar{y}''D/T^2 \\
t &= \bar{t}T & \Omega &= \omega_n/\omega_w = f_n/f_w & \omega_w &= 2\pi/T \\
U &= U_m \sin(\omega_w t) & \bar{\rho} &= \rho_c/\rho.
\end{aligned}
\tag{5.8}
$$

This substitution into Equations 5.6 and 5.7 yields after some algebra

$$
\begin{aligned}
\bar{x}'' + 4\pi\zeta\Omega\bar{x}' + 4\pi^2\Omega^2\bar{x} &= \frac{2}{\pi}\frac{C_{d_x}}{\bar{\rho}+C_a'}(Kc \sin 2\pi\bar{t} - \bar{x}')\,|Kc \sin 2\pi\bar{t} - \bar{x}'| \\
&\quad +2\pi Kc\frac{C_m}{\bar{\rho}+C_a'}\cos 2\pi\bar{t},
\end{aligned}
\tag{5.9}
$$

$$\bar{y}'' + 4\pi\zeta\Omega\bar{y}' + 4\pi^2\Omega^2\bar{y} = \frac{2}{\pi}Kc^2\frac{C_L}{\bar{p} + C_a{}'}\sin(n2\pi\bar{t} + \phi)$$

$$-\frac{2}{\pi}\frac{C_{dy}}{\bar{p} + C_a{}'}\bar{y}'|\bar{y}'|. \tag{5.10}$$

5.3 Modified Uncoupled Model

A possible improvement for the transverse forcing proposed in the simple uncoupled model is to use the transverse force suggested by McConnell and Park [12] previously discussed in Section 2.3. Specifically, the transverse force in this case is given by

$$F_L(t) = \frac{1}{2}\rho DC_L U^2 \sin(n\omega_w t + \phi). \tag{5.11}$$

The only difference from the simple uncoupled model is that the instantaneous fluid velocity is used instead of U_m. The value of n is again based on the number of vortices that are produced per half cycle of fluid motion. This forcing model gives frequency components at $n\omega_w$, $(n + 2)\omega_w$ and $(n - 2)\omega_w$, as previously discussed.

Using the same model for inline forcing as the simple uncoupled model, the resulting equations of motion for the "modified uncoupled model" are

$$(m + \rho AC_a{}')\ddot{x} + c\dot{x} + kx = \rho AC_m\dot{U} + \frac{1}{2}\rho DC_{dx}(U - \dot{x})|U - \dot{x}|, \tag{5.12}$$

$$(m + \rho AC_a{}')\ddot{y} + c\dot{y} + ky = \frac{1}{2}\rho DU^2 C_L \sin(n\omega_w t + \phi) - \frac{1}{2}\rho DC_{dy}\dot{y}|\dot{y}|. \tag{5.13}$$

By substituting in the expressions of Equation 5.8, the nondimensional equations are

$$\bar{x}'' + 4\pi\zeta\Omega\bar{x}' + 4\pi^2\Omega^2\bar{x} = \frac{2}{\pi}\frac{C_{dx}}{\bar{p} + C_a{}'}\left(Kc\sin 2\pi\bar{t} - \bar{x}'\right)|Kc\sin 2\pi\bar{t} - \bar{x}'|$$

$$+2\pi Kc\frac{C_m}{\bar{p} + C_a{}'}\cos 2\pi\bar{t}, \tag{5.14}$$

$$\bar{y}'' + 4\pi\zeta\Omega\bar{y}' + 4\pi^2\Omega^2\bar{y} = \frac{2}{\pi}Kc^2\frac{C_L}{\bar{p} + C_a{}'}\sin(n2\pi\bar{t} + \phi)\sin^2 2\pi\bar{t}$$

$$-\frac{2}{\pi}\frac{C_{dy}}{\bar{p} + C_a{}'}\bar{y}'|\bar{y}'|. \tag{5.15}$$

5.4 Coupled Model

An alternative to simply superimposing the inline and transverse deflections predicted by separate equations is to resolve the lift and drag terms perpendicular to and parallel to the instantaneous direction of relative motion with respect to the fluid, while leaving the inertia terms independent in the inline and transverse directions. Another approach based on resolving inertia terms in the direction of relative acceleration is presented in Appendix A, although with certain assumptions this results in the same equations of motion.

As shown in Figure 5.1, for a cylinder with velocity $\dot{x}\mathbf{i} + \dot{y}\mathbf{j}$, the velocity of the fluid with respect to the cylinder is

$$\mathbf{v}_{F/C} = (U - \dot{x})\mathbf{i} - \dot{y}\mathbf{j}, \tag{5.16}$$

in which the direction of relative velocity is defined by the angle α. Note that positive α is measured clockwise. From Figure 5.1(a),

$$\sin \alpha = \frac{\dot{y}}{v}, \qquad \cos \alpha = \frac{(U - \dot{x})}{v}, \tag{5.17}$$

where v is the magnitude of $\mathbf{v}_{F/C}$ and is

$$v = \sqrt{(U - \dot{x})^2 + \dot{y}^2}. \tag{5.18}$$

Using the lift and drag forces, F_L and F_D, illustrated in Figure 5.1(b), the equations
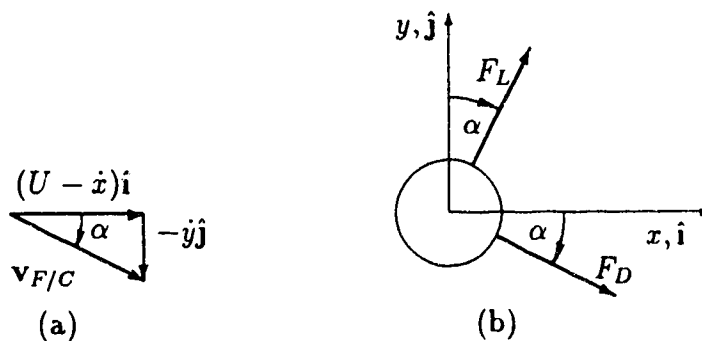
Figure 5.1 Direction of lift and drag for the coupled model.

of motion are

$$m\ddot{x} + c\dot{x} + kx \;=\; F_D\cos\alpha + F_L\sin\alpha + C_m\rho A\dot{U} - C_a'\rho A\ddot{x}, \tag{5.19}$$

$$m\ddot{y} + c\dot{y} + ky \;=\; F_L\cos\alpha - F_D\sin\alpha - C_a'\rho A\ddot{y}, \tag{5.20}$$

where the lift and drag force are

$$F_D = \frac{1}{2}\rho DC_d v^2, \qquad F_L = \frac{1}{2}\rho DC_L v^2 \sin(n\omega_w t + \phi). \tag{5.21}$$

By combining these results the equations of motion become

$$(m + \rho AC_a')\ddot{x} + c\dot{x} + kx \;=\; C_m\rho A\dot{U} + \frac{1}{2}\rho DC_d v^2\cos\alpha$$

$$+\frac{1}{2}\rho DC_L v^2 \sin(n\omega_w t + \phi)\sin\alpha \tag{5.22}$$

$$(m + \rho AC_a')\ddot{y} + c\dot{y} + ky \;=\; \frac{1}{2}\rho DC_L v^2 \sin(n\omega_w t + \phi)\cos\alpha$$

$$-\frac{1}{2}\rho DC_d v^2 \sin\alpha. \tag{5.23}$$

Again using the nondimensionalization given in Equation 5.8, the equations of motion can be written as

$$\bar{x}'' + 4\pi\zeta\Omega\bar{x}' \;+\; 4\pi^2\Omega^2\bar{x} =$$

$$2\pi Kc\frac{C_m}{\bar{\rho} + C_a'}\cos 2\pi\bar{t} \tag{5.24}$$

$$+\frac{2}{\pi}\frac{C_d}{\bar{\rho} + C_a'}(Kc\sin 2\pi\bar{t} - \bar{x}')\left\{(Kc\sin 2\pi\bar{t} - \bar{x}')^2 + \bar{y}'^2\right\}^{\frac{1}{2}}$$

$$+\frac{2}{\pi}\frac{C_L}{\bar{\rho} + C_a'}\bar{y}'\sin(n2\pi t + \phi)\left\{(Kc\sin 2\pi\bar{t} - \bar{x}')^2 + \bar{y}'^2\right\}^{\frac{1}{2}}$$

$$\bar{y}'' \;+\; 4\pi\zeta\Omega\bar{y}' + 4\pi^2\Omega^2\bar{y} =$$

$$\frac{2}{\pi}\frac{C_L}{\bar{\rho} + C_a'}\sin(n2\pi\bar{t} + \phi)(Kc\sin 2\pi\bar{t} - \bar{x}')\left\{(Kc\sin(2\pi\bar{t}) - \bar{x}')^2 + \bar{y}'^2\right\}^{\frac{1}{2}}$$

$$-\frac{2}{\pi}\frac{C_D}{\bar{\rho} + C_a'}\bar{y}'\left\{(Kc\sin 2\pi\bar{t} - \bar{x}')^2 + \bar{y}'^2\right\}^{\frac{1}{2}}. \tag{5.25}$$

The inline equation for the uncoupled models was successfully used by C.H.K. Williamson [18] to predict inline response, but it remains to be seen whether this approach can be successfully used in the context of two-dimensional response. Large discrepancies between observed and predicted behaviour might be expected to occur for flow conditions in which the fluid-structure interaction is significantly different from that for a fixed cylinder, since the coefficients were obtained from data for a fixed cylinder. In such cases an iterative solution might be required.

The solutions to the sets of equations in this chapter cannot be expected to reproduce exactly the observed behaviour because of the assumptions and simplifications made. In particular, lock-in self-limiting amplitudes were not accounted for in the models and are not expected in the results. Other assumptions made include the applicability of fixed cylinder data, the use of constant coefficients, the assumption of independent inline and transverse behaviour, and the omission of inline force due to vortices.

In the next chapter the solutions of the three models developed here are compared to experimentally observed trajectories. This comparison provides a basis for evaluating the usefulness and limitations of the models.

Chapter 6

Numerical Results and Analysis

In this chapter, the computed trajectories from the equations of motion developed in Chapter 5 are compared to experimentally observed trajectories. From this comparison the usefulness and limitations of the different models are identified.

6.1 Solution of the Equations of Motion

The equations of motion presented in Chapter 5 consist of sets of nonlinear second order differential equations that are not readily solved analytically. Consequently, these equations were solved numerically using an adaptive stepsize, fourth order Runge-Kutta algorithm given by Press et al. [31]. To solve the pair of second order equations, they were converted into a set of four first order equations in the variables z_i, such that

$$z_1 = \frac{dx}{dt}, \qquad z_2 = x, \qquad z_3 = \frac{dy}{dt}, \qquad z_4 = y. \tag{6.1}$$

The nondimensional forms of the equations were solved for zero initial conditions and all quickly approached steady-state trajectories. Other initial conditions were also used and the solutions were found not to depend on the initial conditions. In all cases structural damping was set to zero because it is much smaller than fluid damping effects. Additionally, structural damping would have been very difficult

73

to determine experimentally as the very soft springs cannot support the cylinders without the buoyancy provided by the water. The assumption of ignoring the very small structural damping is conservative because it will tend to overestimate the response slightly.

Maximum deflections from the equilibrium position rather than peak to peak measurements are used in the comparison because structural stresses are generally proportional to deflection from equilibrium. If peak to peak measurements were used, any offset of the response in one direction would result in the largest deflection from equilibrium exceeding half of the peak to peak measurement. Therefore if peak to peak measurements were used, the stresses could be underestimated.

6.2   Comparison to Experimental Results

To evaluate the effectiveness of each of the three models in predicting the response of a cylinder to oscillatory flow, five particular cases in the experimental portion of the study were selected for comparison to the numerical predictions, and are referred to as Case 1 through Case 5. In all cases the trajectories chosen were judged as being two-dimensional and repeatable, which permits a meaningful comparison between the experimental and numerical results.

For each of the models developed in the previous chapter, a number of coefficients must be specified. The values of Kc and f_n/f_w characterize the case under consideration, while values of C_L, C_m and C_d were taken from data for a fixed cylinder as measured by Sarpkaya [5]. A summary of the test cases and the coefficients used for all the models is presented in Table 6.1. From free vibration tests of the cylinder in water, the added mass coefficient was found using Equation 5.5 to be very close to 1. This result was expected, since for small amplitude oscillations in which there is little or no separation of the flow, the value of C_a' should be very close to the inviscid flow value of 1. Therefore $C_a' = 1$ was used in all cases. The selection of n and ϕ is discussed in the comparison to the experimental results.
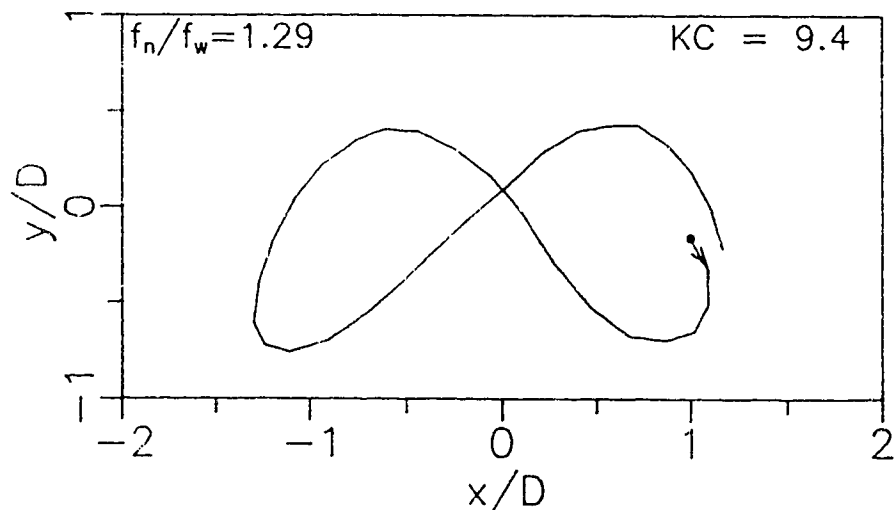
stiffly supported cylinder able to respond in the transverse direction only, and noted very good agreement between the two numbers. The numbers presented by Sarpkaya are a function mainly of Kc but in the experimental portion of the present study the number of transverse cycles for each cycle of water motion was observed to depend on both Kc and frequency ratio f_n/f_w. Therefore the value of n was set by inspection of the experimental results using the number of cycles of transverse motion for each cycle of inline motion. It is worth noting that the selection of n can be made in advance by referring to Figure 4.5 using the values of Kc and f_n/f_w. Each "Group" in the figure is named according to the number of transverse cycles completed for each inline cycle, which corresponds to n for the uncoupled models.

The trajectory produced by the simple uncoupled model is given in Figure 6.2(a) for $\phi = -1.7$. The shape of the numerically predicted trajectory is similar to that in Figure 6.1. The inline response amplitude matches quite closely that observed in the experiment, as shown in Figure 6.1, however the maximum transverse response is slightly larger than the experimentally observed value. Although the shape matches the observed trajectory quite well, the trajectory predicted by the model gives equal maximum transverse deflections both upward and downward. In contrast, the observed trajectory shows an apparent offset so that the largest negative transverse deflections are greater than those in the positive direction. This may be due to unequal development of the vortices, which is not accounted for in the model. The value of ϕ was the one parameter that could not be determined from previous experimental results. The effect of selecting a different value of ϕ is illustrated in Figure 6.2(b) for which $\phi = 0$. For the simple uncoupled model, the inline and transverse response amplitudes do not depend on ϕ. In what follows the value of ϕ is chosen so as to achieve the best match between the experimentally observed trajectory and those calculated numerically.

The modified uncoupled model was able to accurately reproduce the trajectory of Case 1 with $n = 2$ and $\phi = -\pi/2$, as shown in Figure 6.3. This value of ϕ is very close to that required for the simple uncoupled model. The computed inline
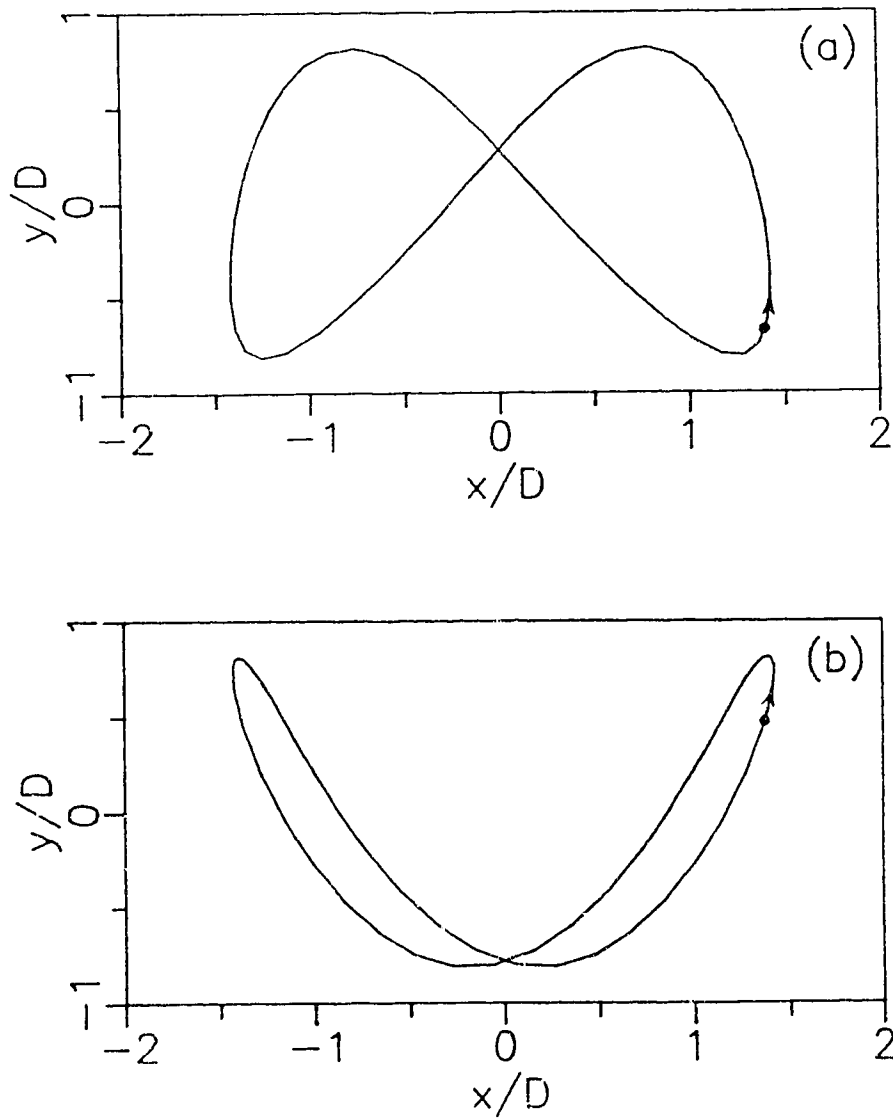
Figure 6.2 Numerically predicted trajectories from the simple uncoupled model for Case 1 with $n = 2$. (a) $\phi = -1.7$, (b) $\phi = 0$.
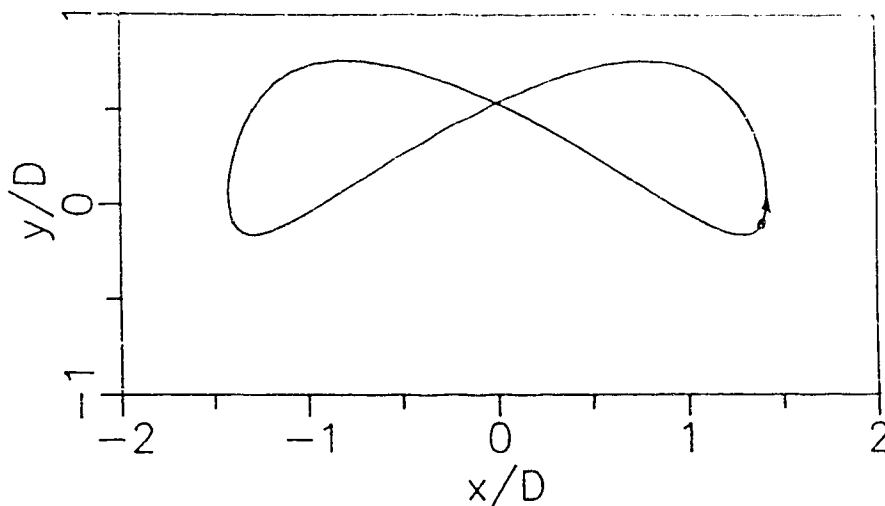
Figure 6.3 Numerically predicted trajectory from the modified uncoupled
model for Case 1 with $n = 2$ and $\phi = -\pi/2$.

response amplitude is in good agreement with the observed response. The main
difference between the observed and predicted amplitudes is that they are shifted in
opposite directions from the equilibrium position. Specifically, the experimentally
observed maximum transverse displacements are about 0.4D upward and 0.7D
downward whereas the predicted trajectory has an even greater offset with maximum
displacements of about 0.7D upward and 0.2D downward.

The coupled model also required values for the coefficients C_d, C_m and C_L, which
were taken from Table 6.1. The remaining parameters are ϕ, which was again varied
to obtain the best trajectory, and n. For the coupled model the value of n no longer
corresponded to the number of transverse cycles for each cycle of water motion, as
it did for the uncoupled models. The reason for this change is most likely due to
the coupling between the lift force, which acts perpendicular to the instantaneous
relative velocity, and the inline motion. An example of the effects of different values
of n can be seen in Figures 6.4(a), (b) and (c) in which n is given values of 1, 2 and 3
respectively, with $\phi = 0$. From these three figures, it is clear that the value of n does
not correspond to the number of transverse cycles for each cycle of inline motion. In
Figure 6.4(d) the value of n is 3 as in 6.4(c), however $\phi = \pi/4$, with the result that
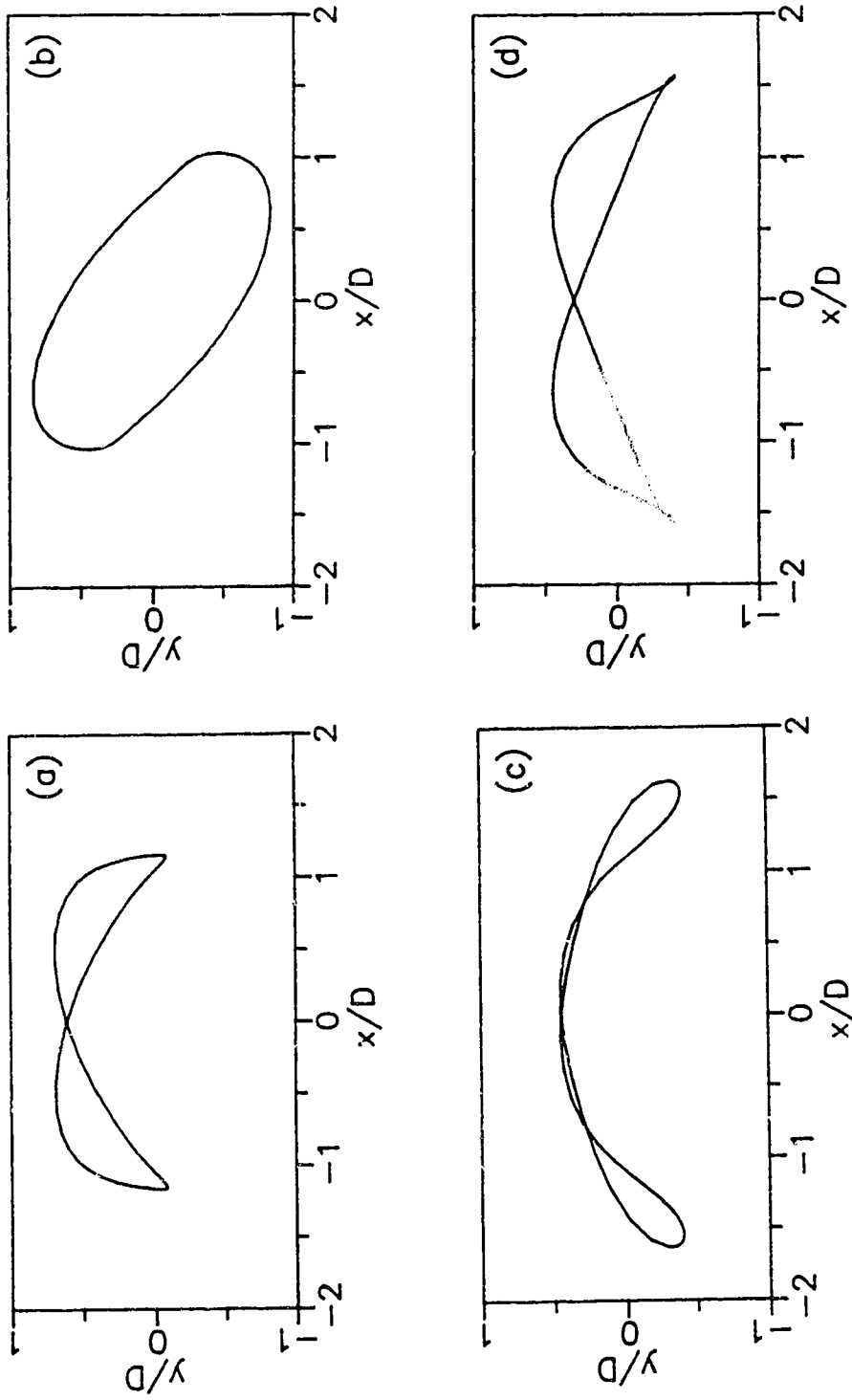
Figure 6.4 Coupled model's dependence on n and ϕ, Case 1. (a) $n = 1$, $\phi = 0$
(b) $n = 2$, $\phi = 0$ (c) $n = 3$, $\phi = 0$ (d) $n = 3$, $\phi = \pi/4$

the trajectory is very similar to that for $\phi = 0$ and $n = 1$ in Figure 6.4($\vdots$`. The result of this phenomenon is that not only ϕ had to be varied, but also n had to be chosen correctly. Based on the trajectories analyzed in this study, the best value for n is either one less than or greater than the observed number of transverse cycles. The closest trajectory to the observed Case 1 is that shown in Figure 6.5 with $n = 3$ and $\phi = -\pi/4$. The shape is quite similar to the observed trajectory, but inline response is overestimated slightly and the transverse response is underestimated.

An additional feature that may be compared between the computed and experimentally observed trajectories is the phase of the response with respect to the water motion and the direction of motion about the trajectory. For this comparison, the trajectory is arbitrarily considered to start at the time corresponding to maximum fluid velocity from left to right, at which time the fluid is passing its equilibrium position. On the plots of both the experimentally observed trajectory and the computed trajectories, the starting point is indicated with a dot, while an arrowhead indicates the direction of motion of the cylinder from the starting point.

Comparison of the starting point for the simple uncoupled model in Figure 6.2(b)
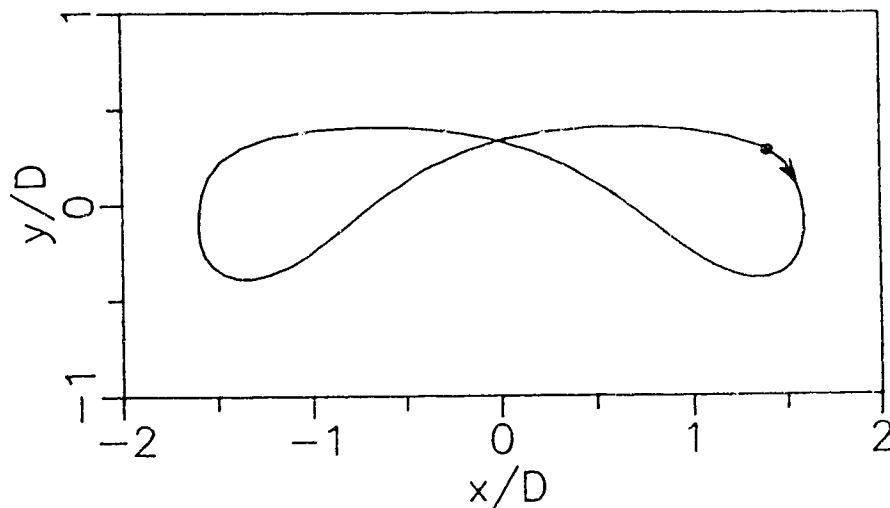

Figure 6.5 Numerically predicted trajectory from the coupled model for Case 1 with $n = 3$ and $\phi = -\pi/4$.

to that of the observed trajectory in Figure 6.1 reveals a very close agreement, but it proceeds in the opposite direction. The modified uncoupled model in Figure 6.3 also starts at about the same point but proceeds in the direction opposite to that observed experimentally. The coupled model in Figure 6.5 is the only model for Case 1 that agrees with the observed trajectory in both direction and starting point. On the basis of the direction of the computed responses it appears that the coupled model is a better predictor of the response in this case.

6.2.2 Case 2

The observed trajectory for Case 2, in which $Kc = 7.7$ and $f_n/f_w = 1.97$, is shown in Figure 6.6. As in the observed trajectory for Case 1, there are two transverse cycles for each cycle of inline motion, so that for both uncoupled models, $n = 2$. However, unlike the infinity shape for Case 1, there are three crossing points in the trajectory and two points where the cylinder changes direction abruptly. With $n = 2$ the frequency of transverse forcing caused by the vortices is defined to be twice the flow frequency. The frequency ratio f_n/f_w is also very close to 2, which indicates that there is a resonance-like condition. It is speculated that the abrupt changes
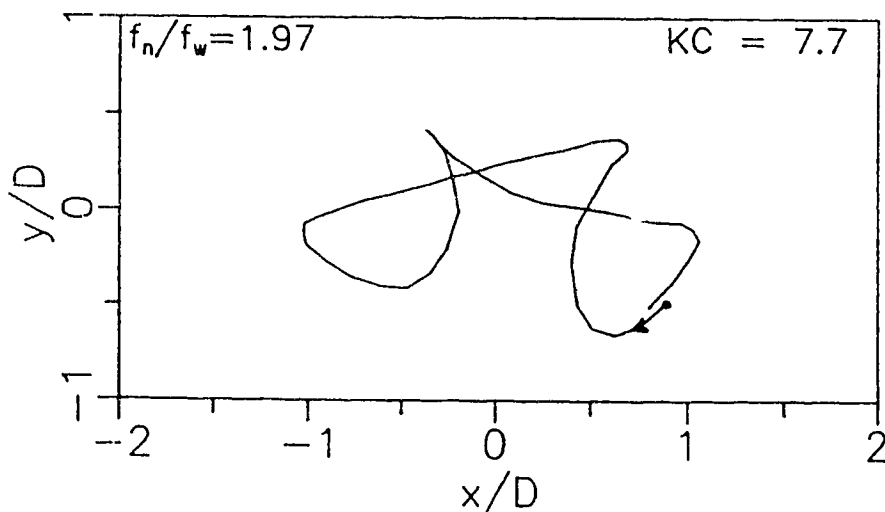

Figure 6.6 Experimentally observed trajectory, Case 2.

in direction are caused by the resonance-like condition and may correspond to the shedding of a strong vortex.

The trajectory predicted by the simple uncoupled model with $\phi = 0$ is shown in Figure 6.7(a) and with $\phi = \pi/2$ in Figure 6.7(b). Other values of ϕ were also tried with similar results. Clearly the abrupt changes in direction are not predicted by the simple uncoupled model. The transverse response amplitudes are overpredicted by the model, while inline responses are underpredicted by about half. The simple uncoupled model is clearly unsuccessful at reproducing this case.

Samples of the modified uncoupled model's predictions for Case 2 are shown in Figure 6.8(a) with $\phi = 0$ and in Figure 6.8(b) with $\phi = -1.8$. In Figure 6.8(b) a slight similarity in shape is evident in that the trajectory shows three crossing points, but otherwise the shape is not very close to the observed one. Inline responses are underpredicted by slightly more than half while the transverse response is quite accurately predicted. By comparing Figures 6.7 and 6.8 it is evident that the modified uncoupled model predicts transverse amplitudes that are less than those of the simple uncoupled model.

In modelling Case 2 with the coupled model, the best trajectory was produced for $n = 1$ and $\phi = -\pi/2$ and is shown in Figure 6.9(a). However, a similar trajectory was produced when $n = 3$ and $\phi = 1.4$, and is shown in Figure 6.9(b). The predictions of inline response were somewhat lower than observed, but transverse response predictions were very close to the observed values. Of interest in modelling Case 2 is the result obtained by setting $\phi = 0$, $n = 1$, $C_L = 3$, $C_m = 2$, and $C_d = 0.8$, shown in Figure 6.10. Although there is no rigorous basis for choosing these coefficients, the similarity between this trajectory and that observed in experiment is very good.

A comparison of the phase and starting points of the computed response from the simple uncoupled model for Case 2 is quite difficult, due to the large differences between the shape of the observed trajectory in Figure 6.6 and the computed
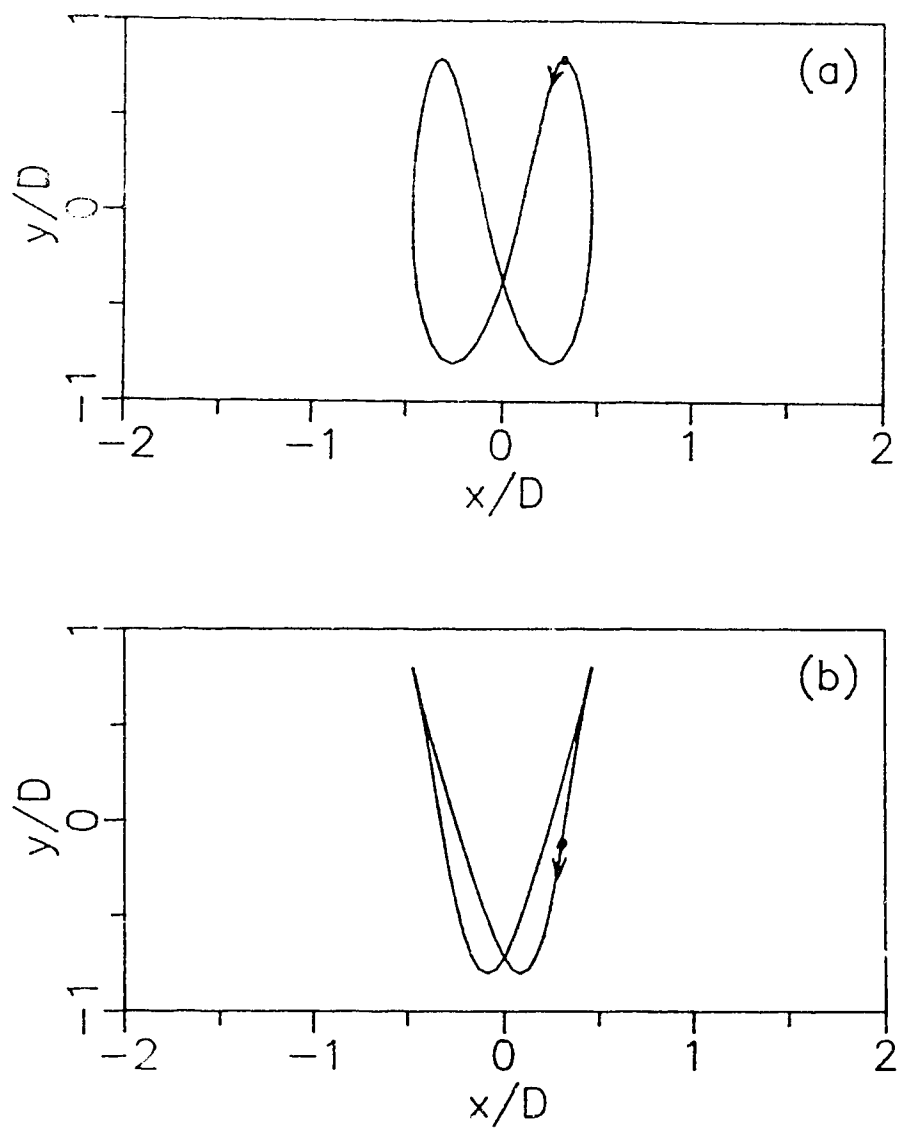
Figure 6.7   Numerically predicted trajectories from the simple uncoupled model
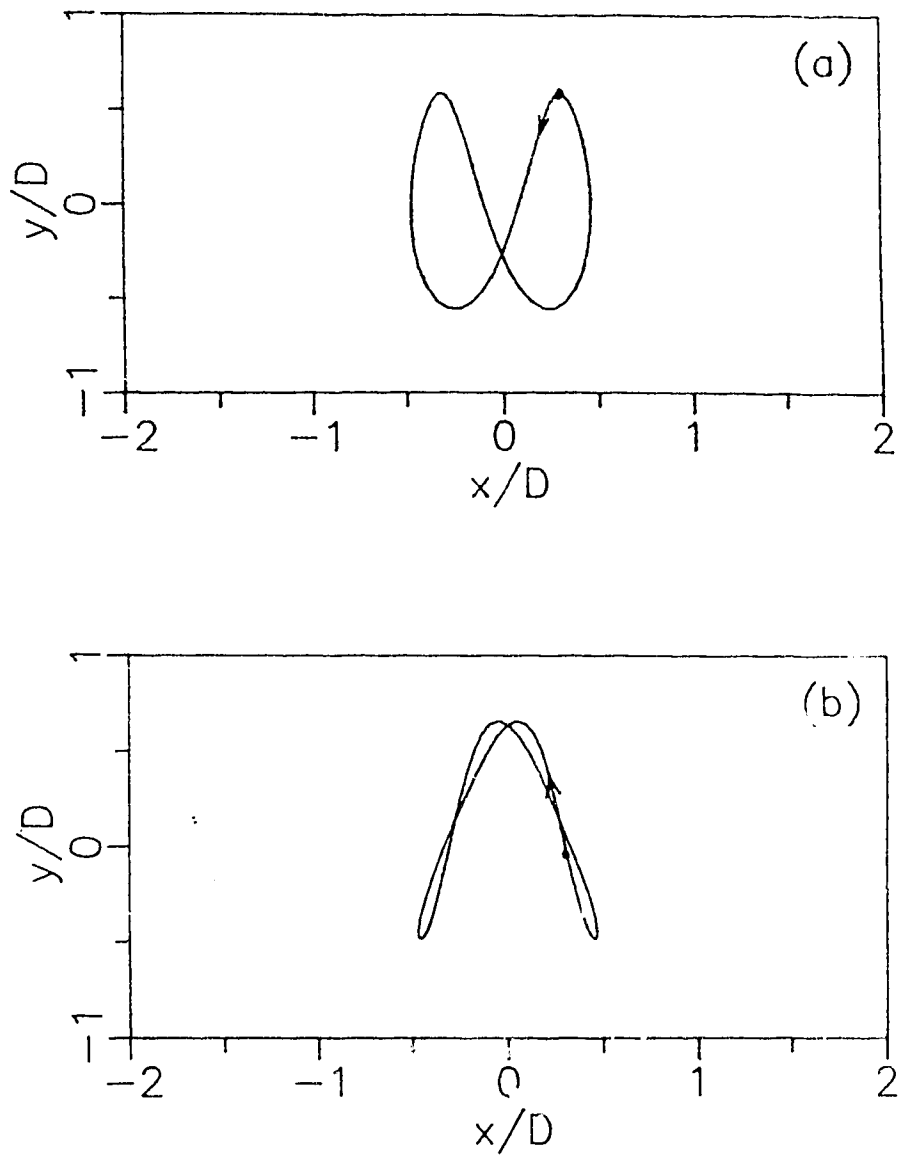for Case 2 with $n = 2$. (a) $\phi = 0$, (b) $\phi = \pi/2$

Figure 6.8   Numerically predicted trajectory from the modified uncoupled model for Case 2 with $n = 2$. (a) $\phi = 0$, (b) $\phi = -1.8$
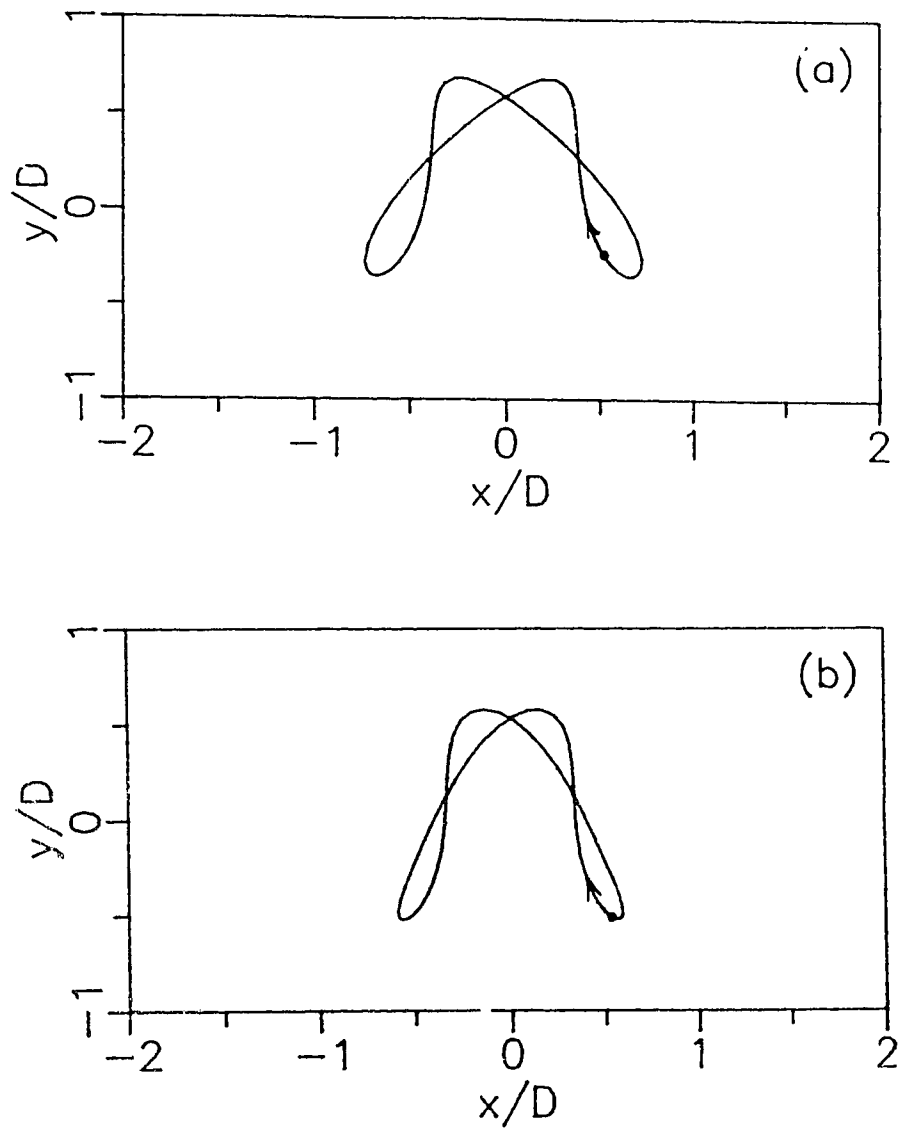
Figure 6.9 Numerically predicted trajectory from the coupled model for Case 2. (a) $n = 1$, $\phi = -\pi/2$, (b) $n = 3$, $\phi = 1.4$
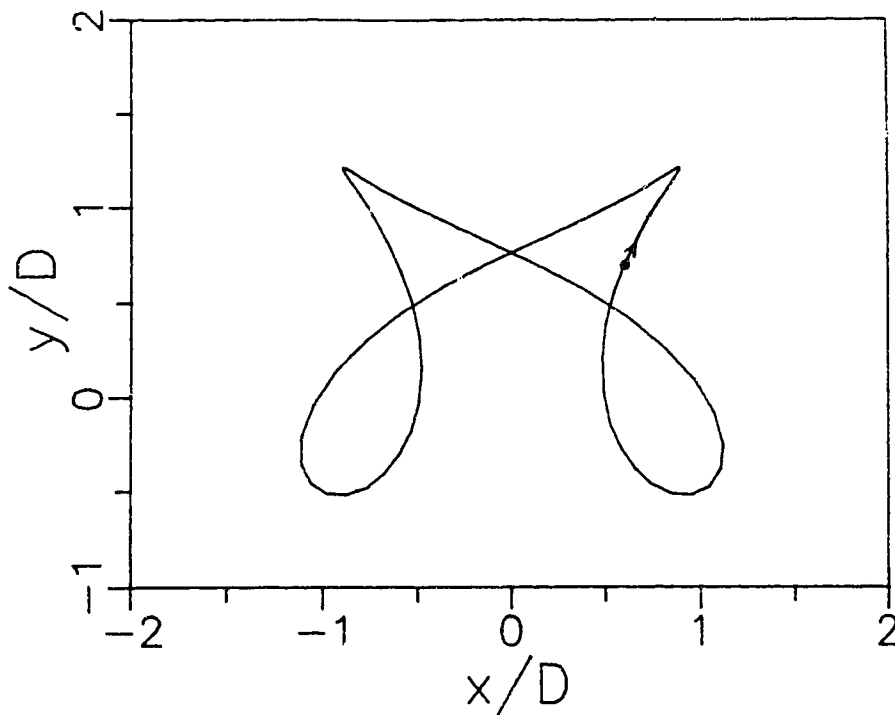
Figure 6.10 Numerically predicted trajectory from the coupled model for Case 2, using modified coefficients.

trajectories in Figure 6.7. However, both the computed and observed starting points agree in that they occur shortly after the cylinder has reached its maximum positive inline deflection. The modified uncoupled model in Figures 6.8(a) and (b) also shows the starting points to occur shortly after maximum positive inline deflection. In Figure 6.8(b), which exhibits three crossing points similar to the observed trajectory, the trajectory proceeds in the same direction about this shape as the experimental trajectory shown in Figure 6.6. The coupled model predictions in Figures 6.9 and 6.10 show the same direction of motion and good agreement in phase is evident in Figure 6.9. Figure 6.10, which was obtained using coefficients to best fit the shape rather than coefficients from empirical data, shows a slight difference in the starting point.

6.2.3 Case 3

The third case for comparison is shown in Figure 6.11, for which Kc 19.7 and $f_n/f_w = 1.97$. This is the same frequency ratio as for Case 2 which w.as identified as a resonance-like condition. Note that in contrast to Case 2, this case corresponds to a trajectory with three transverse cycles for each inline cycle. Additionally, in Case 3 the transverse response is larger than for Case 2. Using the simple uncoupled model with $n = 3$, the third case was most closely reproduced by setting $\phi = -0.4$, with the predicted trajectory shown in Figure 6.12. This model gives a reasonably good prediction of the shape, which is evident by following both trajectories from their starting points. In both the numerically predicted and observed trajectories, the starting point occurs near the right hand side of the trajectory near a very sharp peak. They then proceed to a fairly sharp downward peak, followed by a more rounded upward peak and then to the very sharp downward peak at the lower left corner of the trajectory. The inline response amplitude is well predicted, however transverse response is again overestimated.

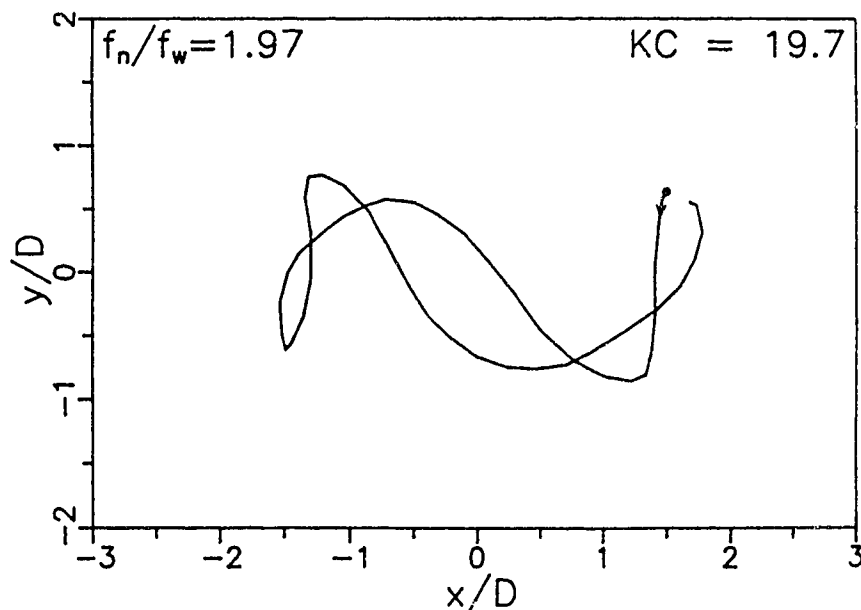The modified uncoupled model's prediction is shown in Figure 6.13 with $\phi = 0$.

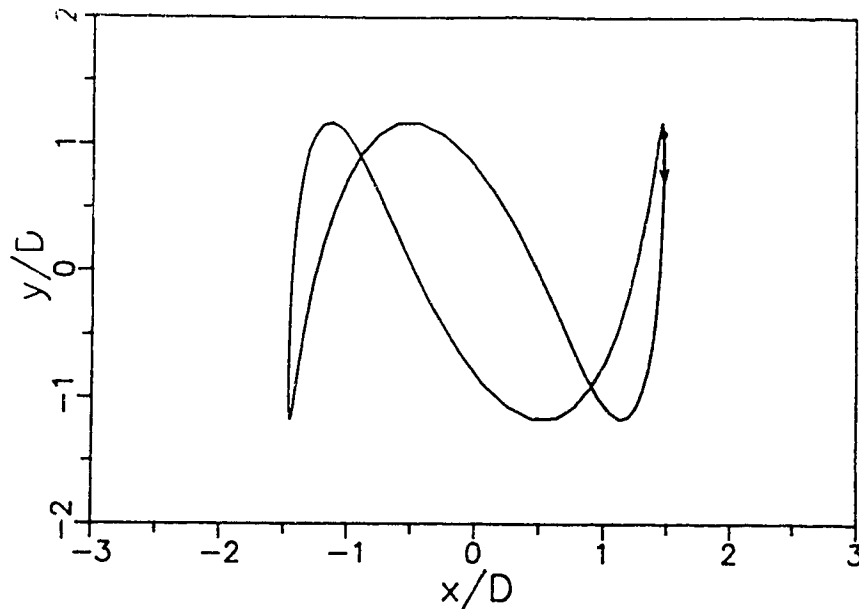Figure 6.11 Experimentally observed trajectory, Case 3.

Figure 6.12 Numerically predicted trajectory from the simple uncoupled model for Case 3 with $n = 3$ and $\phi = -0.4$.

The trajectory shows one sharper peak both upward and downward, similar to the experimentally observed trajectory, however near maximum inline deflection the transverse deflection appears to be shifted vertically. This results in a trajectory that appears to be rotated about 30 degrees from the simple uncoupled model's prediction. Consequently, the largest transverse response is much greater than the observed, but inline amplitude predictions are quite accurate. The best trajectory from the coupled model is that shown in Figure 6.14, for which $n = 4$ and $\phi = 2.5$. The overall shape and transverse response is well duplicated, but the inline response is somewhat overestimated.

The starting point and direction of the observed trajectory for Case 3 in Figure 6.11 shows the trajectory starting at the largest inline and transverse deflection and proceeding first toward a fairly sharp downward peak, as described for the simple uncoupled model. All three models exhibit the same direction of motion and very close agreement in starting point, as can be seen in Figures 6.12, 6.13 and 6.14.
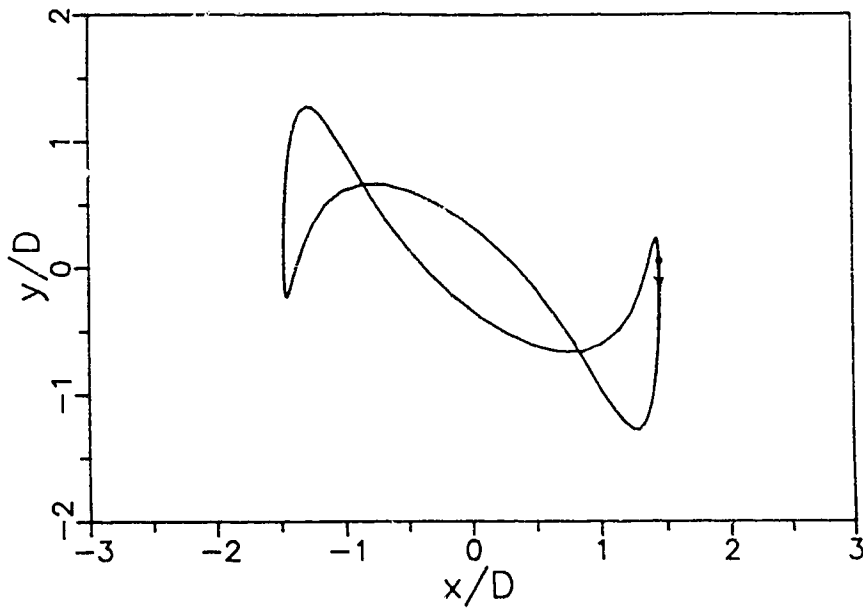
Figure 6.13 Numerically predicted trajectory from the modified uncoupled model for Case 3 with $n = 3$ and $\phi = 0$.
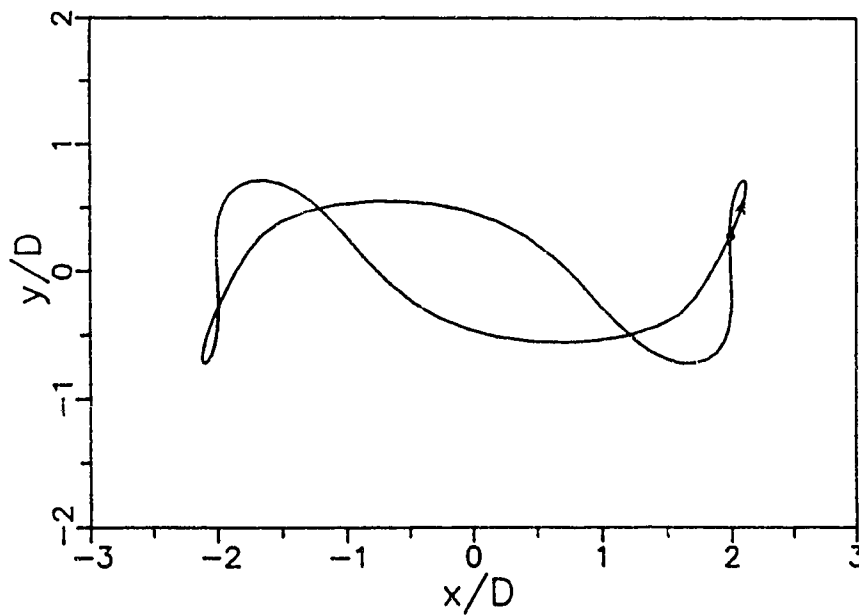

Figure 6.14 Numerically predicted trajectory from the coupled model for Case 3 with $n = 4$ and $= \phi = 2.5$.

6.2.4 Case 4

Figure 6.15 shows the experimentally observed trajectory for Case 4, for which $Kc = 15.0$ and $f_n/f_w = 2.87$. It is similar to Case 2 in that there are abrupt changes in direction which might be attributed to the shedding of a strong vortex. This case could also be considered as a resonance-like situation, since three transverse cycles are completed for each cycle of inline motion and f_n/f_w is close to three. A typical trajectory predicted by the simple uncoupled model is shown in Figure 6.16, with $\phi = 0$. The shape of the trajectory is not very close to the experimental one. The transverse response is somewhat overestimated, while the observed inline response is underestimated by about half.

The predictions of Case 4 from the modified uncoupled model are shown in Figures 6.17(a) and (b) for $\phi = 0$ and $\phi = \pi/3$ respectively. Again, the model does not predict the abrupt changes in direction. As was the case with the simple uncoupled model, the inline deflections are underestimated by about half while the transverse deflections are overestimated slightly.

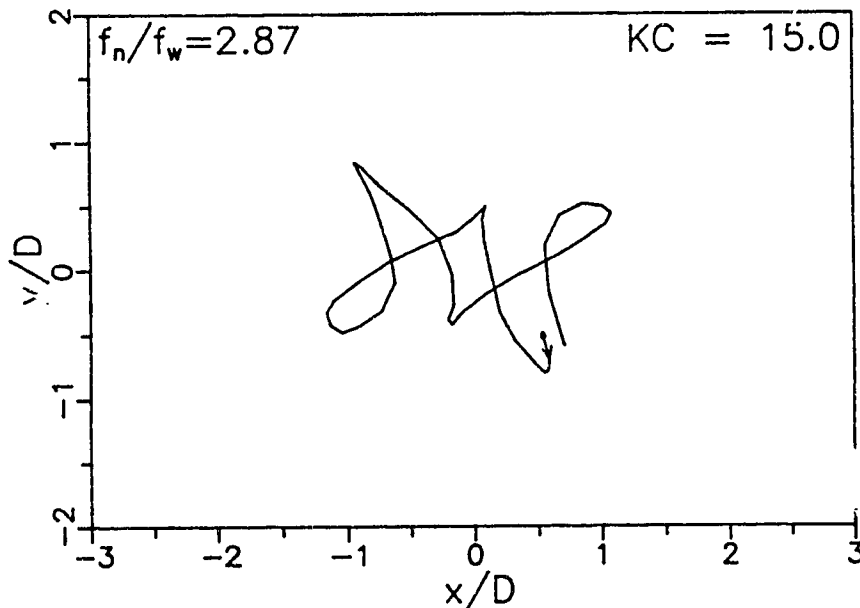The computed response from the coupled model is shown in Figure 6.18, with

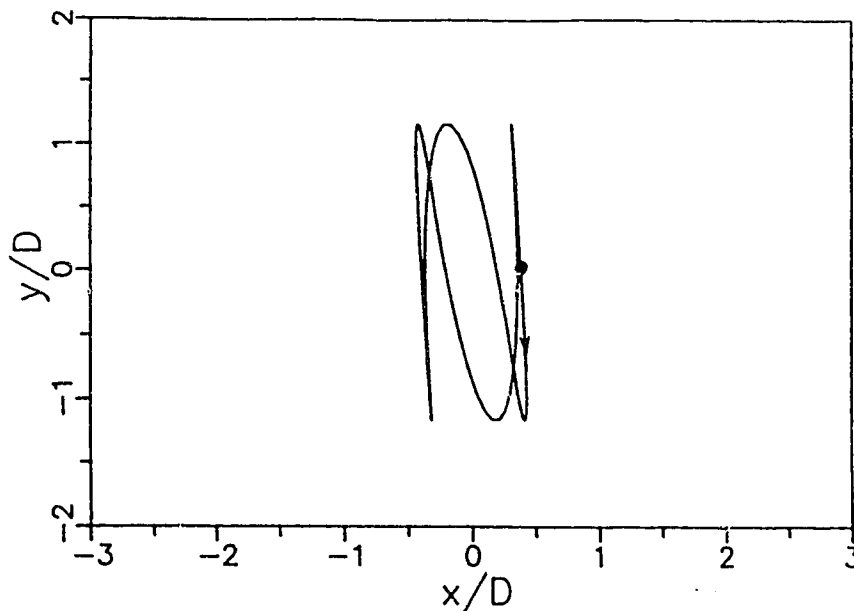Figure 6.15 Experimentally observed trajectory, Case 4.

Figure 6.16 Numerically predicted trajectory from the simple uncoupled model for Case 4 with $n = 3$ and $\phi = 0$.

$\phi = 0$ and $n = 4$. In this case the transverse and inline amplitudes of motion are both well estimated and the shape bears some resemblance to the experimentally observed trajectory.

A comparison of the starting points and directions for the computed trajectories for Case 4 is difficult to make, due to the differences in shape from the observed trajectory, however they all start near maximum positive inline deflection. The coupled model is the only one for which the direction of motion may be compared, and it proceeds in the opposite direction from the experimentally observed trajectory.

6.2.5 Case 5

The experimentally observed trajectory for Case 5 is shown in Figure 6.19, for which $Kc = 48$ and $f_n/f_w = 6.43$. This case is significantly different from the others in that both Kc and f_n/f_w are much larger. The larger cycle to cycle variations observed experimentally for larger Kc, as discussed in Chapter 4, are evident in that the end of the cycle shown is not coincident with the start of the cycle. Nevertheless, this trajectory is repeatable in terms of the number of transverse cycles completed
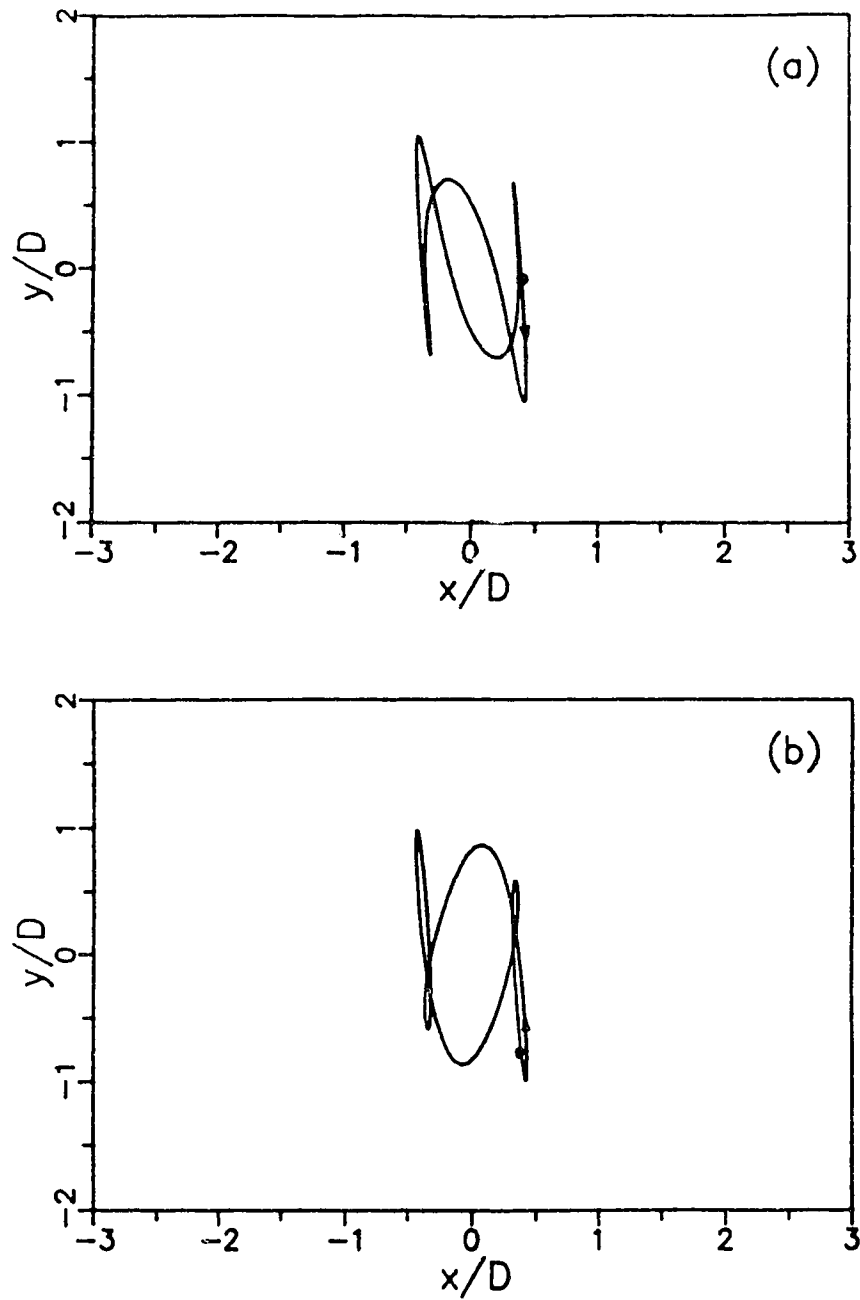
Figure 6.17 Numerically predicted trajectory from the modified uncoupled model for Case 4. (a) $\phi = 0$, (b) $\phi = \pi/3$.
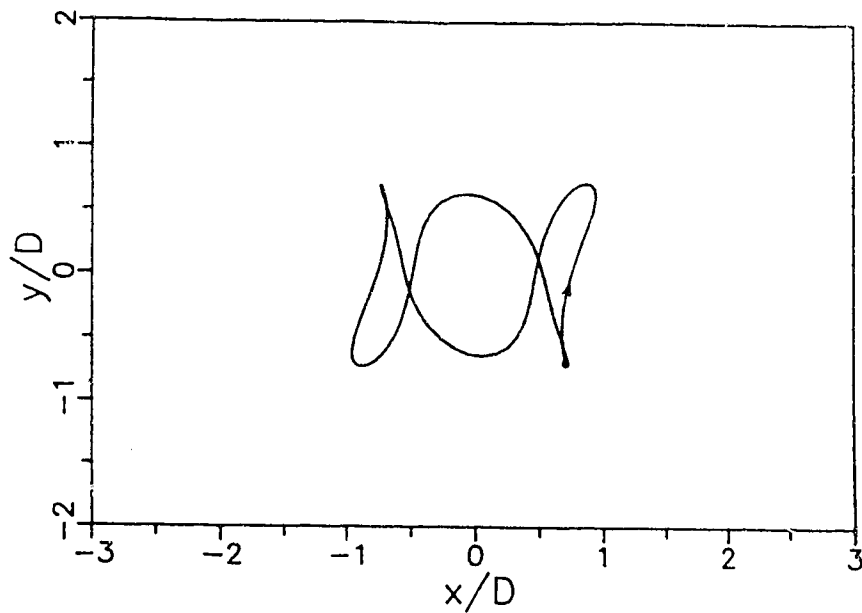
Figure 6.18   Numerically predicted trajectory from the coupled model for Case 4
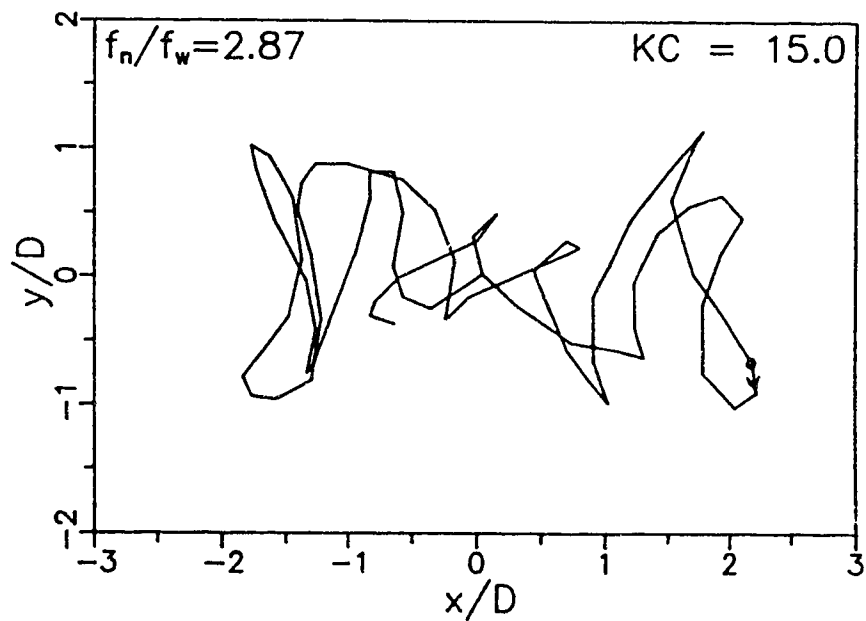with $n = 4$ and $\phi = 0$.

Figure 6.19 Experimentally observed trajectory, Case 5.

and the orientation of the transverse cycles within each cycle of inline motion. The number of transverse cycles completed per inline cycle is 7, including the smaller cycles in the centre of the trajectory. Therefore n should be chosen as 7 for the uncoupled models. The abrupt changes in direction and the similarity between $f_n/f_w = 6.43$ and the number of transverse cycles completed in one cycle of water motion indicates that this is also a resonance-like condition.

The simple uncoupled model's prediction for $n = 7$ and $\phi = 0$ is shown in Figure 6.20. Seven transverse cycles can be identified, and they all are of the same amplitude, as expected from the simple uncoupled model. In contrast, the experimental trajectory shows larger transverse amplitude corresponding to large inline displacement. Both inline and transverse displacement amplitudes are underestimated, probably due to an amplification of lift and drag forces similar to that experienced under lock-in conditions in steady flow. The modified uncoupled model's predictions with $n = 7$ and $\phi = 0$, shown in Figure 6.21, displayed some
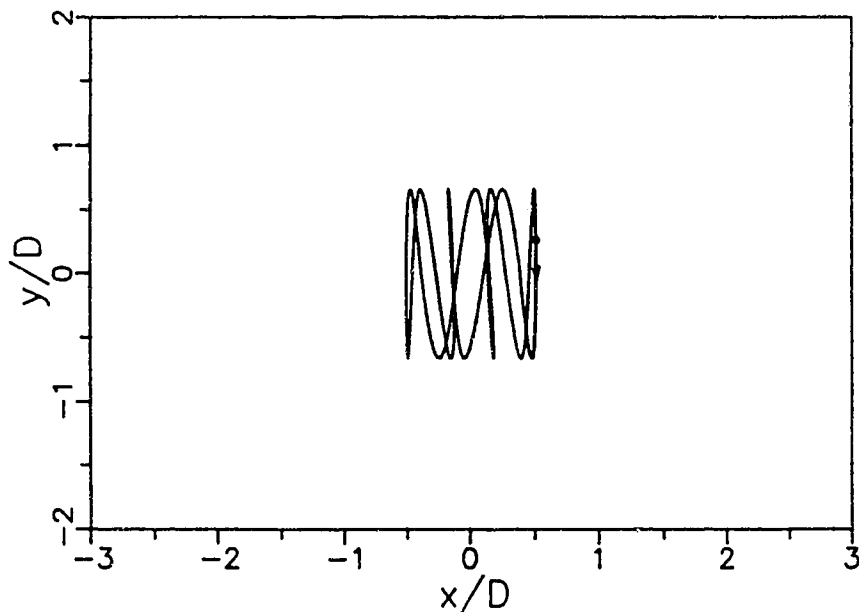

Figure 6.20 Numerically predicted trajectory from the simple uncoupled model for Case 5 with $n = 7$ and $\phi = 0$.

Figure 6.21 Numerically predicted trajectory from the modified uncoupled model for Case 5 with $n = 7$ and $\phi = 0$.

modulation of the transverse response but also underestimated the amplitude of inline and transverse response.

A typical trajectory from the coupled model for Case 5 is shown in Figure 6.22 with $n = 6$ and $\phi = 0$. The amplitudes of response are again underestimated. Comparison of the starting points show that all the models start near the maximum inline deflection, as observed in the experimental trajectory, but the direction of motion is difficult to compare.

6.3   Conclusions

The numerical results of the three models developed to predict the response of a cylinder to oscillatory flow were compared to experimentally observed trajectories. The agreement between the predicted and experimentally observed trajectories was generally quite good considering the simplicity of the models and the complex nature
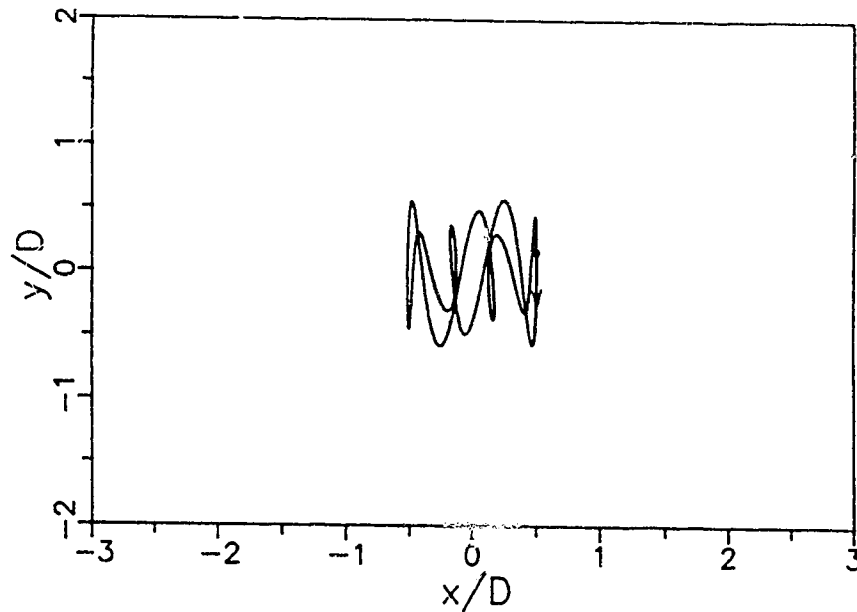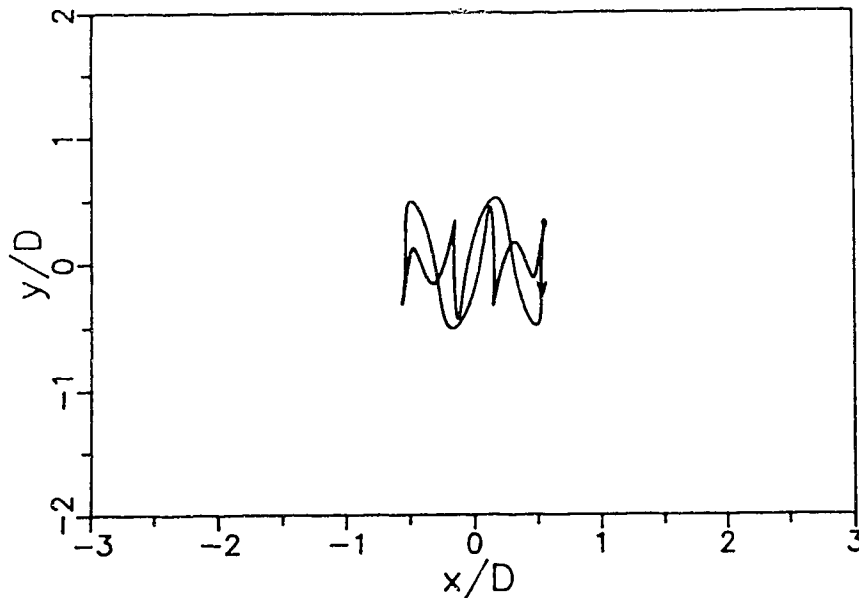
Figure 6.22 Numerically predicted trajectory from the coupled model for Case 5
with $n = 6$ and $\phi = 0$.

of the interaction between the cylinder and the flow. The comparison showed that there was particularly good agreement for the trajectories which did not have abrupt changes in direction and resonance-like conditions. This limitation is not as serious as one might expect, with respect to transverse oscillations, since non-resonant cases such as Case 3 often produced larger transverse deflections than the resonant cases. However, significant underestimation of the inline response for the resonant cases is a greater limitation.

The simple uncoupled model best predicted trajectories that were smoothly curved. The transverse response peaks were all of the same amplitude due to the nature of the simple harmonic forcing in the transverse direction, and consequently the modulation of the transverse response observed experimentally was not predicted. Of the predictions by the simple uncoupled model that were close enough in shape to permit a comparison of the starting points and direction, only Case 3 showed the correct direction and starting point.

The modified forcing model showe᠄ some improvement over the simple uncoupled model's predictions. In general the transverse responses were closer to the experimentally observed values than for the simple uncoupled model. The reason that the modified uncoupled model does not overpredict the transverse responses to the same extent as the simple uncoupled model is the use of the instantaneous fluid velocity, rather than U_m, in the expression for the lift force. As expected the inline response amplitudes for ᠄e modified uncoupled model were the same as for the simple uncoupled model because the inline equation of motion is the same for both. The model displayed some modulation of the amplitude of transverse response, and it is in this respect that the modified uncoupled model was noticeably better than the simple uncoupled model. In every case except 4 and 5, where the similarity in shape was not sufficient to permit a clear comparison of the direction of motion, good agreement in starting point and direction of motion about the trajectory was evident. This result helps to discount the possibility ᠄hat the agreement in shape between the numerical and experimental trajectories is caused by a combination of coincidence and adjustment of the parameter ϕ.

The coupled model showed considerably different types of trajectories from those produced by the uncoupled models. Although the selection of the parameters n and ϕ was more difficult to define, the overall shape and proportions of the trajectories were in better agreement than the two uncoupled models. In particular, the transverse displacements for Cases 2, and 4 were not so highly overestimated, while the shape of Case 3 was predicted in quite good detail. For Case 5, in which $Kc = 48$, the coupled model was least successful. This might indicate that it is best suited to cases where a large part of the vortex motion consists of attached vortices being swept around the cylinder, as opposed to vortex shedding in the quasi-steady flow encountered for large Kc. In this respect, the coupled model showed potential, with the excellent agreement in shape that was obtained for Case 2 with different coefficients. This result may be an indication that alternative methods of selecting coefficients need to be developed, perhaps involving iterative solutions. The coupled model also exhibited

good agreement in starting point and direction of motion in cases where the shapes were similar enough to permit the comparisons.

One reason for the consistent overprediction of amplitudes of transverse response by the simple uncoupled model in Cases 1 to 4 may be that the structural damping was ignored in the numerical solution. This problem could also be addressed by using a more suitable lift coefficient. In the results given here, the lift coefficient was $C_{L_{max}}$ reported by Sarpkaya [5], which was the largest of the maximum values of the lift coefficient over many cycles. Instead, the average maximum value of the lift coefficient could be used. Another approach would be to employ an amplitude dependent lift coefficient, although such a source of data is not currently available.

The trajectories show that a different model is required to reproduce exactly the shapes of the trajectories that have abrupt changes in direction, or "corners", which are likely caused by the strong and distinct shedding of an individual vortex. Inline response amplitudes are quite well predicted for Cases 1 and 3, which are smoothly curved trajectories, but the inline response for trajectories exhibiting "corners" are underpredicted by about half. It would appear that there is a considerable difference in the fluid-structure interaction between these two types of cases. The result of this fluid-structure interaction is that inline deflections may be underestimated for conditions involving transverse resonance. To gain a better understanding of the fluid-structure interaction a flow visualization study of the vortex shedding should be undertaken and compared to the flow visualization studies by C.H.K. Williamson [18] and C.H.K. Williamson and Roshko [19]. Due to resonance-like phenomena, the use of constant empirical coefficients from fixed cylinder data is probably in error. One possibility to investigate is the use of iteratively determined coefficients similar to those used by C.H.K. Williamson [20] for inline response.

An alternative method of obtaining better agreement in the shapes of the trajectories is to use a more complex forcing expression. In an attempt to improve the shape of the trajectories an additional term was added to the inline forcing terms in the simple uncoupled model to account for vortex forces in the inline direction.

The numerical results of this model were not presented here, however it is worth noting that the trajectories often lost symmetry and gained complexity, proving to be worse predictions of the cylinder's response than the simple uncoupled model.

A further refinement that could be made to the modified uncoupled model would be to use the forcing expression of Bearman et al. [17] as discussed in Section 2.2.2. By using this model, additional components at multiples of the flow frequency would be included.

Although some success was achieved with the three models it is clear that further improvements are needed to accurately predict the cylinder's response. The possibility of a wake oscillator model similar to that for steady flow seems to be the next step, although greatly increased complexity might be anticipated due to the need to account for the incident wake and vortices from the previous half cycle. In this respect, a vortex tracking numerical model might hold some promise, but such a model would first require a knowledge of vortex motion for the case in which the cylinder is free to respond in two dimensions.

Chapter 7

Conclusions and

Recommendations

In this study, the response of a flexibly mounted rigid cylinder to oscillatory flow was investigated experimentally. It was found that the cylinder tended to respond in trajectories that varied in size and shape depending on the Keulegan-Carpenter number, Kc, and frequency ratio, f_n/f_w. Kc was varied between 2 and 60 in the study, while f_n/f_w was varied between 1 and 8.6. When the trajectories were placed on a plot with Kc as the ordinate and f_n/f_w as the abcissa, it was found that the trajectories in certain areas of the plot were similar and could be grouped on the basis of the number of transverse cycles completed for each cycle of water motion. In all cases, one principal cycle of inline motion was observed for each cycle of water motion. For the range of parameters investigated, trajectories with as few as 2 or as many as 8 transverse cycles were identified. The boundaries for these groups were most clearly defined for lower values of Kc and f_n/f_w. For conditions corresponding to the boundaries between trajectories with different numbers of transverse cycles, smaller, and often three-dimensional response was observed. Amplitudes of transverse response appeared to be limited to about 1.2 diameters, similar to the largest amplitudes observed in studies of transverse-only

response in oscillatory flow and of response to steady flow. Amplitudes of inline response of slightly over two diameters were observed, however no limit to their amplitude was evident.

It was found that when the cylinder can respond in two dimensions the number of transverse cycles completed in one cycle of water motion tended to assume integer multiples of the flow frequency. For example, as Kc was increased for a cylinder with f_n/f_w fixed at 1.97, the transverse response occurred first at 2 and then at 3 times the flow frequency. By comparison, in studies of transverse response alone it has been reported that the frequency of response shows a strong tendency to assume an integer multiple of the flow frequency, but the integer multiple is such that the principal frequency of transverse response remains very close to the natural frequency of the cylinder. In the example cited from the present study, the response at 3 times the flow frequency for a cylinder with $f_n/f_w = 1.97$ is not consistent with the results of transverse response only. The reason for this inconsistency is that transverse response at 2 times the flow frequency, rather than 3, would result in a response frequency closer to the natural frequency. In addition, the studies of transverse response alone have shown that larger transverse responses occur when the ratio of the natural frequency to the flow frequency is an integer multiple, although this was not evident in the present study. The reasons for these differences can be attributed to the inline response of the cylinder which can significantly alter the timing of the incident vortices from the previous half cycle with the response of the cylinder.

Three numerical models of the two-dimensional response of a cylinder to oscillatory flow were developed and compared to experimentally observed trajectories. The "simple uncoupled" model and the "modified uncoupled model" used the relative velocity formulation of the Morison equation for the inline fluid force, and different expressions for the transverse forcing. The "coupled model" involved lift and drag terms that act perpendicular and parallel to the direction of instantaneous relative velocity between the cylinder and the flow. In all models empirical coefficients from studies of fixed cylinders in oscillatory flow were used.

It was found that the models predicted the behaviour quite well considering the simplicity of the models and the complexity of the fluid-structure interaction. In particular, the models were more successful at predicting the response for cases where the trajectories were smoothly curved, rather that the cases that appeared to involve resonant behaviour and abrupt changes in direction. The modified uncoupled model was significantly better than the simple uncoupled model because it was able to predict some modulation of the transverse response. It was also more successful at predicting the direction of motion about the trajectory and the phase relationship between the water motion and the trajectories. Despite these successes, it was also evident that improvements need to be made to accomodate the resonant cases. The main shortcoming of the models was that the inline response for these resonant cases was significantly underestimated, especially for cases corresponding to high Kc. In this regard, the coupled model showed some promise in that, with appropriate coefficients, it could model some of the resonant cases more successfully. This may be an indication that alternative methods may be required to select the empirical coefficients, perhaps involving iterative approaches which account for the structural response. Obviously many other different models could be formulated which may prove useful. In this regard the independent flow fields model could be used for the inline force, and different models for the lift force such as the one proposed by Bearman et al. [17] should be considered.

For this study, it is clearly evident that the next step in understanding the fluid-structure interaction is to conduct a flow visualization study to determine the fluid and vortex dynamics involved. Such a study should be able to identify the causes of the well defined groups of trajectories observed, and perhaps provide some insight for the modelling of the response, particularly the resonant cases.

References

[1] R.D. Blevins, *Flow Induced Vibrations*, Second Edition, Van Nostrand Reinhold, New York, 1990.

[2] P.W. Bearman, "Vortex Shedding from Oscillating Bluff Bodies", *Ann. Rev. Fluid Mech.*, Vol. 16, pp. 195–222, 1984.

[3] H. Schlicting, *Boundary Layer Theory*, Seventh Edition, McGraw-Hill, New York, 1979.

[4] T. Sarpkaya and M. Isaacson, *Mechanics of Wave Forces on Offshore Structures*, Van Nostrand Reinhold, New York, 1981.

[5] T. Sarpkaya, "Vortex Shedding and Resistance in Harmonic Flow about Smooth and Rough Circular Cylinders at High Reynolds Numbers", Report NPS-59SL76021, Naval Postgraduate School, Monterey, California, 1976.

[6] T. Sarpkaya, "In-line and Transverse Forces on Smooth and Sand Roughened Cylinders in Oscillatory Flow at High Reynolds Numbers", Report NPS-69SL76062, Naval Postgraduate School, Monterey, California, 1976.

[7] T. Sarpkaya, "In-line and Transverse Forces on Cylinders in Oscillatory Flow at High Reynolds Numbers", *Journal of Ship Research*, Vol. 21, No. 4, pp. 200–216, 1977.

[8] T. Sarpkaya, "In-line and Transverse Forces on Smooth and Sand Roughened Cylinders in Oscillatory Flow at High Reynolds Numbers", Report NPS-69-86-003, Naval Postgraduate School, Monterey, California, 1986.

[9] P.W. Bearman and J.M.R. Graham, "Hydrodynamic Forces on Cylindrical Bodies in Oscillatory Flow", *BOSS '79 Second Int'l Conf. on Behaviour of Off-Shore Structures*, Vol. 1, pp. 309–322, Imperial College, London 1979.

[10] D.J. Maull and M.G. Milliner, "Sinusoidal Flow Past a Circular Cylinder", *Coastal Engineering*, Vol. 2, pp. 149–168, 1978.

[11] C. J. Garrison, "Drag and Inertia Forces on Circular Cylinders in Harmaonic Flow", *Journal of Waterway Port Coastal and Ocean Engineering ASCE*, Vol. 116, No. 2, pp. 169–190, 1990.

[12] K.G. McConell and Y.S. Park, "The Frequency Components of Fluid-Lift Forces Acting on a Cylinder Oscillating in Still Water", *Experimental Mechanics*, Vol. 22, No. 6, pp. 216–222, 1982.

[13] K.G. McConell and Y.S. Park, "The Response and the Lift-Force Analysis of an Elastically Mounted Cylinder Oscillating in Still Water", *Behaviour of Offshore Structures Proceedings of the 3rd Int'l BOSS '82 Conference*, Vol. 2, pp. 671–680, 1982.

[14] J. R. Morison, M. P. O'Brien, ?. W. Johnson and S. A. Schaaf, "The Force Exerted by Surface Waves on Piles", *Transactions of the American Institute of Mining and Metallurgical Engineers*, Vol. 189, pp. 149–154, 1950.

[15] G.H. Keulegan and L.H. Carpenter, "Forces on Cylinders and Plates in Oscillating Fluid", *Journal of Research of the National Bureau of Standards*, Vol. 60, No. 5, pp. 423–440, 1958.

[16] J.F. Wilson, *Dynamics of Offshore Structures*, John Wiley & Sons, New York, 1984.

[17] P.W. Bearman and J.M.R. Graham and E.D. Obasaju, "A Model Equation for the Transverse Forces on Cylinders in Oscillatory Flow", *Applied Ocean Research*, Vol. 6, No. 3 pp. 166–172, 1984.

[18] C. H. K. Williamson, "Sinusoidal Flow Relative to Circular Cylinders", *Journal of Fluid Mechanics*, Vol. 155, pp. 141–174, 1985.

[19] C. H. K. Williamson and A. Roshko, "Vortex Formation in the Wake of an Oscillating Cylinder", *Journal of Fluids and Structures*, Vol. 2, No. 4, pp. 355–382. July 1988.

[20] C.H.K. Williamson, "In-line Response of a Cylinder in Oscillatory Flow," *Applied Ocean Research*, Vol. 7, No. 2, pp. 97–106, 1985.

[21] T. Sarpkaya and F. Rajabi, "Dynamic Response of Piles to Vortex Shedding in Oscillating Flows", *Proceedings of the 11th Annual Offshore Technology Conference in Houston Tex.*, OTC paper 3647, pp. 2523–2528, 1979.

[22] P.W. Bearman and P.F. Hall, "Dynamic Response of Circular Cylinders in Oscillatory Flow and Waves", *Proceedings of the 1st International Conference on Flow Induced Vibrations*, R. King (ed.), pp. 183–190, June 1987.

[23] B.M. Sumer and J. Fredsøe, "Transverse Vibrations of an Elastically Mounted Cylinder Exposed to an Oscillating Flow", *Journal of Offshore Mechanics and Arctic Engineering*, Vol. 110, No. 4. pp. 387–394, 1988.

[24] B.M. Sumer, J. Fredsøe, H. Gravesen and R. Bruschi, "Response of Marine Pipelines in Scour Trenches", *Journal of Waterway, Port, Coastal and Ocean Engineering*, Vol. 115, No. 4, pp. 477–496, 1989.

[25] M.F. Zedan, J.Y. Yeung, H.J. Salane and F.J. Fischer, "Dynamic Response of a Cantilever Pile to Vortex Shedding in Regular Waves", *Proceedings of the 12th Offhore Technology Conference*, OTC paper 3799, pp. 45–59, 1980.

[26] M.F. Zedan and F. Rajabi, "Lift Forces on Cylinders Undergoing Hydroelastic Oscillations in Waves and in Two-Dimensional Harmonic Flow", *Int'l Symp. on Hydrodynamics in Ocean Engineering*, pp. 239–261, Trondheim, Norway, 1981.

[27] T. Sawaragi, T. Nakamura and H. Miki, "Dynamic Behaviour of Circular Pile Due to Eddy Shedding in Waves", *Coastal Engineering in Japan*, Vol. 20, pp. 109–120, 1977.

[28] A.G.L. Borthwick and D.M. Herbert, "Loading and Response of a Small Diameter Flexibly Mounted Cylinder in Waves," *Journal of Fluids and Structures*, Vol. 2, No. 5, pp. 479-501, 1988.

[29] F. Rajabi, "Hydroelastic Oscillations of Smooth and Rough Cylinders in Harmonic Flow," PhD. Thesis, Naval Postgraduate School, Monterey, California. 1979.

[30] S.K. Chakrabarti, *Hydrodynamics of Offshore Structures*, Springer-Verlag, London, 1987.

[31] W.H. Press, B.P. Flannery, S.A. Teukolsky, W.T. Vetterling, *Numerical Recipes*, Cambridge University Press, Cambridge, 1986.

Appendix A

Resolving Inertia Terms in an Equation of Motion

This appendix describes an alternative method of deriving the inertia terms for the resolved lift and drag model discussed in section 5.4. The inertia terms due to the flow field and the acceleration of the cylinder with respect to the fluid are resolved in the direction of relative acceleration, with the inline and transverse components separated.

The direction of the acceleration of the cylinder with respect to the fluid, $a_{C/F}$, is not necessarily the same as the direction of instantaneous relative velocity. The inertia terms must therefore be resolved along a direction separate from the direction of relative velocity. Recall that the velocity of the fluid with respect to the cylinder is $v_{F/C}$ as defined in Eq. 5.16. The inertia terms depend on the acceleration of the cylinder with respect to the fluid,

$$a_{C/F} = (\ddot{x} - \dot{U})\hat{\imath} + \ddot{y}\hat{\jmath}, \tag{A.1}$$

as shown in Figure A.1. The angle γ can be defined such that

$$\sin\gamma = \ddot{y}/a \quad \text{and} \quad \cos\gamma = (\ddot{x} - \dot{U})/a, \tag{A.2}$$

where $a = \sqrt{(\ddot{x} - \dot{U})^2 + \ddot{y}^2}$ is the magnitude of a. The inertia term for the x direction
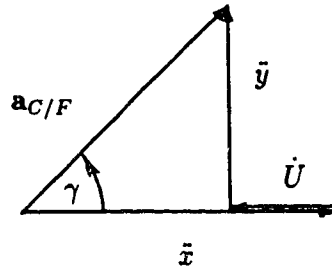
Figure A.1 Components of the direction of relative acceleration.

will include a pressure gradient term that is causing the fluid acceleration, $\dot{U}$. This force is independent of cylinder motion and acts only in the x direction. Additionally there will be a term to account for the relative acceleration of the cylinder with respect to the fluid. Therefore

$$
\begin{aligned}
[\text{inertia}]_x &= \rho A \dot{U} - \rho A C_a (\mathbf{a}_{C/F})_x \\
&= \rho A \dot{U} - \rho A C_a a \cos\gamma \\
&= \rho A \dot{U} - \rho A C_a (\ddot{x} - \dot{U}),
\end{aligned}
\tag{A.3}
$$

using the second of Equation A.2. In general the coefficient C_a will depend on the relative motion which is not known *a priori*. At this point it is necessary to make some assumptions to avoid an iterative solution. It is convenient to extract the $-\rho A C_a \ddot{x}$ term for use as an added mass in the equation of motion, which causes the natural frequency of the structure in the fluid to appear as a term in the equation of motion. The remaining inertia terms are $\rho A \dot{U}(1 + C_a)$. By including added mass with the structural mass, one is committed to treating the inertia terms on an independent flow field basis because the relative acceleration term $(\ddot{x} - \dot{U})$ has been separated. C_m should then be used in place of $(1 + C_a)$ as it is known to account for the effects of the fluid motion past the cylinder when held fixed.

The inertia term for the y direction is similarly shown to be

$$\begin{aligned}
[\text{inertia}]_y &= -\rho A C_a (\mathbf{a}_{C/F})_y \\
&= -\rho A C_a a \sin \gamma \\
&= -\rho A C_a \ddot{y}.
\end{aligned} \tag{A.4}$$

as it only consists of effects due to the acceleration of the cylinder with respect to the fluid. The inertia terms derived in this appendix are identical to those assumed in the resolved lift and drag model and used in equations 5.19 and 5.20.